AN OBJECT DESCRIPTION AND CATEGORIZATION METHOD BASED ON SHAPE AND APPEARANCE FEATURES

by

M.Sc. Leonardo Chang Fernández

A THESIS SUBMITTED IN PARTIAL FULFILLMENT OF
THE REQUIREMENTS FOR THE DEGREE OF

DOCTOR IN COMPUTER SCIENCE

at the

Instituto Nacional de Astrofísica, Óptica y Electrónica
Tonantzintla, Puebla, Mexico
2015

Advisors:

Dr. Miguel Octavio Arias Estrada, INAOE, Mexico
Dr. Luis Enrique Sucar Succar, INAOE, Mexico
Dr. José Hernández Palancar, CENATAV, Cuba

A mis padres y hermana
este minúsculo paso
en mi camino
a ser como ustedes.

Agradecimientos

Quiero expresar mis más sinceros agradecimientos a mis asesores Dr. Luis Enrique Sucar, Dr. Miguel Arias Estrada y Dr. José Hernández Palancar, por todo el apoyo, guía y conocimiento brindados durante el desarrollo de esta investigación. Sus enseñanzas han sido fundamentales para el desarrollo de esta tesis doctoral y para el mío propio como investigador.

A mis sinodales Dra. Angélica Muñoz Meléndez, Dr. Eduardo Morales Manzanares, Dr. Jesús Antonio González Bernal, Dr. Hugo Jair Escalante Balderas y Dr. Gustavo Olague Caballero por sus certeras observaciones y sugerencias que ayudaron a mejorar la calidad de esta tesis.

Al CENATAV, por formarme como profesional e investigador, por darme un lugar donde sentirme como en casa.

A Shul, por su inagotable energía en la tarea de convertirnos en mejores investigadores y profesionales. A Isneri, por su apoyo y ejemplo.

A mis padres, por toda la sabiduría, educación, consejos y amor que me han brindado, ustedes son lo máximo.

A mi hermana, por ser mi mejor amiga, mi cómplice incondicional, mi complemento.

A mi cuñado Ariel, por cuidar y amar a mi ser más querido. También por las construcciones de las que me he librado durante este período.

A toda mi familia y amigos, por hacer mi vida muy feliz.

A todos mis compañeros del CENATAV, todos han sido parte de esta etapa de mi vida y me han ayudado de una forma u otra. En especial a Yoanna, Airel, Heydi, Annette, Noslen, Yenisel, Nelson, Raudel por todo lo que hemos compartido cada día.

A mis amigos-hermanos, a Alfre por siempre estar ahí, ya son casi 20 años bro! Al flaco por ser un amigo incondicional y también por la parte que compartimos de la investigación. A

Jasan que aunque lejos y distantes seguimos siendo hermanos. A mis hermanos de Ciego, Andrés, Tavo y Migue en quienes gracias a esta tesis encontré excelentes amigos.

A todos aquellos que conocí durante mis días en México, hicieron de esto una experiencia excepcional.

Al INAOE por brindarme un espacio para desarrollar mis estudios, no hubiera preferido otro. A todos los investigadores de la Coordinación de Ciencias Computacionales, en especial al Dr. Ariel Carrasco Ochoa, quien siempre nos ha brindado su ayuda y hospitalidad.

Al CONACYT (a través de la beca No. 240251) por brindarme los medios materiales y económicos para realizar esta investigación.

A mi Patria y a mi bandera.

Leonardo Chang Fernández.
Tonantzintla, Puebla. 15 de Junio de 2015.

Abstract

Object recognition in images is one of the oldest problems in Computer Vision. In this thesis, we focus on the problem of category-level object recognition, based on the use of shape features as a more generic representation of object classes than appearance features, while the latest are used as second-level features.

In this research work we propose an invariant shape feature extraction, description and matching method for binary images, named LISF. The proposed method extracts local features from the contour to describe shape and these features are later matched globally. Combining local features with global matching allows us to obtain a trade-off between discriminative power and robustness to noise and occlusion in the contour. The proposed extraction, description and matching methods are invariant to rotation, translation and scale, and present certain robustness to partial occlusion. The conducted experiments showed that, for larger occlusion levels, the better was the performance of LISF with respect to other popular shape description methods, with about 20% higher bull's eye score and 25% higher accuracy in classification in images with a 60% occlusion. Also, we present a massively parallel implementation in GPU of LISF, which achieves a speed-up of up to 34x.

In order to deal with the intrinsic problems derived from using edges extracted from real images, in this thesis we propose a shape descriptor, named OCTAR, that is particularly suitable for partial shape matching of open/closed contours extracted from edgemap images. Based on this descriptor, we also propose a partial shape matching method robust to partial occlusion, noise, rotation and translation. Our approach allows to combine shape and appearance through the evaluation of object detection hypothesis based on its appearance, providing more distinctiveness. The conducted experiments showed competitive results compared to the state of the art, in both binary and gray scale images.

Further, we introduce three properties and their corresponding quantitative evaluation measures to assess the ability of a visual word to represent and discriminate an object class, in the context of the BoW approach. Based on these properties, we propose a methodology for reducing the size of the visual vocabulary, retaining those visual words that best describe an object class. Reducing the vocabulary will provide a more reliable and compact image representation. This representation is used by the OCTAR method to evaluate the appearance of object detection hypotheses. Experiments were performed using different size vocabularies, different appearance descriptors, different weighting schemas, and different classifiers, which showed that using our reduced vocabulary improves the classification performance with a significant reduction of the image representation size.

Resumen

El reconocimiento de objetos en imágenes es uno de los problemas más antiguos en el campo de la visión por computadoras. En esta tesis, con el objetivo de lograr mejores resultados en la categorización de objetos, se utilizan características de forma como una representación más genérica de los objetos que la brindada por las características de apariencia, las que son usadas como características de segundo nivel.

En esta tesis se propone un método, denominado LISF, para la extracción, descripción y comparación de características de forma para imágenes binarias. LISF extrae y describe la forma de manera local pero halla correspondencias usando información global con el fin de obtener un balance entre el poder discriminativo y la robustez al ruido y oclusión parcial en el contorno. Los experimentos realizados muestran que para mayores niveles de oclusión en la forma, mejores son los resultados de LISF con respecto a otros métodos del estado del arte, con mejorías del 20% en la medida *bull's eye* y del 25% de exactitud en la clasificación para una oclusión del 60%. También, se propone una implementación masivamente paralela en GPU de LISF, que alcanza una aceleración de hasta 34x.

Para poder lidiar con los problemas intrínsecos del uso de la información de forma obtenida a partir de bordes extraídos de imágenes reales, como parte de este trabajo se propone un descriptor de forma, al que denominamos OCTAR, particularmente diseñado para hallar correspondencias parciales entre contornos abiertos o cerrados extraídos de imágenes de mapas de bordes. Basados en este descriptor, se propuso además un método de comparación parcial de formas, que es robusto a la oclusión parcial, ruido, rotación y traslación. Este método permite combinar la forma con la apariencia a partir de la evaluación de hipótesis de objetos basados en la información de apariencia, brindando mayor poder discriminativo. Los experimentos realizados muestran su efectividad tanto en imágenes binarias como en imágenes reales.

Por último, se proponen tres propiedades y sus correspondientes medidas de evaluación cualitativas para expresar la habilidad de una palabra visual de representar y discriminar una categoría de objetos, dentro del enfoque de bolsas de palabras visuales. Basado en estas propiedades, se propone una metodología para reducir el tamaño de los vocabularios visuales, obteniendo vocabularios más compactos pero que a su vez mejor describen y discriminan a las categorías de objetos. Esta representación es usada para evaluar la apariencia en el método OCTAR. Los experimentos, que se realizaron usando diferentes tamaños de vocabularios, varios descriptores de apariencia, diferentes esquemas de pesado y diferentes clasificadores, mostraron que usando nuestros vocabularios reducidos se obtenían mejores resultados en la categorización que usando los vocabularios completos, con una significativa reducción en el tamaño de la representación de las imágenes.

Contents

1 Introduction 1

1.1 Problem Description 4

1.2 Objectives 6

1.3 Contributions 7

1.4 Thesis Structure 8

2 Related Work 10

2.1 Object Recognition Evolution 10

2.2 Shape-based Category-level Object Recognition 13

2.3 Appearance-based Category-level Object Recognition 14

2.4 Shape Feature Descriptors 16

2.5 Triangle Area-based Shape Feature Descriptors 18

2.6 Building More Discriminative and Representative Visual Vocabularies . . . 20

2.7 Summary 22

3 The Invariant Local Shape Features Method 23

3.1 Proposed Local Shape Feature Descriptor 24

3.1.1 Feature Extraction 24

3.1.2 Feature Description 26

3.1.3 Robustness and Invariability Considerations 26

3.2 Proposed Feature Matching 28

3.2.1 Finding Candidate Matches 28

3.2.2 Rejecting Casual Matches 30

3.3 Efficient LISF Feature Extraction and Matching 32

3.3.1 Implementation of Feature Extraction using CUDA 32

3.3.2 Implementation of Feature Matching using CUDA 33

3.4 Experimental Results 35

3.4.1 Shape Retrieval and Classification Experiments 35

3.4.2 Efficiency Evaluation 39

3.5 Summary 41

4 The Open/Closed Contours Triangle Area Representation Method 42

4.1 Proposed Shape Descriptor 44

4.2 Proposed Partial Shape Matching Method 46

4.3 Object Hypotheses Formation and Evaluation 48

4.3.1 Covering Criterion 50

4.3.2 Object Hypothesis Contour Estimation Criterion 50

4.3.3 Fitted Object Hypothesis Criterion 51

4.3.4 Appearance-based Evaluation Criterion 52

4.4 Experimental Results 53

4.4.1 Performance Evaluation on Real Scenes 53

4.4.2 Performance Evaluation on Occluded Shapes 56

4.5 Summary 58

5 Improving Visual Vocabularies 59

5.1 Proposed Method 61

5.1.1 Inter-class Representativeness Measure 62

5.1.2 Intra-class Representativeness Measure 62

5.1.3 Inter-class Distinctiveness Measure 65

5.1.4 On Ranking and Reducing the Size of Visual Vocabularies 66

5.2 Experimental Evaluation 67

5.2.1 Assessing the Validity in a Classic BoW-based Classification Task . 68

5.2.2 Comparison with Other Kinds of Feature Selection Algorithms . . . 76

5.2.3 Computation Time of the Visual Vocabulary Ranking 78
5.3 Summary 78

6 Conclusions 79

6.1 Summary and Conclusions 79
6.2 Main Contributions 80
6.3 Future Work 81
6.4 Publications 82

References 84

A The Mann-Whitney Test 99

B Acronyms 101

C Notations 103

List of Figures

1.1 Object recognition. 2

2.1 Evolution of object recognition. 11

3.1 Detection of contour fragments in LISF method. 25

3.2 LISF contour fragment descriptor. 27

3.3 LISF contour fragment scale and orientation. 29

3.4 Casual matches rejection stage of the LISF method. 31

3.5 Matches between local shape descriptors in two images using LISF method. 32

3.6 Overview of the proposed LISF feature comparison method in GPU. 34

3.7 Example images and categories from the Shapes99, Shapes216 and the MPEG-7 datasets. 35

3.8 Example images from the MPEG-7 dataset with different levels of occlusion used in the experiments. 36

3.9 Bull's eye score comparison between LISF, shape context, Zernike moments and Legendre moments. 37

3.10 Top 5 retrieved images by LISF and its similarity score. 38

3.11 Classification accuracy comparison between LISF, shape context, Zernike moments and Legendre moments. 39

3.12 Computation time and achieved speed-up by the proposed massively parallel implementation of LISF in CUDA. 40

4.1 Problems derived from using edgemaps extracted from real images. 43

4.2 The OCTAR descriptor computation. 45

4.3 The OCTAR descriptor self-containing property. 46

4.4 The OCTAR partial shape matching process. 48

4.5 OCTAR spatial relation constraints graph. 49

4.6 Extended OCTAR descriptor for contours spatial configuration. 49

4.7 Example images from the ETHZ Shape Classes dataset. 53

4.8 Example edgemap images from the ETHZ Shape Classes dataset. 54

4.9 Example image from the Shapes216 dataset with different levels of occlusion. 56

4.10 Bull's eye score comparison between OCTAR, shape context and IDSC. . . 57

5.1 BoW approach overview. 60

5.2 Examples of $\mathcal{M}_1$ measure values. 63

5.3 Examples of $\mathcal{M}_2$ measure values. 64

5.4 Example of $\mathcal{M}_3$ measure for two visual words. 66

5.5 Mean classification accuracy results for SVM cross-validation on the Caltech-101 dataset. 71

5.6 Mean classification accuracy results for KNN cross-validation on the Caltech-101 dataset. 72

5.7 Mean classification accuracy results for SVM cross-validation on the Pascal VOC 2006 dataset. 73

5.8 Mean classification accuracy results for KNN cross-validation on the Pascal VOC 2006 dataset. 74

5.9 Comparison of classification accuracy results with the state of the art. . . . 77

List of Tables

3.1 Average feature extraction and matching time for two images of the MPEG7 database, in seconds. 39

4.1 Comparison of interpolated average precision (AP) on the ETHZ Shape Classes dataset. 55

4.2 Comparison of classification accuracy on the ETHZ Shape Classes dataset. 55

4.3 OCTAR average feature extraction and matching time comparison. 57

5.1 Summarized classification accuracy results for the Caltech-101 dataset. . . 75

5.2 Summarized classification accuracy results for the Pascal VOC 2006 dataset. 75

5.3 Computation time of visual vocabulary ranking compared to vocabulary building. 75

Chapter 1

Introduction

Object recognition is one of the oldest problems in the field of Computer Vision. However, it still remains an open problem. Object recognition can be divided into two distinct groups:

- **Specific object recognition:** Let us assume the problem of finding John's car in an image. In this case, the object we are looking for is a car, but the key here is that we are not looking for any car, we are looking for an object that has unique and distinctive features, in this case John's car. (See Figure 1.1 (a))

- **Category-level object recognition:** This is a more general problem. Following the same example, the problem here is to detect every car in the image, see Figure 1.1 (b). In this case, we would have to use training data to create a model of a car able to generalize the class of cars. Then, with this model, detect all objects and classify them as a car or not. Hence, it follows that the class of objects we want to recognize can be as specific (*e.g.*, Toyota cars) or as general (*e.g.*, every ground transportation) as needed. Taking this into account, the case of specific object recognition could be seen as the more specific case of category-level object recognition.

In the present doctoral research, we focus on the problem of category-level object recognition (also referred to as object categorization, object class recognition, generic object recognition and classification of objects). More formally, it can be defined as:

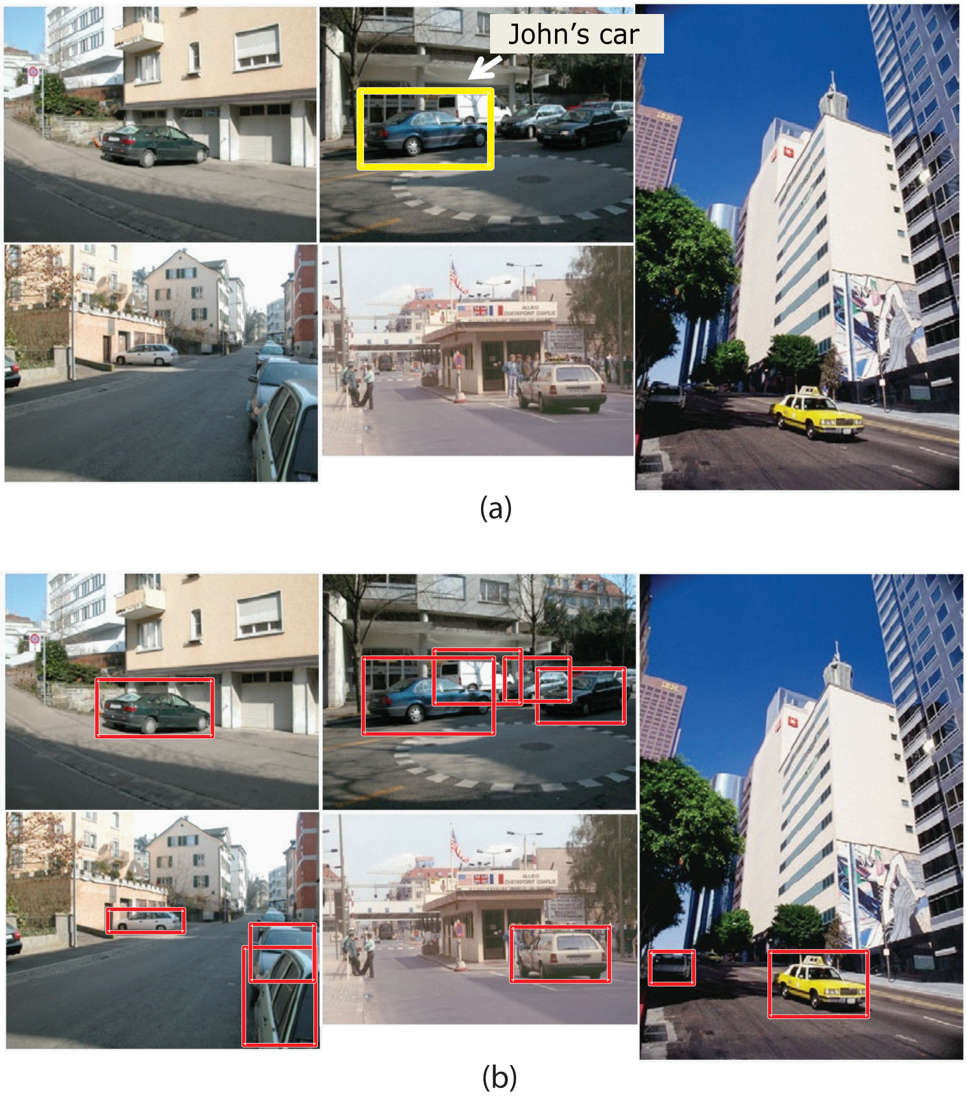

Figure 1.1: Object recognition could be seen under two different groups: (a) specific object recognition and (b) category-level object recognition.

given a number of training images from a category or a class of objects, recognize unseen instances of that category and assign the appropriate label to them.

In recent years, the field of specific object recognition has made significant progress with the emergence of local appearance-based features (*e.g.*, SIFT (Lowe, 2004), SURF (Bay *et al.*, 2008), ORB (Rublee *et al.*, 2011), Harris-Affine (Mikolajczyk and Schmid, 2002)(Mikolajczyk, 2004), Hessian-Affine (Mikolajczyk and Schmid, 2002)(Mikolajczyk, 2004), MSER (Matas, 2004)). Local appearance-based features have proven to be very effective in finding distinctive features between different views of the same object in the presence of variations in viewpoint, illumination, scale, rotation, partial occlusion, translation and affine transformations. The traditional idea of these methods is to first identify representative structures or points in the image and then to obtain a distinctive description from their neighborhood (Tuytelaars and Mikolajczyk, 2007).

Motivated by the good results obtained by the local appearance-based features in the specific object recognition field, in the last years we have seen a large interest in applying these techniques to the problem of object classification (*e.g.*, (Qin and Yung, 2012; Jégou *et al.*, 2011; Zhang *et al.*, 2007; Lazebnik *et al.*, 2006)) in order to take advantage of the aforementioned virtues of local appearance-based features. One of the most popular and effective approaches is the Bag of Visual Words (BoW) representation (Csurka *et al.*, 2004). Usually the visual vocabulary is obtained through the clustering of local features extracted, being K-Means (Hartigan and Wong, 1979) the most used algorithm for this purpose.

Since local features were designed to recognize specific objects, it is suspected that these techniques are not intended to completely succeed in object class recognition tasks. The extracted features are little generic to a category (in fact, it is highly unlikely that images of two different object instances within the same object class share some feature). The causes of this phenomenon can be that these methods are based on appearance and it is believed that the appearance is more related to the identification of specific objects, while shape features are more related to the classification of objects (Dickinson, 2009; Kimia, 2009; Biederman and Ju, 1988). There are even certain classes of objects where methods based on appearance features largely fail (Stark and Schiele, 2007) and the best choice are features based on shape, mainly in man-made object classes which lack of texture or have a largely variable texture (*e.g.*, bottles, cups, tools, etc.). However, there are other classes where the role of appearance is essential to differentiate classes of objects (*e.g.*, horses from zebras, leopards from panthers, etc.).

In Section 2.2 and 2.3, the main advantages and limitations of the appearance-based and shape-based approaches for object categorization are stated. As it can be seen, many of the limitations of one of theses approaches are complemented by the other advantages.

In this doctoral research, we propose to combine appearance and shape features by taking advantage of each of these representations in the classification of objects. With the combination of both kind of features we expect better classification results than when using these features separately.

On the other hand, historically, the researchers in this area have been more focused on obtaining accurate methods leaving aside efficiency. However, the latter has become an increasingly important issue, mainly motivated by the need to recognize object classes in real-time applications or other applications where execution time is a critical resource.

An example of this would be the representation of visual information according to the MPEG-7 standard (Martínez, 2004). The main difference of this standard to its predecessor MPEG-4 is that it includes labelling of multimedia content through metadata, including the category to which each object belongs. Another example could be robotics or video surveillance applications where certain categories of objects have to be found in a scene in real time ($\sim$ 30 fps).

A technology that has proven to be successful in accelerating several computing tasks is the use of GPUs (Graphics Processing Units). GPUs are processors initially designed to perform the calculations involved in the generation of interactive 3D graphics. However, some of their main characteristics (low price in relation to its computing power, high parallelism capabilities, floating point operations optimization) have led the scientific community to extend their use to a wider range of computing tasks, to what has been called General-Purpose Computing on Graphics Processing Units (GPGPU).

In this dissertation, we also propose a massively parallel GPU implementation in CUDA, to ensure an acceleration of the recognition of classes of objects in images that favor their use in applications where time is a critical factor.

1.1 Problem Description

During the historical development of object recognition there has been a trend towards recognizing specific objects, leaving aside the recognition of object classes, so that the greatest achievements and developments have been reached in the first of these. Having now attained great progress in recognizing specific objects (emergence of the appearance-based invariant local features, *e.g.*, SIFT, SURF, ORB, Harris-Affine, Hessian-Affine, MSER), a boom in applying appearance-based local features techniques to the more general problem of object classification has been seen, constituting these schemas the state of the art in the subject.

From the above, it is suspected that appearance-based local features methods can not completely succeed, because these methods from their theoretical conception were designed to recognize specific objects and the features extracted are little generic to a category. Local appearance features are structures on the objects that are present in different views of the same object, but in their theoretical basis there is nothing to indicate that these features are capable of abstracting the appearance of an object class (beyond a specific object), in fact, it is very unlikely that two images of different objects belonging to the same class share a local appearance feature.

What we propose in this thesis, and that has become a trend in recent research, is returning to the use of shape as a more generic representation of objects. Also, by combining shape features with the progress made in the description of the appearance, we expect to be able to achieve better results in object categorization. Throughout the evolution of object recognition, shape features have shown greater ability to represent object categories than appearance features. Furthermore, studies on how humans identify object categories have shown that humans rely primarily on shape features, leaving appearance features as a second-level features (Biederman and Ju, 1988). On the other hand, recent studies on the use of appearance have shown its importance in object categorization, specifically in object classes with similar shape (*e.g.*, cougar vs. panther, zebra vs. horse, etc.), hence the need to combine together shape and appearance.

When using shape information extracted from real images, *e.g.*, edgemaps obtained using Canny or any other edge extraction technique, we have to deal with several problems imposed by using edgemaps. In edges extracted from real images, edge fragments representing part of the object can be missing, contours could be broken into several fragments, and part of the true contour of the object of interest can be incorrectly connected to edge fragments belonging to the background or another object, resulting in a single edge fragment. Dealing with the three aforementioned problems implies that the shape descriptor should be able to represent both open and closed contours, and that part of the contour fragments should match with one or more parts of the shape model, which makes the shape matching problem more difficult than that for closed shapes. Other considerations are the robustness with respect to the image scale, rotation and translation.

The Bag of Visual Words approach is one of the most widely used approaches for representing objects based on their appearance. One of the main limitations of the BoW approach is that the visual vocabulary is built using features that belong to both the object and the background, including the noise extracted from the image background as part of the object class description. Also, every visual word is used, regardless of its low representativeness or discriminative power. Additionally, for some applications the obtained vocabulary is of considerable size ($> 100K$ visual words), so the size of the object representation makes the classifiers computationally expensive. These limitations could be addressed by only using the more discriminative and representative visual words in the vocabulary, which will also lead to a more compact image representation.

Another problem, which has been identified as one of the major drawbacks of existing systems so far, is their high computational cost. This is an issue that has not received much attention, perhaps because the research community in this area is more focused on accuracy than on efficiency. But computational efficiency is increasingly taking a significant role in object recognition systems, specially in those solving applied problems where it is necessary to perform the recognition in real time, using high-resolution images, on large volumes of data or in any application where time is a critical issue. Examples of these applications are the representation of visual information according to the MPEG-

7 standard, applications of robotics where the detection of certain object categories is needed, or video surveillance applications where certain objects must be found to launch an alarm.

1.2 Objectives

The **general objective** of this doctoral research is to develop a method for category-level object recognition in images, based on local shape and appearance features, competitive against state-of-the-art methods in terms of accuracy, and at the same time more robust to occlusions.

Our **specific objectives** are:

1. To propose an invariant shape features extraction, description and matching method for binary images robust to partial occlusions.

2. To propose a shape descriptor able to deal with the intrinsic problems derived from using edges extracted from real images.

3. To propose a shape matching method able to deal with the intrinsic problems derived from using edges extracted from real images and that uses the above descriptor.

4. To propose a method for obtaining a compact, discriminative and representative appearance BoW-based representation.

5. To propose a method for category-level object recognition that equally favors both shape and appearance cues, improving the accuracy of reported results.

6. To develop a massively parallel GPU implementation of the most time consuming parts and exceed by at least 10 times in terms of efficiency the CPU implementation.

1.3 Contributions

The main contribution of this doctoral dissertation is the proposal of a method for category-level object recognition that favors both shape and appearance cues.

We introduce a shape-based object recognition method, named LISF, that is invariant to rotation, translation and scale, and present robustness to partial occlusion. LISF, for highly occluded images largely outperformed other popular shape description methods and retain comparable results for not occluded images. We also propose a massively parallel implementation in CUDA of the two most time-consuming stages of LISF, *i.e.*, the feature extraction and feature matching steps, which achieves speed-ups of up to 32x and 34x, respectively.

Further, we introduce a shape-based object recognition method, named OCTAR, able to deal with the intrinsic problems derived from using edges extracted from real images, *i.e.*, broken and missing edge fragments that represent the target object, edge fragment wrongly connected to another object or background edges, and background cluttering. In this method is where the combination of shape and appearance features is performed. Appearance cues are used as a second-level features. OCTAR, for highly occluded images largely outperformed other popular shape description methods and retained comparable results for not occluded images. Also, outperformed other methods in the state of the art in object detection in real images.

Additionally, we propose three properties and their corresponding quantitative evaluation measures to assess the ability of a visual word to represent and discriminate an object class, in the context of the BoW approach. Also, based on these properties, we proposed a methodology for reducing the size of the visual vocabulary, retaining those visual words that best describe an object class. Using our reduced vocabularies the classification performance is improved with a significant reduction of the image representation size.

1.4 Thesis Structure

The content of this thesis is organized in six chapters. Chapter 2 points some key issues in the evolution of the object recognition field that support our proposal. Also, it presents a critical review of the main approaches in the state of the art of the shape and appearance-based category-level object recognition.

In Chapter 3, we introduce an invariant shape feature extraction, description and matching method for binary images, named LISF. Also, in this chapter, we propose a massively parallel implementation in CUDA of the two most time-consuming stages of LISF, *i.e.*, the feature extraction and feature matching steps. Finally, we present several experiments to show the robustness of the LISF method to partial occlusion in the shape and in order to provide an efficiency evaluation of the proposed GPU parallel implementation.

In Chapter 4, we propose the OCTAR descriptor, a shape descriptor that is particularly suitable for partial shape matching of open/closed contours extracted from edge map images, *e.g.*, using Canny or any other edge extraction method from gray or color images. Based on this descriptor, we also introduce a partial shape matching method robust to partial occlusion and noise in the extracted contour. In OCTAR we combine shape and appearance features, specifically by using appearance as a second level feature. Finally, several experiments to show the advantages of the OCTAR description and matching method in binary and edge images (extracted from color images) are presented.

In Chapter 5, we introduce three properties and their corresponding qualitative evaluation measures to assess the ability of a visual word to represent and discriminate an object class, in the context of the BoW approach. Also, based on these properties, we propose a methodology for reducing the size of the visual vocabulary, retaining those visual words that best describe an object class. Further, we present several experiments in well-known datasets in order to show that using only the most discriminative and representative visual words obtained by our proposed methodology improves the classification performance.

Finally, Chapter 6 concludes the thesis, and presents our future work, contributions and the publications obtained as result of this thesis.

Chapter 2

Related Work

2.1 Object Recognition Evolution

The evolution of object recognition over the past 40 years has followed a very clear path, as illustrated in Figure 2.1. In the 1970's, the main research on object recognition focused on obtaining generic representations of the objects 3D shape. The objects were represented mostly as construction of volumetric parts, *e.g.*, cylinders (Binford, 1971; Agin and Binford, 1976; Brooks, 1983), superquadrics (Ferrie *et al.*, 1993; Solina and Bajcsy, 1990; Pentland, 1986; Terzopoulos and Metaxas, 1991), and geons (Biederman, 1985). The main drawback that these early systems were facing was the representational gap that existed between the low-level features that could be effectively extracted from the image and the abstract nature of the model components. Instead of trying to eliminate this gap by creating more effective mechanisms for abstraction, the trend was to bring the images closer to the model. Therefore, in order to obtain generic representations of the objects 3D shape, it was necessary to eliminate the objects surface textures and other structural details, control the illumination conditions and use more uniform backgrounds. As a result, the obtained systems were not able to recognize objects in images obtained in real conditions. However, several basic principles emerged in that decade, such as the importance of shape, the significance of invariance to viewpoint and the importance of 3D representations, among others.

In the 1980's, the main trend was to obtain 3D models that represent the exact shape of

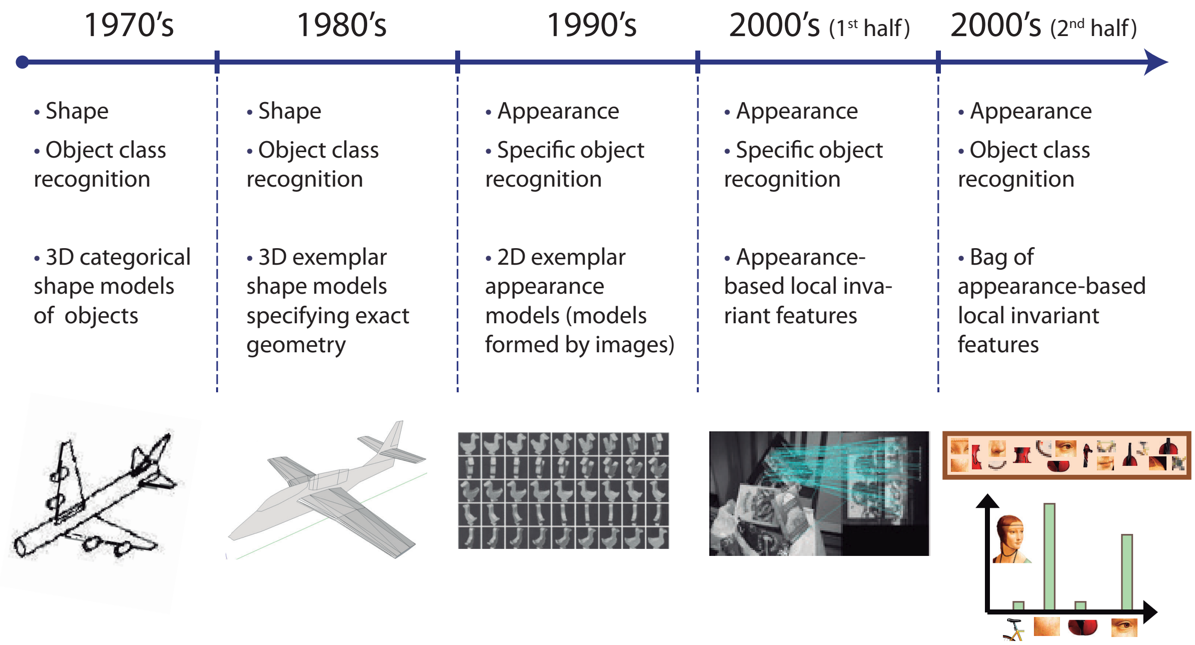
1970's
1980's
1990's
2000's (1st half)
2000's (2nd half)
• Shape
• Object class recognition
• 3D categorical shape models of objects
• Shape
• Object class recognition
• 3D exemplar shape models specifying exact geometry
• Appearance
• Specific object recognition
• 2D exemplar appearance models (models formed by images)
• Appearance
• Specific object recognition
• Appearance-based local invariant features
• Appearance
• Object class recognition
• Bag of appearance-based local invariant features

Figure 2.1: Evolution of object recognition.

objects (*e.g.*, (Grimson and Lozano-Perez, 1984; Silberberg *et al.*, 1986; Huttenlocher and Ullman, 1990)). These models, inspired by the CAD (Computer Aided Design) models, were 3D templates. Since these models could be obtained for real objects (although at a high cost), it was possible to build systems capable of recognizing real objects (still several restrictions). As the models were three-dimensional, these methods remained view point invariant. On this occasion, to eliminate the representational gap, the model was moved toward the object in the image, requiring the model to capture the exact geometry of the object. Since the presence of texture severely affected the complexity of these methods, the objects were not textured. Therefore, these systems were not able to recognize complex objects with complex textures. Moreover, the cost of obtaining the precise 3D models, either automatically or manually, was significant.

Since in the two generations above mentioned, a one-to-one correspondence was assumed between the image features and the model features, a turn and redefinition of the problem from object classes recognition to specific object recognition was evidenced.

In the early 1990's several factors led to a paradigm shift within the object recognition community. 3D shape models were made aside in order to introduce the appearance-based object recognition. For the first time, it was possible to recognize complex objects with complex textures (*e.g.*, (Kirby and Sirovich, 1990; Turk and Pentland, 1991; Murase and Nayar, 1995)). This time the representational gap was eliminated by bringing the model closer to the images, obtaining models that were images. Therefore, these methods could only recognize specific objects, *i.e.*, objects that have been present in training. These approaches had several limitations, mainly related with dealing with occlusion, non-uniform illumination, translation, rotation and scale changes. Several of these limitations were resolved, but the models remained global and failed to achieve invariance to occlusion, and scale and viewpoint changes.

To solve the aforementioned problems, in the early 2000's, researchers in the field took a turn from the global representations to local representations, and to the use of structured representations that were invariant to changes in illumination, rotation, scale, translation and viewpoint (*e.g.*, (Lowe, 1999, 2004; Weber *et al.*, 2000; Agarwal *et al.*, 2004)). Local invariant appearance features are local patterns that differ from its immediate neighborhood. Usually related to variations in one or several image properties, *e.g.*, color, texture and intensity. Typically, these local features are described from its surrounding, transforming its neighborhood into a descriptor, in order to provide distinctiveness. In this case, the models were also formulated closer to the images, but unlike the previous three decades, the representational gap has not been completely eliminated. In this decade, the idea of local features has evolved from one pixel to a scale invariant patch or structure. Moreover, this patch may contain not only the pixel values but a small abstraction of it, *e.g.*, the histogram of gradients of SIFT descriptor (Lowe, 2004).

Thanks to the achievements obtained in the recognition of specific objects with the emergence of local appearance features, in the second half of the 2000's, researchers began to use these features in the more general problem of object class recognition. Although the obtained results, in certain extent are satisfactory, it is believed that the methods based only on appearance features are not intended to fully resolve the problem of categorization. It is believed that appearance features are more related to the specific object recognition problem and so shape features with object categorization (Dickinson, 2009; Kimia, 2009; Biederman and Ju, 1988), as evidenced throughout the evolution of this field when a turn towards using appearance features, inevitably turned to the recognition of specific objects.

2.2 Shape-based Category-level Object Recognition

Since the beginning of research in the field of object recognition, shape features have been widely used. The primary motivation was given that shape is the most natural characteristic that humans use in the process of object categories recognition.

According to (Zhang, 2004), shape recognition methods can be classified in contour-based methods and region-based methods. This classification is based on whether the features are extracted only from the outline of the shape (*e.g.*, (Belongie *et al.*, 2001; Van Otterloo, 1991; Kliot and Rivlin, 1998; Asada and Brady, 1986; Chang *et al.*, 2014b,a)) or are extracted from the entire region of the shape (*e.g.*, (Blum, 1967; Hu, 1962; Kim and Kim, 2000; Zhang and Lu, 2002a)), respectively. In addition, the latest are divided into global approaches and structural approaches. This sub-classification is based on whether the shape is represented holistically or represented by segments or sections. The aforementioned classification is the most general and most widely used, however, according to (Zhang, 2004), it can also be classified into groups based on spatial domain and transformation domain methods.

The vast majority of the shape-based object recognition methods assumed that objects could be accurately segmented from the image. Since the first researches on this area, this assumption was justified by the extensive research in the field of image segmentation that was taking place simultaneously. Today, it is a generalized criterion that the problem of image segmentation, by itself, still remains as an open problem. The main limitation and the fundamental reason of why they have not succeeded in real applications lies in its dependence on an effective segmentation. However, the advances in the area have identified several key elements in shape representation and have recognized the main challenges in this area such as dealing with the problems of occlusion, noise, articulation and affine transformations, among others.

The following summarizes the main advantages and limitations we have identified in the shape-based methods.

Advantages:

- Shape has proven to be effective in describing object categories as a more generic feature than appearance.
- Within this group there are several global descriptors that are compact and easy to compute, and that combined could achieve good results in practice. However, restricted to applications where there are few variations between the different views of the objects. Global region methods compared to contour-based methods, introduce an improvement in this respect, although not sufficient.

Limitations:

- The main and major drawback of these methods is that they assume that the object is separated from the background (effective segmentation).
- In real applications it is always necessary to find the right balance between accuracy and efficiency since the simplest methods are not robust to variations and noise; and the more robust methods are very complex and have a high computational cost.
- The main drawback of structural approaches is the process of generating the sections or segments, as their number and characteristics required for each shape is unknown. Therefore, the success of structural methods depends on the a priori knowledge about the objects in the database. This element leads to its impractical use in general applications.
- Another shortcoming of structural approaches is their high computational complexity, specifically in the matching stage. In such methods the computational cost becomes more noticeable because in order to support partial correspondences between shapes, finding correspondences between sub-graphs is inevitable.

2.3 Appearance-based Category-level Object Recognition

As mentioned in Section 2.1, in the last decade the trend has been to use local appearance features; thanks to the emergence of methods able to find local structures that will be present in different views of the image. Moreover, having a description of these structures largely invariant to translation, rotation, scale, affined deformations, illumination and viewpoint changes in the image. Examples of local appearance features methods are SIFT (Lowe, 2004), SURF (Bay *et al.*, 2008), Harris-Affine (Mikolajczyk and Schmid, 2002; Mikolajczyk, 2004), Hessian-Affine (Mikolajczyk and Schmid, 2002; Mikolajczyk, 2004), MSER (Matas, 2004) and ORB (Rublee *et al.*, 2011).

One of the predominant and more popular approaches on using local appearance feature in the category-level object recognition task is the use of Bags of Visual Words (BoW) representation (Csurka *et al.*, 2004). The general idea is to discretize the entire space of features extracted from the images in the training set, aiming to group features that are visually similar. Therefore, clustering on the feature descriptor space is performed, and the centroid of each cluster constitutes a visual word. Later, for an unseen image, one of these visual words is assigned for each feature extracted from the image, and the image is represented as a histogram of visual word occurrences. Then, several machine learning and pattern recognition techniques can be used to determine the category of the object from its BoW-based representation. Examples of these kind of approaches are (Dork and Schmid, 2005; Mikolajczyk *et al.*, 2005; Zhang *et al.*, 2007; Chang *et al.*, 2010, 2012).

In addition, other studies have tried to learn the spatial relationships between features, visual words are related using various connectivity structures (a description of several of these methods is provided in (Carneiro and Lowe, 2006)). The main structures that have been used are constellation (Fei-fei *et al.*, 2003; Fergus *et al.*, 2003), star (Leibe *et al.*, 2004, 2007), tree (Felzenszwalb and Huttenlocher, 2005), hierarchy (Bouchard and Triggs, 2005) and sparse flexible model (Carneiro and Lowe, 2006).

The main advantages and limitations we have identified in the appearance-based methods are:

Advantages:

- The main advantages of these methods are their flexibility to different geometries, deformations and viewpoints.
- A compact description of the image content is provided.
- A vector representation is provided which allows the use of several machine learning and artificial intelligence algorithms based on this kind of representation.
- They have achieved good recognition results in real scene images.

Limitations:

- Low description power of several object categories, specifically those categories of untextured objects (*e.g.*, man made objects, bottles, cups, tools, etc.).
- The basic BoW-based representations ignore the object geometry and the spatial relationships between visual words.
- In the Bag of Words are mixed features that belong to both the object and the background.
- The optimal method to build the visual vocabulary is unclear (clustering algorithm used, number of clusters, level of cohesion within each visual word, etc.). Generally, K-means is used to obtain a single vocabulary of size K, determined empirically.
- These methods are based on appearance features, which is believed are more related with the identification of specific objects, without taking into account shape information.

2.4 Shape Feature Descriptors

Some recent works, where shape descriptors are extracted using all the pixel information within a shape region, include Zernike moments (Kim and Kim, 2000), Legendre moments (Chong *et al.*, 2004), and generic Fourier descriptor (Zhang and Lu, 2002b). The main limitation of region-based approaches resides in that only global shape characteristics are captured, without taking into account important shape details. Hence, the discriminative power of these approaches is limited in applications with large intra-class variations or with databases of considerable size.

Curvature Scale Space (CSS) (Mokhtarian and Bober, 2003), Multi-scale Convexity Concavity (MCC) (Adamek and O'Connor, 2004) and multi-scale Fourier-based descriptor (Direkoglu and Nixon, 2011) are shape descriptors defined in a multi-scale space. In CSS and MCC, by changing the sizes of Gaussian kernels in contour convolution, several shape approximations of the shape contour at different scales are obtained. CSS uses the number of zero-crossing points at these different scale levels. In MCC, a curvature measure based on the relative displacement of a contour point between every two consecutive scale levels is proposed. The multi-scale Fourier-based descriptor uses a low-pass Gaussian filter and a high-pass Gaussian filter, separately, at different scales. The main drawback of multi-scale space approaches is that determining the optimal parameter of each scale is a very difficult and application dependent task.

Geometric relationships between sampled contour points have been exploited effectively for shape description. Shape context (SC) (Belongie *et al.*, 2002) finds the vectors of every sample point to all the other boundary points. The length and orientation of the vectors are quantized to create a histogram map which is used to represent each point. To make the histogram more sensitive to nearby points than to points farther away, these vectors are put into log-polar space. The triangle-area representation (TAR) (Alajlan *et al.*, 2007) signature is computed from the area of the triangles formed by the points on the shape boundary. TAR measures the convexity or concavity of each sample contour point using the signed areas of triangles formed by contour points at different scales. In these approaches, the contour of each object is represented by a fixed number of sample points and when comparing two shapes, both contours must be represented by the same fixed number of points. Hence, how these approaches work under occluded or uncompleted contours is not well-defined. Also, most of these kinds of approaches can only deal with closed contours and/or assume a one-to-one correspondence in the matching step.

In addition to shape representations, in order to improve the performance of shape matching, researchers have also proposed alternative matching methods designed to get the most out of their shape representations. In (McNeill and Vijayakumar, 2006), the authors proposed a hierarchical segment-based matching method that proceeds in a global to local direction. The locally constrained diffusion process proposed in (Yang *et al.*, 2009) uses a diffusion process to propagate the beneficial influence that offer other shapes in the similarity measure of each pair of shapes. Authors in (Bai *et al.*, 2010) replace the original distances between two shapes with distances induced by geodesic paths in the shape manifold.

Shape descriptors which only use global or local information will probably fail in presence of transformations and perturbations of shape contour. Local descriptors are accurate to represent local shape features, however, are very sensitive to noise. On the other hand, global descriptors are robust to local deformations, but can not capture the local details of the shape contour. In order to balance discriminative power and robustness, in this work we use local features (contour fragments) for shape representation; later, in the matching step, in a global manner, the structure and spatial relationships between the extracted local features are taken into account to compute shapes similarity. To improve matching performance, specific characteristics such as scale and orientation of the extracted features are used. The extraction, description and matching processes are invariant to rotation, translation and scale changes. In addition, there is not restriction about only dealing with closed contours or silhouettes, *i.e.*, the method also extracts features from open contours.

The shape representation method used in our proposed LISF method to describe the extracted contour fragments is similar to that of shape context (Belongie *et al.*, 2002).

Besides locality, the main difference between these descriptors is that in (Belongie *et al.*, 2002) the authors obtain a histogram for each point in the contour, while we only use one histogram for each contour fragment, *i.e.*, our representation is more compact. Unlike our proposed method, shape context assumes a one-to-one correspondence between points in the matching step, which makes it more sensitive to occlusion.

2.5 Triangle Area-based Shape Feature Descriptors

Several methods have used the area of triangles formed by contour points as the basis for shape representations. In (Roh and Kweon, 1998), authors proposed the use of shape features based on triangle area using five equally spaced contour points $p_1(t), p_2(t), p_3(t), p_4(t)$ and $p_5(t)$ from a closed boundary of N points. For each selection $t = \{1, 2, ..., N\}$ they defined the shape invariant as indicated in Formula 2.1.

$$I(t) = \frac{A(p_5(t)p_1(t)p_4(t)) \cdot A(p_5(t)p_2(t)p_3(t))}{A(p_5(t)p_1(t)p_3(t)) \cdot A(p_5(t)p_2(t)p_4(t))}, \tag{2.1}$$

where $A(p_a(t)p_b(t)p_c(t))$ is the area of the triangle formed by points $p_a(t)$, $p_b(t)$ and $p_c(t)$. Finally, the shape signature of a boundary is obtained by plotting the value $I(t)$ versus t for the different values of $t = \{1, 2, 3, ..., N\}$.

Rube *et al.* (2005) proposed a method named Multi-scale Triangle-Area Representation (MTAR). This representation uses the area of the triangles formed by each three consecutive and equally spaced points on a closed boundary. A MTAR image is obtained by thresholding the area function at zero and taking the locations of the negative values. To reduce noise effect, they apply a Dynamic Wavelet Transform to each contour sequence at various scale levels. At each wavelet scale level a TAR image is computed. In order to match two MTAR image sets of two shapes, several global features are used to discard very dissimilar shapes. Then, a similarity measure D_s between each two MTAR images at certain scale is computed. D_s is based on finding a number of initial correspondences between two sets of maxima in the MTAR images using only two maxima in each image. After that, the lowest cost node is extended to include all other maxima and its cost is considered as D_s.

More recently, the triangle-area representation signature (TAR) proposed by (Alajlan *et al.*, 2007) have shown very good results in shape retrieval. TAR is computed from the area of the triangles formed by the points on the shape boundary at different scales. For the matching, the optimal correspondence between the points of two shapes is searched using a Dynamic Space Warping algorithm. Based on the established correspondence, a distance is derived, and global features are incorporated in the distance to increase the discrimination ability and to facilitate the indexing in large shape databases.

The aforementioned approaches can only deal with shapes of closed boundary. Also, the contour of each object is represented by a fixed number of sample points and no partial matches of the shape are allowed, hence, how these approaches work under occluded, noisy or uncompleted contours is not well-defined. In this thesis, in Chapter 4, we propose a self-containing, triangle area-based shape descriptor able to represent both open and closed contours. We also propose a partial matching method that takes advantage of the properties of the proposed descriptor to provide robustness to partial occlusion and noise in the contour.

2.6 Building More Discriminative and Representative Visual Vocabularies

Several methods have been proposed in the literature to overcome the limitations of the BoW approach (Tsai, 2012). These include part generative models and frameworks that use geometric correspondence (Zhang *et al.*, 2011b; Lu and Ip, 2009), works that deal with the quantization artifacts introduced while assigning features to visual words (Jégou *et al.*, 2011; Fernando *et al.*, 2012), techniques that explore different features and descriptors (Qin and Yung, 2012; Gehler and Nowozin, 2009), among many others. In this section, we briefly review some recent methods aimed to build more discriminative and representative visual vocabularies, which are more related to our work.

Kesorn and Poslad (2012) presented a framework to improve the quality of visual words by constructing visual words from representative keypoints. Also, domain specific non-informative visual words are detected using two main characteristics for non-informative visual words: high document frequency and a small statistical association with all the concepts in the collection. In addition, the vector space model of visual words is restructured with respect to a structural ontology model in order to solve visual synonym and polysemy problems.

Zhang *et al.* (2011a) proposed to obtain a visual vocabulary comprised of descriptive visual words and descriptive visual phrases as the visual correspondences to text words and phrases. Authors state that a descriptive visual element can be composed by the visual words and their combinations and that these combinations are effective in representing certain visual objects or scenes. Therefore, they define visual phrases as frequently co-occurring visual word pairs.

Lopez-Sastre *et al.* (2011) presented a method for building a more discriminative visual vocabulary by taking into account the class labels of images. The authors proposed a cluster precision criterion based on class labels in order to obtain class representative visual words through a Reciprocal Nearest Neighbors clustering algorithm. Also, they introduced an adaptive threshold refinement scheme aimed to increase vocabulary compactness.

Liu (2010) builds a visual vocabulary based on a Gaussian Mixed Model (GMM). After K-Means clusters are obtained, GMM is then used to model the distribution of each cluster. Each GMM will be used as a visual word of the visual vocabulary. Also, a soft assignment schema for the bag of words is proposed based on the soft assignment of image features to each GMM visual word.

Liu and Shah (2008) exploit mutual information maximization techniques to learn a compact set of visual words and to determine the size of the codebook. In their proposal two codebook entries are merged if they have comparable distributions. In addition, spatio-temporal pyramid matching is used to exploit temporal information in videos.

The most popular visual descriptors are histograms of image measurements. It has been shown that with histogram features, the Histogram Intersection Kernel (HIK) is more effective than the Euclidean distance in supervised learning tasks. Based on this assumption, Wu *et al.* (2011) proposed a histogram kernel k-means algorithm which uses

HIK in an unsupervised manner to improve the generation of visual codebooks.

In (Chandra *et al.*, 2012), in order to use low level features extracted from images to create higher level features, Chandra *et al.* proposed a hierarchical feature learning framework that uses a Naive Bayes clustering algorithm. First, SIFT features over a dense grid are quantized using K-Means to obtain the first level symbol image. Later, features from the current level are clustered using a Naive Bayes-based clustering and quantized to get the symbol image at the next level. Bag of words representations can be computed using the symbol image at any level of the hierarchy.

Jiu *et al.* (2012), motivated for obtaining a visual vocabulary highly correlated to the recognition problem, proposed a supervised method for joint visual vocabulary creation and class learning, which uses the class labels of the training set to learn the visual words. In order to achieve that, they proposed two different learning algorithms, one based on error backpropagation and the other based on cluster label reassignment.

Zhang *et al.* (2014) proposed a supervised Mutual Information (MI) based feature selection method. This algorithm uses MI between each dimension of the image descriptor and the image class label to compute the dimension importance. Finally, using the highest importance values, they reduce the image representation size. This method achieve higher accuracy and less computational cost than feature compression methods such as product quantization (Jégou *et al.*, 2011) and BPBC (Gong *et al.*, 2013).

In Chapter 5, similarly to (Kesorn and Poslad, 2012; Lopez-Sastre *et al.*, 2011; Jiu *et al.*, 2012), we also use the class labels of images. However, we do not use the class labels to create a new visual vocabulary but for scoring the set of visual words, according to their distinctiveness and representativeness for each class. It is important to emphasize that our proposal does not depend on the algorithm used for building the set of visual words, the descriptor or the weighting scheme used. The previously mentioned characteristics make our approach suitable to any visual vocabulary since it does not build a new visual vocabulary, it rather finds the best visual words of a given visual vocabulary. In fact, our proposal could directly complement all the above discussed methods, by ranking their resulting vocabularies according to the distinctiveness and representativeness of the obtained visual words, although is out of the scope of this thesis to explore it.

2.7 Summary

In this Chapter we presented the most closely related work to our doctoral research. First, some important issues of the evolution of the object recognition field were exposed, in order to show the role of shape and appearance features. The main advantages and limitations of both shape and appearance-based methods for object categorization were also presented. Several relevant shape feature descriptors were discussed in Section 2.4. In Section 2.5 we presented some shape feature descriptors based on the triangle area representation, which are more related with our proposed shape feature descriptor, OCTAR. Finally, we reviewed some recent methods aimed to build more discriminative and representative visual vocabularies, which are related to our proposed methodology for improving the distinctiveness and representativeness of visual vocabularies.

Chapter 3

The Invariant Local Shape Features Method

Shape descriptors have proven to be useful in many image processing and computer vision applications (*e.g.*, object detection (Toshev *et al.*, 2011) (Wang *et al.*, 2012), image retrieval (Shu and Wu, 2011) (Yang *et al.*, 2013), object categorization (Trinh and Kimia, 2011) (Gonzalez-Aguirre *et al.*, 2011), etc.). However, shape representation and description remains as one of the most challenging topics in computer vision. The shape representation problem has proven to be hard because shapes are usually more complex than appearance. Shape representation inherits some of the most important considerations in computer vision such as the robustness with respect to the image scale, rotation, translation, occlusion, noise and viewpoint. A good shape description and matching method should be able to tolerate geometric intra-class variations, but at the same time should be able to discriminate from objects of different classes.

In this work, we describe object shape locally, but global information is used in the matching step to obtain a trade-off between discriminative power and robustness. The proposed approach has been named Invariant Local Shape Features (LISF), as it extracts, describes, and matches local shape features that are invariant to rotation, translation and scale. LISF, besides closed contours, extracts and matches features from open contours, which in conjunction with its local character and its global matching schema, makes it appropriate for matching occluded or incomplete shape contours. Conducted experiments showed that while increasing the occlusion level in the shape contour, the difference in terms of bull's eye score, and accuracy of the classification gets larger in favor of LISF compared to other state-of-the-art methods.

Another important requirement for a promising shape descriptor is computational efficiency. Several applications demand real time processing or handling large image datasets. General-Purpose Computing on Graphics Processing Units (GPGPU) is the utilization of GPUs to perform computation in applications traditionally handled by a CPU, having obtained considerable speed-ups in many computing tasks. In this chapter, we also propose a massively parallel implementation in GPUs of the two most time consuming stages of LISF, namely, the feature extraction and feature matching stages. Our proposed GPU implementation achieves a speed-up of up to 32x and 34x for the feature extraction and matching steps, respectively.

3.1 Proposed Local Shape Feature Descriptor

Psychological studies (Biederman and Ju, 1988) (De Winter and Wagemans, 2004) show that humans are able to recognize objects from fragments of contours and edges. Hence, if the appropriate contour fragments of an object are selected, they should be representative of it.

Straight lines are not very discriminative since they are only defined by their length (which is useless when looking for scale invariance). However, curves provide a richer description of the object as they are defined, in addition to their length, by their curvature. A line can be seen as a specific case of a curve, *i.e.*, a curve with null curvature. Furthermore, in the presence of variations such as changes in scale, rotation, translation, affine transformations, illumination and texture, the curves tend to remain present. In this thesis we use contour fragments as repetitive and discriminant local features.

3.1.1 Feature Extraction

The detection of high curvature contour fragments is based on the method proposed by Chetverikov (Chetverikov, 2003). Chetverikov's method inscribes triangles in a segment of contour points and evaluates the angle of the median vertex which must be smaller than α_{max} and bigger than α_{min}. The sides of the triangle that lie on the median vertex are required to be larger than d_{min} and smaller than d_{max}, as indicated in Formulas 3.1, 3.2 and 3.3.

$$d_{min} \leq ||p \quad - \quad p^{+}|| \leq d_{max}, \tag{3.1}$$

$$d_{min} \leq ||p \quad - \quad p^{-}|| \leq d_{max}, \tag{3.2}$$

$$\alpha_{min} \leq \quad \alpha \quad \leq \alpha_{max}, \tag{3.3}$$

where p, p^{+} and p^{-} are the triangle points and α is the angle of the median vertex, p, of the triangle. d_{min} and d_{max} define the scale limits, and are set empirically in order to avoid detecting contour fragments that are known to be too small or too large. α_{min} and α_{max} are the angle limits that determine the minimum and maximum sharpness accepted as high curvature. In our experiments we set $d_{min} = 10$ pixels, $d_{max} = 300$ pixels, $\alpha_{min} = 5°$, and $\alpha_{max} = 150°$.

Several triangles can be found over the same point or over adjacent points at the same curve, hence it is selected the point with the highest curvature. Each selected contour fragment i is defined by a triangle (p_i^{-}, p_i, p_i^{+}), where p_i is the median vertex and the points p_i^{-} and p_i^{+} define the endpoints of the contour fragment. See Figure 3.1 (a).

The Chetverikov's corners detector has the disadvantage of not being very stable to noisy contours or highly branched contours, which may cause that false corners are selected. For example, see Figure 3.1(b). In order to deal with this problem, another restriction is introduced to the Chetverikov's method. Each candidate triangle (p_k^{-}, p_k, p_k^{+}) will grow while the points p_k^{-} and p_k^{+} do not match any p_j point of another corner. Figure 3.1(c) shows how this restriction overcome the false detection in the example in Figure 3.1(b).

Then, each feature ς_i extracted from the contour is defined by $\langle P_i, T_i \rangle$, where $T_i = (p_i^{-}, p_i, p_i^{+})$ is the triangle inscribed in the contour fragment and $P_i = \{p_1, ..., p_n\}, p_j \in \mathbb{R}^2$ is the set of n points which form the contour fragment ς_i, ordered so that the point p_j is adjacent to the point p_{j-1} and p_{j+1}. Points $p_1, p_n \in P_i$ match with points $p_i^{-}, p_i^{+} \in T_i$,

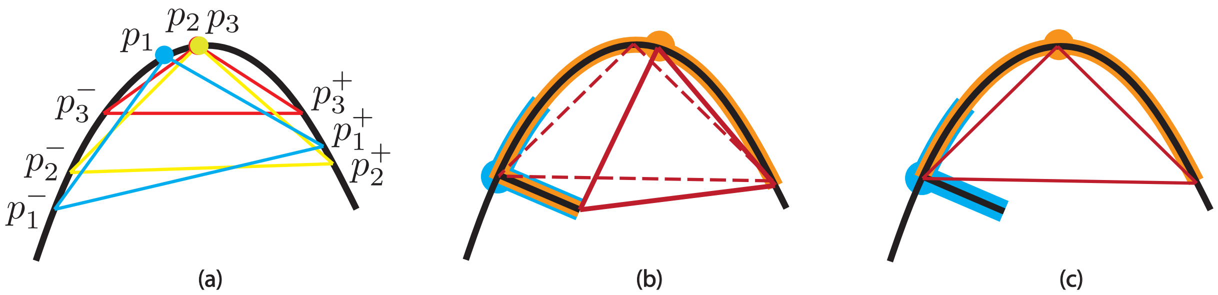

Figure 3.1: (*best seen in color*). Detection of contour fragments. (a) Those contour fragments where it is possible to inscribe a triangle with aperture between α_{min} and α_{max}, and adjacent sides with lengths between d_{min} and d_{max} are considered as candidate contour fragments. If several triangles are found on the same point or near points, the sharpest triangle in a neighborhood is selected. (b) Noise can introduce false contour fragments (the contour fragment in orange). (c) To counteract the false contour phenomenon we introduce another restriction, candidate triangles will grow until another corner is reached.

respectively.

3.1.2 Feature Description

The definition of contour fragment given by the extraction process (specifically the triangle (p_i^-, p_i, p_i^+)) provides a compact description of the contour fragment as it gives evidence of amplitude, orientation and length; however, it has low distinctiveness due to the fact that different curves can share the same triangle.

In order to give more distinctiveness to the extracted features, we represent each contour fragment in a polar space of origin p_i (see Figure 3.2), where the length r and the orientation θ of each point are discretized to form a two-dimensional histogram, H_i, of $n_r \times n_\theta$ bins, as expressed in Formula 3.4.

$$H_i(b) = |\{w \in P_i : (w - p_i) \in \text{bin}(b)\}| \quad , \tag{3.4}$$

where b is a given bin of the histogram H_i and w is a point in the contour fragment P_i.

Note that for a sufficiently large number of n_r and n_θ this is an exact representation of the contour fragment.

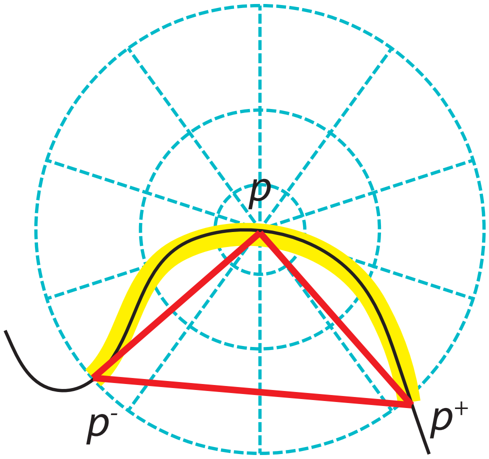

Figure 3.2: (*best seen in color*). LISF contour fragment descriptor. Every point in the contour fragment defined by the triangle (p_i^-, p_i, p_i^+) is represented in a polar space of origin p_i. The length r and the orientation θ of each point in the contour fragment are discretized to form a two-dimensional histogram.

3.1.3 Robustness and Invariability Considerations

In order to have a robust and invariant description method, several properties are met by the proposed description method:

Locality: the locality property is met directly from the definitions of interest contour fragment and its descriptor given in Sections 3.1.1 and 3.1.2. A contour fragment and its descriptor only depend on a point and a set of points in a neighborhood much smaller than the image area, therefore, in both the extraction and description processes, a change or variation in a portion of the contour (produced, for example, by noise, partial occlusion or other deformation of the object), only affects the features extracted in that portion.

Translation invariance: by construction, both the feature extraction and description processes are inherently invariant to translation since they are based on relative coordinates of the points of interest.

Rotation invariance: the contour fragment extraction process is invariant to rotation by construction. An interest contour fragment is defined by a triangle inscribed in a contour segment, which only depends on the shape of the contour segment rather than its orientation. In the description process, it is possible to achieve rotation invariance by rotating each feature coordinate systems until alignment with the bisectrix of the vertex p_i.

Scale invariance: this could be achieved in the extraction process by extracting contour fragments at different values of d_{min} and d_{max}. In the description process it is achieved by sampling contour fragments (*i.e.*, P_i) to a fixed number M of points or by normalizing the histograms.

3.2 Proposed Feature Matching

In this section we describe our proposed method for finding correspondences between LISF features extracted from two images. Let us consider the situation of finding correspondences between N_Q features $\{a_i\}$, with descriptors $\{H_i^a\}$, extracted from the query image and N_C features $\{b_i\}$, with descriptors $\{H_i^b\}$, extracted from the database image.

The simplest criterion to establish a match between two features is to establish a global threshold over the distance between the descriptors, *i.e.*, each feature a_i will match with those features $\{b_j\}$ which are at distance $D(a_i, b_j)$ below a given threshold. Usually, matches are restricted to nearest neighbors in order to limit multiple false positives. Some intrinsic disadvantages of this approach limit its use; such as determining the number of nearest neighbors depends on the specific application and type of features and objects. The mentioned approach obviates the spatial relations between the parts (local features) of objects, which is a determining factor. Also, it fails in the case of objects with multiple occurrences of the structure of interest or objects with repetitive parts (*e.g.*, buildings with several equal windows). In addition, the large variability of distances between the descriptors of different features makes the task of finding an appropriate threshold a very difficult task.

To overcome the previous limitations, we propose an alternative for feature matching that takes into account the structure and spatial organization of the features. The matches between the query features and database features are validated by rejecting casual or wrong matches.

3.2.1 Finding Candidate Matches

Let us first define the scale and orientation of a contour fragment (see Figure 3.3).

Let the feature ς_i be defined by $\langle P_i, T_i \rangle$, its scale s_{ς_i} is defined as the magnitude of the vector $\mathbf{p_i^+} + \mathbf{p_i^-}$, where $\mathbf{p_i^+}$ and $\mathbf{p_i^-}$ are the vectors with initial point in p_i and terminal points in p_i^+ and p_i^- (see Figure), respectively, as expressed in Formula 3.5,

$$s_{\varsigma_i} = |\mathbf{p_i^+} + \mathbf{p_i^-}|. \tag{3.5}$$

The orientation ϕ_{ς_i} of the feature ς_i is given by the direction of vector $\mathbf{p_i}$, which we will call orientation vector of feature ς_i, and it is defined as the vector that is just in the middle of vector $\mathbf{p_i^+}$ and vector $\mathbf{p_i^-}$, as indicated in Formula 3.6,

$$\mathbf{p_i} = \hat{\mathbf{p}}_\mathbf{i}^+ + \hat{\mathbf{p}}_\mathbf{i}^-, \tag{3.6}$$

where $\hat{\mathbf{p}}_\mathbf{i}^+$ and $\hat{\mathbf{p}}_\mathbf{i}^-$ are the unit vectors with same direction and origin that $\mathbf{p_i^+}$ and $\mathbf{p_i^-}$, respectively.

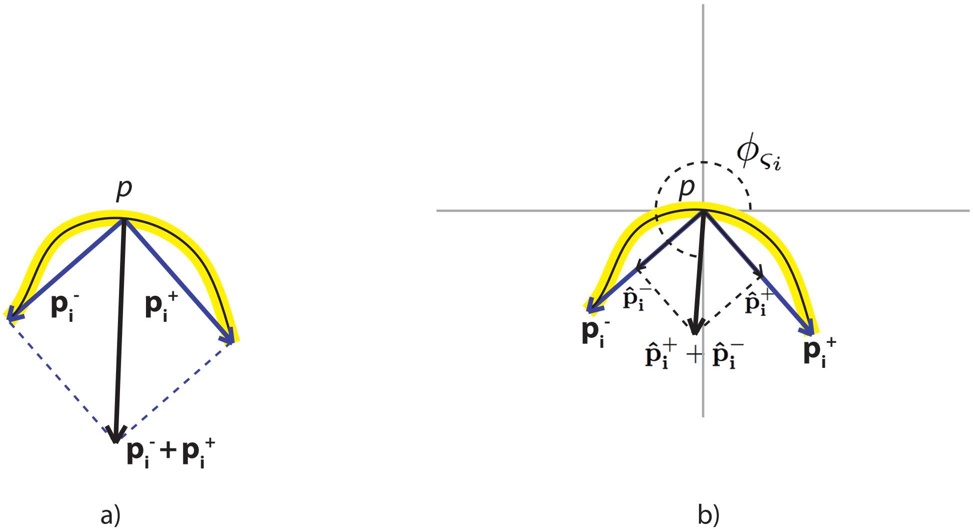
p
$\mathbf{p_i^-}$
$\mathbf{p_i^+}$
$\mathbf{p_i^-+p_i^+}$
a)
ϕ_{ς_i}
p
$\hat{\mathbf{p}}_\mathbf{i}^-$
$\hat{\mathbf{p}}_\mathbf{i}^+$
$\mathbf{p_i^-}$
$\hat{\mathbf{p}}_\mathbf{i}^+ + \hat{\mathbf{p}}_\mathbf{i}^-$
$\mathbf{p_i^+}$
b)

Figure 3.3: (*best seen in color*). LISF contour fragment a) scale and b) orientation.

We already defined the terms scale and orientation of a feature ς_i. In the process of finding candidate matches, for each feature a_i, its K nearest neighbors $\{b_j^K\}$ in the candidate image are found by comparing their descriptors; in this work we use χ^2 distance to compare histograms. Our method tries to find among the K nearest neighbors the best match (if any), so K can be seen as an accuracy parameter. To provide the method with rotation invariance the feature descriptors are normalized in terms of orientation. This normalization is performed by rotating the polar coordinate system of each feature by a value equal to $-\phi_{\varsigma_i}$ (*i.e.*, all features are set to orientation zero) and calculating their descriptors. The scale and translation invariance in the descriptors is accomplished by construction (for details see Section 3.1.2).

3.2.2 Rejecting Casual Matches

For each pair $\langle a_i, b_j^k \rangle$, the query image features $\{a_i\}$ are aligned according to the correspondence $\langle a_i, b_j^k \rangle$:

$$a_i' = (a_i \cdot s + \mathbf{t}) \cdot R(\theta(a_i, b_j^k)),$$

where $s = s_{a_i}/s_{b_j^K}$ is the scale ratio between the features a_i and b_j^k, $\mathbf{t} = p_{a_i} - p_{b_j^k}$ is the translation vector from point p_{a_i} to point $p_k^{b_j}$, $R(\theta(a_i, b_j^k))$ is the rotation matrix for a rotation, around point p_{a_i}, equal to the direction of the orientation vector of feature a_i with respect to the orientation of b_j^k, *i.e.*, $\phi_{a_i} - \phi_{b_j^k}$.

Once both images are aligned (same scale, rotation and translation) according to correspondence $\langle a_i, b_j^k \rangle$ (see Figure 3.4 a) and b)), the nearest neighbor $b_v \in \{b_j^k\}$ of each feature a_i' is found. Then, a vector $\mathbf{m}$ defined by (l, φ) is calculated; being l the distance from point p_{b_v} of feature b_v to a reference point $p_\bullet$ in the candidate object (*e.g.*, the object centroid, the point p of some feature or any other point, but always the same point for every candidate image), and φ the orientation of feature b_v with respect to the reference point $p_\bullet$, *i.e.*, the angle between the orientation vector $\mathbf{p_{b_v}}$ of feature b_v and the vector $\mathbf{p_\bullet}$, the latter defined from point p_{b_v} to point $p_\bullet$, as expressed in Formulas 3.7 and 3.8 and depicted in Figure 3.4 c).

$$l = ||p_{b_v} - p_\bullet||, \tag{3.7}$$

$$\varphi = \arccos\left(\frac{\mathbf{p_{b_v}} \cdot \mathbf{p_\bullet}}{||\mathbf{p_{b_v}}||\ ||\mathbf{p_\bullet}||}\right). \tag{3.8}$$

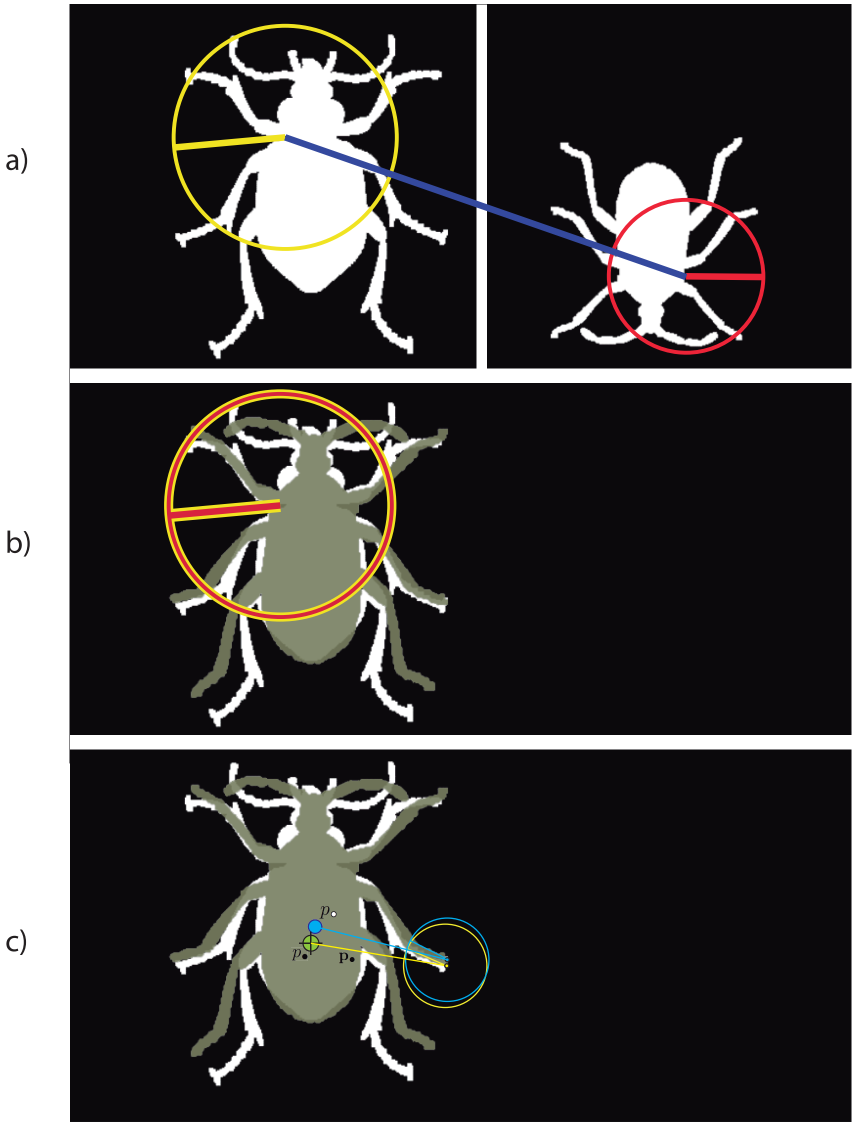

Figure 3.4: (*best seen in color*). a) A candidate match, b) images alignment according to the candidate match in a). c)

Once obtained $\mathbf{m}$, the point $p_\circ$, given by the point at a distance l from point $p_{a'_i}$ of feature a'_i and orientation φ respect to its orientation vector $\mathbf{p_{a'_i}}$, is found as indicated in Formulas 3.9 and 3.10,

$$p^x_\circ = p^x_{a'_i} + l \cdot \cos(\phi_{a'_i} + \varphi), \tag{3.9}$$

$$p^y_\circ = p^y_{a'_i} + l \cdot \sin(\phi_{a'_i} + \varphi). \tag{3.10}$$

Intuitively, if $\langle a_i, b^k_j \rangle$ is a correct match, most of the points $p_\circ$ should be concentrated around the point $p_\bullet$. This idea is what allows us to accept or reject a candidate match $\langle a_i, b_j^k \rangle$. With this aim, we defined a matching measure Ω between features a_i and b_j^k as a measure of dispersion of points $p_\circ$ around point $p_\bullet$, as expressed in Formula 3.11,

$$\Omega = \sqrt{\frac{\sum_{i=1}^{N_Q} ||p_\circ^i - p_\bullet||^2}{N_Q}}. \tag{3.11}$$

Using this measure, Ω, we can determine the best match for each feature a_i of the query image in the candidate image, or reject any weak match having Ω above a given threshold λ_Ω. A higher threshold means supporting larger deformations of the shape, but also more false matches. In Figure 3.5, the matches between features extracted from silhouettes of two different instances of the same object class are shown, the robustness to changes in scale, rotation and translation can be appreciated.

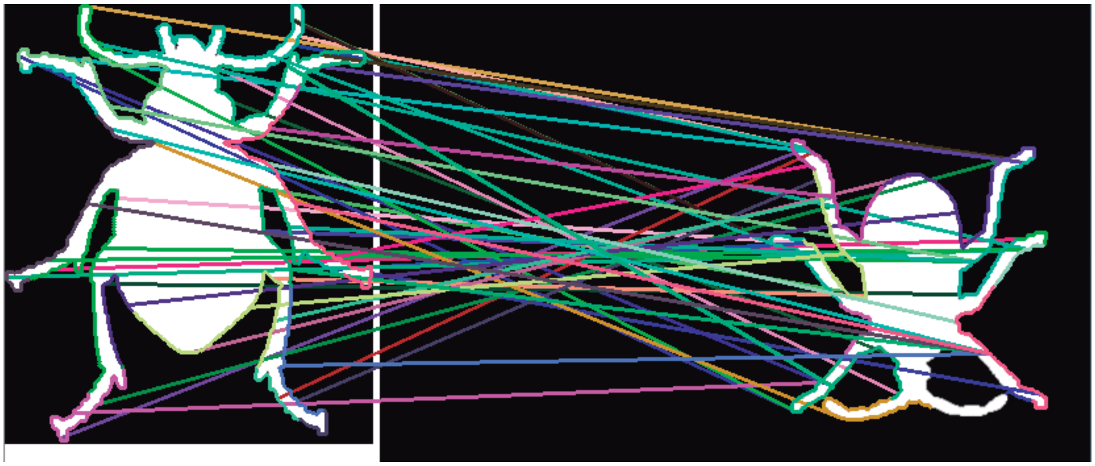

Figure 3.5: Matches between local shape descriptors in two images. It can be seen how these matches were found even in presence of rotation, scale and translation changes. Also, some false matches could be seen, but notice that they are consistent with the resemblance of the rotated shapes.

3.3 Efficient LISF Feature Extraction and Matching

In this section, we present a massively parallel implementation in GPUs of the two most time-consuming stages of LISF, *i.e.*, the feature extraction and the feature matching steps.

3.3.1 Implementation of Feature Extraction using CUDA

As mentioned in Section 3.1.1, in the feature extraction step, for each point p_i in the contour, up to P triangles are evaluated, where P is the contour size. Each one of these evaluations are independent from each other, so there is a great potential for parallelism. We present a massively parallel implementation in CUDA of this stage by obtaining in parallel the candidate triangle of each point p_i in the contour.

All the triangles of a point p_i are evaluated in a block. The constraints of each triangle (Formulas 3.1 - 3.3) are evaluated in a thread. Threads in a single block will be executed on a single multiprocessor, sharing the software data cache, and can synchronize and share data with threads in the same block. Triangles that fulfill these constrains, *i.e.*, candidate triangles, are tiled into the shared memory. Tiling is a common strategy used in order to increase data reutilization by decreasing global memory accesses, where the data is partitioned into subsets called tiles, such that each tile fits into the shared memory. Later, in each block the highest curvature candidate triangle of corresponding point p_i is selected. The final step, *i.e.*, the selection of the shaper triangle in the neighborhood, is performed in the host. As there are only a few candidate triangles in a neighborhood, this is a task which is more favored to be performed in the CPU.

3.3.2 Implementation of Feature Matching using CUDA

Finding candidate matches involves $N_Q \times N_C$ chi-squared comparisons of feature descriptors, where N_Q and N_C are the number of features extracted from the query and the database images, respectively. Also, rejecting casual matches needs $N_Q \times N_C$ chi-squared comparisons after alignment. Each chi-squared feature comparison is independent from the others, therefore, a great potential for parallelism is also present in these stages. We propose a massively parallel implementation in CUDA for the chi-squared comparison of $N_Q \times N_C$ descriptors.

Given the sets of descriptors extracted from the query and the candidate image, *i.e.*, $Q = \{q_1, q_2, ..., q_{N_Q}\}$ and $C = \{c_1, c_2, ..., c_{N_C}\}$, respectively, where the size of each de-

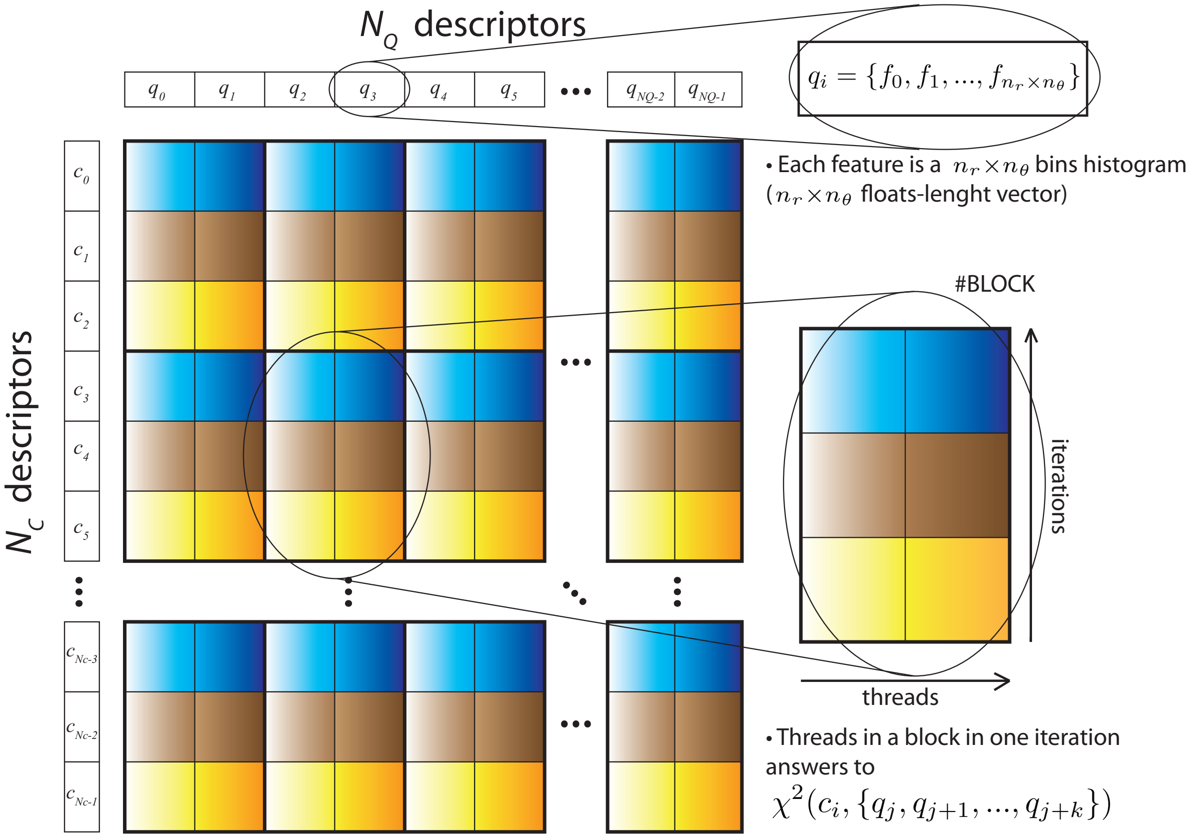
N_Q descriptors
q_0
q_1
q_2
q_3
q_4
q_5
q_{NQ-2}
q_{NQ-1}
$q_i = \{f_0, f_1, ..., f_{n_r \times n_\theta}\}$
• Each feature is a $n_r \times n_\theta$ bins histogram ($n_r \times n_\theta$ floats-lenght vector)
N_C descriptors
c_0
c_1
c_2
c_3
c_4
c_5
c_{Nc-3}
c_{Nc-2}
c_{Nc-1}
#BLOCK
iterations
threads
• Threads in a block in one iteration answers to $\chi^2(c_i, \{q_j, q_{j+1}, ..., q_{j+k}\})$

Figure 3.6: Overview of the proposed feature comparison method in GPU.

scriptor is given by $n_r \times n_\theta$. To perform $N_Q \times N_C$ chi-squared comparisons each value in descriptor q_i is used N_C times. In order to increase data reutilization and decrease global memory accesses, Q and C are tiled into the shared memory. In each device block the chi-squared distances between every pair of descriptors $a \subset Q$ and $b \subset C$ are computed, where $|a| \ll N_Q$ and $|b| \ll N_C$. In Figure 3.6 each bold-lined cell represents the processing performed in a block and each thin-lined cell represents the comparison of a descriptor $\hat{a} \in a$ with a descriptor $\hat{b} \in b$, where the different tones of a color represent separated threads and horizontal items separated iterations. Then, all the comparisons are obtained in $|b|$ iterations, where in the j^{th} iteration the threads in the block compute the chi-squared distance of the j^{th} descriptor in b against every descriptor in a.

For values of N_Q and N_C such that the features and comparison results do not fit in the device global memory, the data could be partitioned and the kernel launched several times.

3.4 Experimental Results

The performance of the proposed LISF method has been evaluated on three different well-known datasets. The first dataset is the Kimia Shapes99 dataset (Sebastian *et al.*, 2004), which includes nine categories and eleven shapes in each category with variations in form, occlusion, articulation and missing parts. The second dataset is the Kimia Shapes216 dataset (Sebastian *et al.*, 2004). This database consists of 18 categories with 12 shapes in each category. The third dataset is the MPEG-7 CE-Shape-1 dataset (Latecki *et al.*, 2000), which consists of 1400 images (70 object categories with 20 instances per category). In the three datasets, in each image there is only one object, defined by its silhouette, and at different scales and rotations. Example shapes are shown in Figure 3.7.

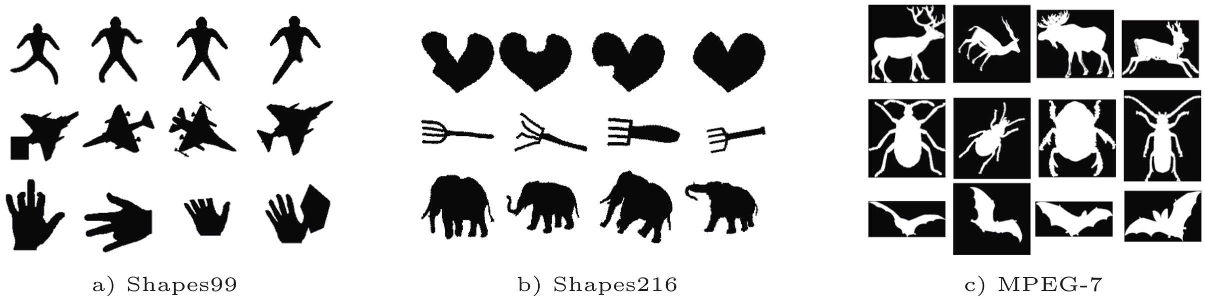

Figure 3.7: Example images and categories from a) the Shapes99 dataset, b) the Shapes216 dataset, and c) the MPEG-7 dataset.

3.4.1 Shape Retrieval and Classification Experiments

In order to show the robustness of the LISF method to partial occlusion in the shape, we generated another 15 datasets by artificially introducing occlusion of different magnitudes (10%, 20%, 30%, 45% and 60%) to the Shapes99, Shapes216 and MPEG-7 datasets. Occlusion was added by randomly choosing rectangles that occlude the desired portion of the shape contour. A sample image from the MPEG-7 dataset at different occlusion levels is shown in Figure 3.8.

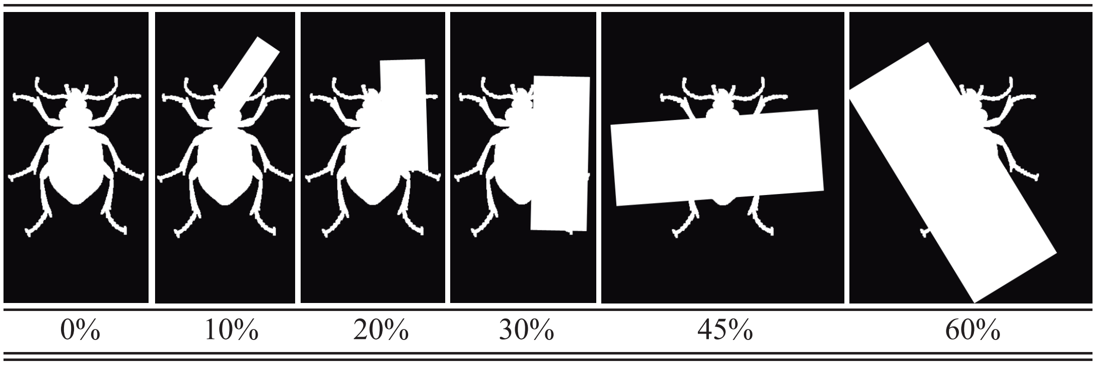

Figure 3.8: Example images from the MPEG-7 dataset with different levels of occlusion (0%, 10%, 20%, 30%, 45% and 60%) used in the experiments.

As a measure to evaluate and compare the performance of the proposed shape matching schema in a shape retrieval scenario we use the so-called bull's eye score. Each shape in the database is compared with every other shape model, and the number of shapes of the same class that are among the $2N_c$ most similar is reported, where N_c is the number of instances per class. The bull's eye score is the ratio between the total number of shapes of the same class and the largest possible value.

The results obtained by LISF ($n_r = 5$, $n_\theta = 12$, $\lambda_\Omega = 0.9$) were compared with those of the popular shape context descriptor (100 points, $n_r = 5$, $n_\theta = 12$) (Belongie *et al.*, 2002), the Zernike moments (using 47 features) (Khotanzad and Hong, 1988) and the Legendre moments (using 66 features) (Chong *et al.*, 2004). Rotation invariance can be achieved by shape context, but it has several drawbacks, as mentioned in (Belongie *et al.*, 2002). In order to perform a fair comparison between LISF (which is rotation invariant) and shape context, in our experiments the non-rotation invariant implementation of shape context is used, and images used by shape context were rotated so that the objects had the same rotation.

Motivated by efficiency issues, for the MPEG-7 CE-Shape-1 dataset we randomly selected 10 of the 70 categories and used the 20 samples per class. The bull's eye score implies all-against-all comparisons and experiments had to be done across the 18 datasets for the LISF, shape context, Zernike moments and Legendre moments methods. It is important to highlight that there is no loss of generality in using a subset of the MPEG-7 dataset, since the aim of the experiment is to compare the behavior of the LISF method against other methods, across increasing levels of occlusion.

As a similarity measure of image a with image b, with local features $\{a_i\}$ and $\{b_j\}$ respectively, we use the ratio between the number of features in $\{a_i\}$ that found matches in $\{b_j\}$ and the total number of features extracted from a.

Figure 3.9 shows the behavior of the bull's eye score of each method while increasing partial occlusion in the Shapes99, Shapes216 and MPEG-7 datasets. Bull's eye score is computed for each of the 18 datasets independently.

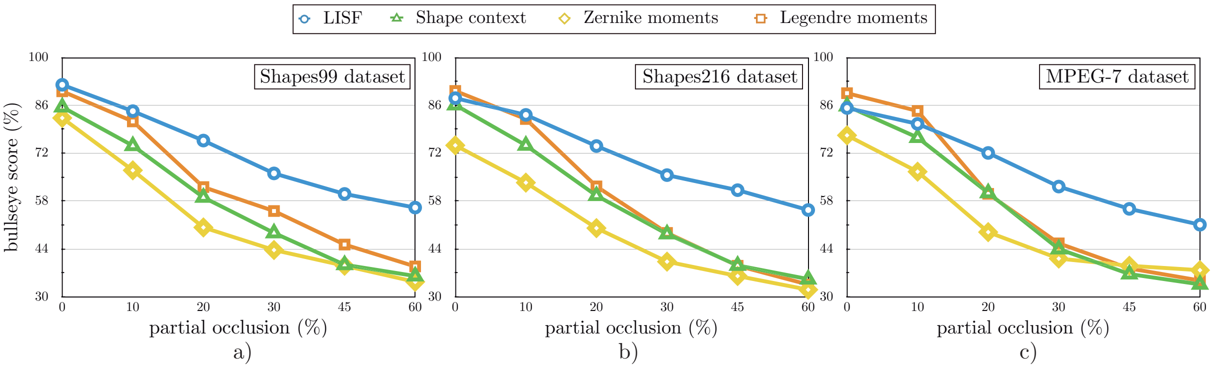

Figure 3.9: (*best seen in color*). Bull's eye score comparison between LISF, shape context, Zernike moments and Legendre moments in the a) Shapes99, b) Shapes216 and c) MPEG-7 datasets with different partial occlusions (0%, 10%, 20%, 30%, 45% and 60%).

As expected, the LISF method outperforms the shape context, Zernike moments and Legendre moments methods. Moreover, while increasing the occlusion level, the difference in terms of bull's eye score gets bigger, with about 15 - 20% higher bull's eye score across highly occluded images; which shows the advantages of the proposed method over the other three.

Figure 3.10 shows the top 5 retrieved images and its retrieval score for the *beetle-5* image from the MPEG-7 dataset, with different occlusion levels (0% to 60% partial occlusion) using the LISF method. The robustness to partial occlusion of the LISF method can be appreciated. Retrieval score of images that do not belong to the same class as the query image are depicted in bold italic.

In a second set of experiments, the proposed method is tested and compared to shape

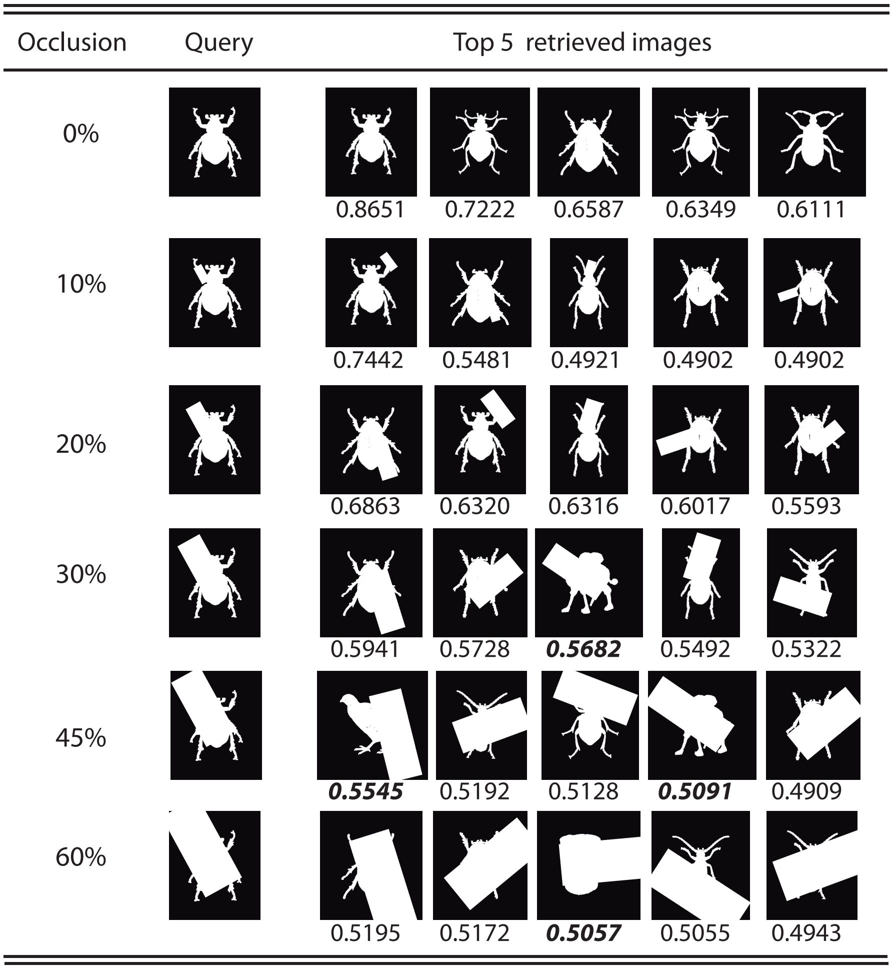

Figure 3.10: Top 5 retrieved images and its similarity score obtained by LISF. In each row retrieval results for the *beetle-5* image in the six MPEG-7 based databases. Retrieval scores in bold italic represent images that do not belong to the same class of the query image.

context, Zernike moments and Legendre moments in a classification task also under varying occlusion conditions. A 1-NN classifier was used, *i.e.*, we assigned to each instance the class of its nearest neighbor. The same data as in the first set of experiments is used. In order to measure the classification performance, the accuracy measure was used. Accuracy measures the percentage of data that are correctly classified. Figure 3.11 shows the results of classification under different occlusion magnitudes (0%, 10%, 20%, 30%, 45% and 60% occlusion).

In this set of experiments, a better performance of the LISF method compared to pre-

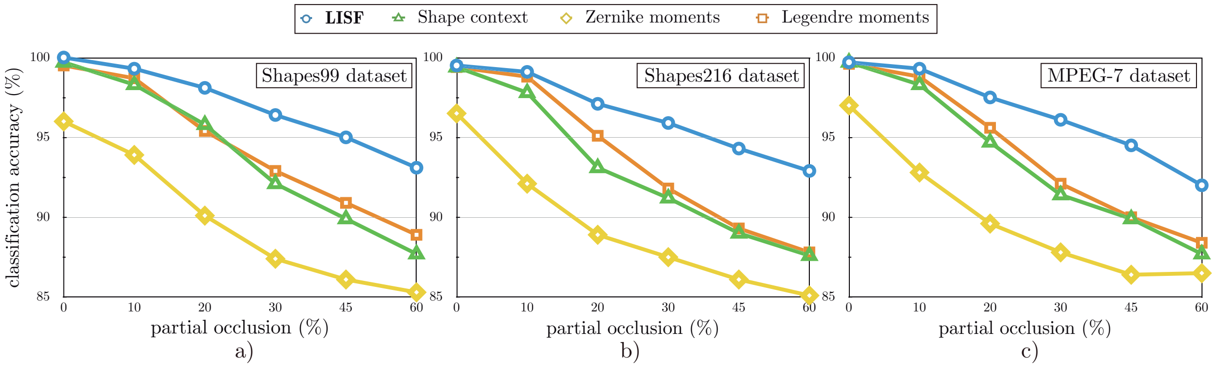

Figure 3.11: (*best seen in color*). Classification accuracy comparison between LISF, shape context, Zernike moments and Legendre moments in the a) Shapes99, b) Shape 216, and c) MPEG-7 dataset, with different partial occlusions (0%, 10%, 20%, 30%, 45% and 60%).

vious work can also be appreciated. As in the shape retrieval experiment, while increasing the occlusion level in the test images, the better is the performance of the proposed method with respect to shape context, Zernike moments and Legendre moments, with more than 25% higher results in accuracy.

3.4.2 Efficiency Evaluation

The computation time of LISF has been evaluated and compared to other methods. Table 3.1 shows the comparison of LISF computation time against shape context, Legendre moments, and Zernike moments. The reported times correspond to the average time needed to describe and match two shapes of the MPEG-7 database over 500 runs. The LISF_CPU, shape context, Legendre and Zernike moments results were obtained on a single thread of a 2.2 GHz processor and 8GB RAM PC, and the LISF_GPU results were obtained on a NVIDIA GeForce GT 610 GPU with 48 CUDA cores and 1GB of global memory. As can be seen in Table 3.1, both implementations of LISF are the least time-consuming compared with shape context, Legendre moments, and Zernike moments.

In order to show the scalability of our proposed massively parallel implementation in CUDA, we reported the time and achieved speed-up while increasing the contour size and the number of features to match for the feature extraction and feature matching stages, respectively. These results were obtained on a NVIDIA GeForce GTX 480 GPU with 480

Table 3.1: Average feature extraction and matching time for two images of the MPEG7 database, in seconds.

Method	Avg. computation time (s)	Std dev
Shape context	2.66	0.09
Legendre moments	7.48	0.12
Zernike moments	26.47	0.14
LISF_CPU	**0.47**	0.04
LISF_GPU	**0.16**	0.01

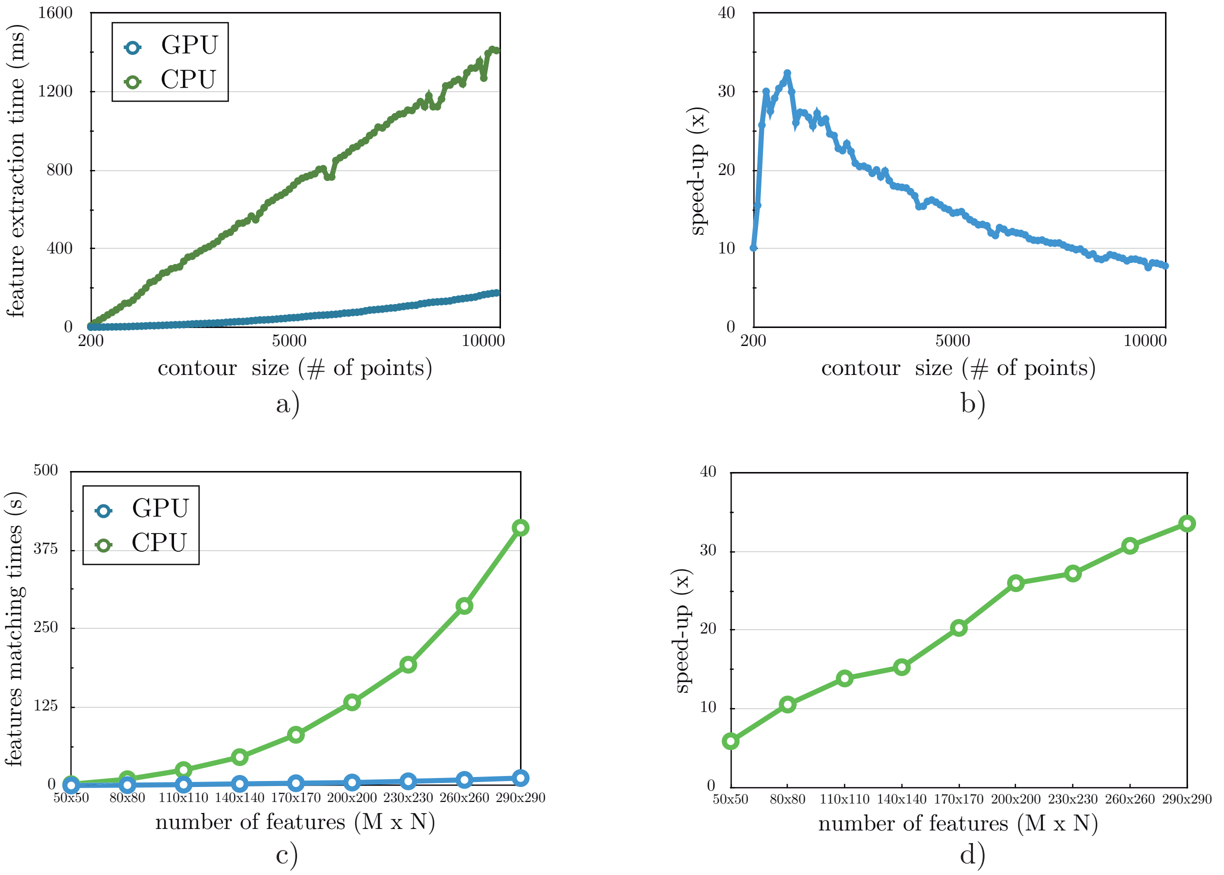

a) b) c) d)

Figure 3.12: (*best seen in color*). Computation time and achieved speed-up by the proposed massively parallel implementation in CUDA with respect to the CPU implementation for the a,b) feature extraction and c,d) feature matching stages of LISF.

CUDA cores and 1GB of global memory, and were compared with those obtained in a single threaded Intel CPU Processor at 3.4GHz with 64GB of RAM PC.

As it can be seen in Figures 3.12(a) and 3.12(b), tested on contours of sizes ranging from 200 to 10 000 points, the proposed feature extraction implementation on GPU achieves up to a 32x speed-up and a 16x average speed-up. The peak in Figure 3.12(b) represents the point where the used GPU board (approximately at contours of size bigger than 1000 points), due to its technical specifications, must enqueue the computations that from the logical programming were determined to be executed in parallel. For the feature matching step (see Figures 3.12(c) and 3.12(d)), the proposed GPU implementation were tested comparing from 50 vs. 50 to 290 vs. 290 features. The GPU implementation showed linear scaling against exponential scaling of the CPU implementation and it obtained a 34x speed-up when comparing 290 vs. 290 LISF features.

3.5 Summary

In this chapter we introduced a method for shape feature extraction, description and matching, invariant to rotation, translation and scale. The proposed method allows us to overcome the intrinsic disadvantages of only using local or global features by capturing both local and global information. The conducted experiments supported the mentioned contributions, showing larger robustness to partial occlusion than other methods in the state of the art. It is also more efficient in terms of computational time than the other techniques. Also, we proposed a massively parallel implementation in CUDA of the two most time-consuming stages of LISF, *i.e.*, the feature extraction and feature matching steps, which achieve speed-ups of up to 32x and 34x, respectively. In this chapter we have presented a shape description and matching method for binary images, in the next chapter we propose a shape description and matching method for real images (RGB or grayscale images).

Chapter 4

The Open/Closed Contours Triangle Area Representation Method

Shape information have proven to be useful in many image processing and computer vision applications such as object detection, image retrieval and 3D curve reconstruction. However, shape representation and matching remains as one of the most challenging topics in computer vision, partly because of partial occlusion and noise in the shape information extracted from real images. Figure 4.1 shows a realistic image and the edges extracted from it using the Pb edge detector (Martin *et al.*, 2004). In edges extracted from real images, edge fragments that represent part of the object might be missing, *e.g.*, the lower part of the chair or the left part of the notebook in Figure 4.1 b). Also, contours could be broken into several fragments. In Figure 4.1 b) we can appreciate that the contours of the bottle and notebook are broken into several pieces. Furthermore, part of the true contour of the object of interest can be incorrectly connected to edge fragments belonging to the background or another object, resulting in a single edge fragment. An example can be appreciated in Figure 4.1 c), where the bottom of the bottle is connected with edges from the note and its reflection in the bottle.

Dealing with the three aforementioned problems derived from using edges extracted from real images implies that the shape descriptor should be able to represent both open and closed contours, and that part of the contour fragments should match with one or more parts of the shape model, which makes the shape matching problem more difficult than that of closed shapes. Other considerations are the robustness with respect to the

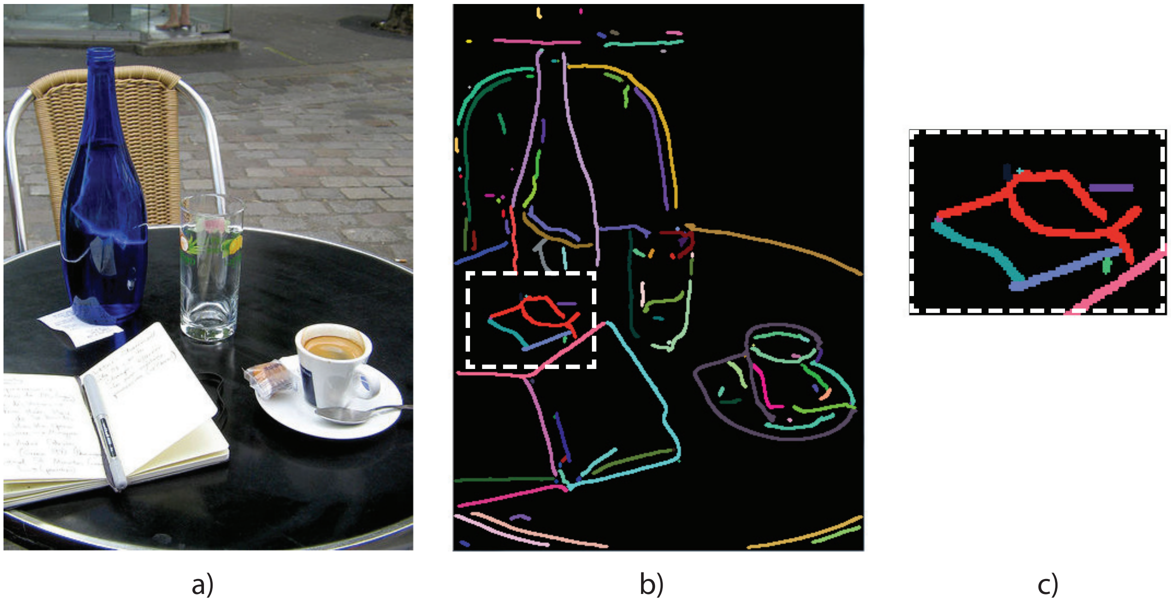

Figure 4.1: Problems derived from using edgemaps extracted from real images. a) original image, b) edge fragments extracted from a). c) closeup of the bottom part of the bottle.

image scale, rotation and translation.

The LISF method, presented in Chapter 3, is able to deal with partial occlusion, able to describe open and closed contours, and invariant to scale, rotation and translation changes. However, LISF cannot perform partial contour matching which is fundamental when dealing with edgemaps, as above mentioned. Further, LISF description is based on high curvature contour fragments, ignoring straight line fragments which are in many cases the primarily structure found in edgemaps obtained from real images.

In this work, we propose a shape descriptor that is particularly suitable for partial shape matching of open/closed contours extracted from edgemap images, *e.g.*, using Canny or any other edge extraction method from gray or color images. Our descriptor, named OCTAR (Open/Closed contours Triangle Area Representation), measures the convexity or concavity of contour segments using the signed areas of triangles formed by every pair of contour points and their middle point. Based on this descriptor, we also propose a partial shape matching method robust to partial occlusion and noise in the extracted contour. The matching method finds for every contour fragment in the query shape its best match in the shape model. We extend the OCTAR descriptor to represent the spatial configuration of two contour fragments. Individual matches with coherent spatial configurations with respect to the model are joined to form object hypotheses in an agglomerative hierarchical process. Later, hypotheses are evaluated based on the coverage of the model contour, measuring the global shape similarity and its appearance.

4.1 Proposed Shape Descriptor

In order to find partial shape correspondences between contour fragments and a model, a shape descriptor must be able to represent both open and closed contours, must be self-contained, and invariant to rotation and translation. In this thesis, we propose a shape descriptor based on the triangle area representation, that meets these properties. The proposed descriptor is named OCTAR, from Open/Closed contour Triangle Area Representation. The use of triangle areas provides discriminative data about shape features such as the convexity/concavity at each curve segment. For contour sequences represented in counter clockwise direction, positive, negative and zero values of OCTAR indicate convex, concave and straight-line points, respectively.

Given a sequence of N ordered points, $\mathcal{P} = \{p_1, p_2, ..., p_N\}, p_i \in \mathbb{R}^2$, representing a contour fragment, for each pair of points $\langle p_i, p_j \rangle$ in $\mathcal{P}$ we compute the area of the triangle formed by these two points and their middle point $p_* \in \mathcal{P}$ (see Figure 4.2(a)). The signed area of the triangle formed by these points is given by Formula 4.1,

$$TAR(i, j, *) = \frac{1}{2} \det \begin{pmatrix} x_i & y_i & 1 \\ x_* & y_* & 1 \\ x_j & y_j & 1 \end{pmatrix}, \tag{4.1}$$

where det() is the matrix determinant. If the middle point between $\langle p_i, p_j \rangle$ does not exist, *i.e.*, $(i - j)$ is odd, p_* is interpolated from $p_{\lfloor (i+j)/2 \rfloor}$ and $p_{\lceil (i+j)/2 \rceil}$.

To obtain the OCTAR descriptor of contour fragment $\mathcal{P}$, denoted as $\Theta^{\mathcal{P}}$, the triangle area is normalized by the area of the equilateral triangle inscribed in the minimum enclosing circle of the sub-contour $\{p_i, ..., p_j\} \subseteq \mathcal{P}$ (it can be proved that this is the maximum area triangle of all possible triangles inside a circle). In Figure 4.2 (b), the equilateral normalization triangle is depicted in orange and the minimum enclosing circle of the sub-

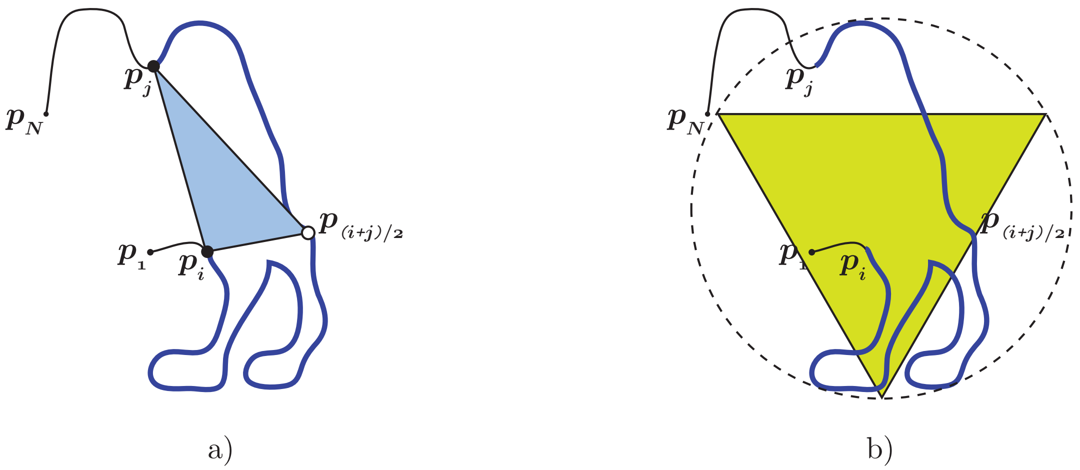

Figure 4.2: *(best seen in color.)* (a) The OCTAR descriptor is computed from the area of the triangles formed by every pair of points in the shape and their middle point, and (b) its normalized by the area of the equilateral triangle inscribed in the minimum enclosing circle of the sub-contour $\{p_i, ..., p_j\} \subseteq \mathcal{P}$.

contour $\{p_i, ..., p_j\} \subseteq \mathcal{P}$ is illustrated by the dashed circle. OCTAR is represented in a log space to make the descriptor more sensitive to the area of nearby contour points than to those of points farther away. The OCTAR value of each pair of points $\langle p_i, p_j \rangle$ in $\mathcal{P}$ is obtained as expressed in Formula 4.2.

$$\Theta^{\mathcal{P}}(i,j) = \log\left(1 + \frac{TAR(i,j,*)}{\mathcal{A}(\{p_i, ..., p_j\})}\right), \tag{4.2}$$

where $\mathcal{A}(\{p_i, ..., p_j\})$ is the area of the equilateral triangle inscribed in the minimum enclosing circle of the sub-contour $\{p_i, ..., p_j\} \subseteq \mathcal{P}$. We add one to the normalized triangle area to make $\Theta^{\mathcal{P}}(i,j)$ positive.

The similarity of two OCTAR descriptors Θ^P and Θ^Q of the same size is given by Formula 4.3.

$$\Phi(P,Q) = 1 - \left(\frac{1}{MN}\sum_{i=1}^{M}\sum_{j=1}^{N}\left|\Theta^P(i,j) - \Theta^Q(i,j)\right|\right), \tag{4.3}$$

where $M \times N$ is the size of the descriptor matrices.

The proposed shape descriptor has three important properties. i) OCTAR is able to represent both open and closed contours, since it does not make any assumption over the contour closeness. ii) The triangle area based representation makes it invariant to rotation and translation. iii) OCTAR is self-contained as for any $C \subset \mathcal{P}$ it holds that $\Theta^C \subset \Theta^{\mathcal{P}}$, this property implicitly allows to retrieve partial matches from the contour description. Figure 4.3 shows the OCTAR descriptor (Formula 4.2) of two shapes, being the second shape a subset of the first. As it can be appreciated, the OCTAR descriptor of the second shape is contained in that of the first shape.

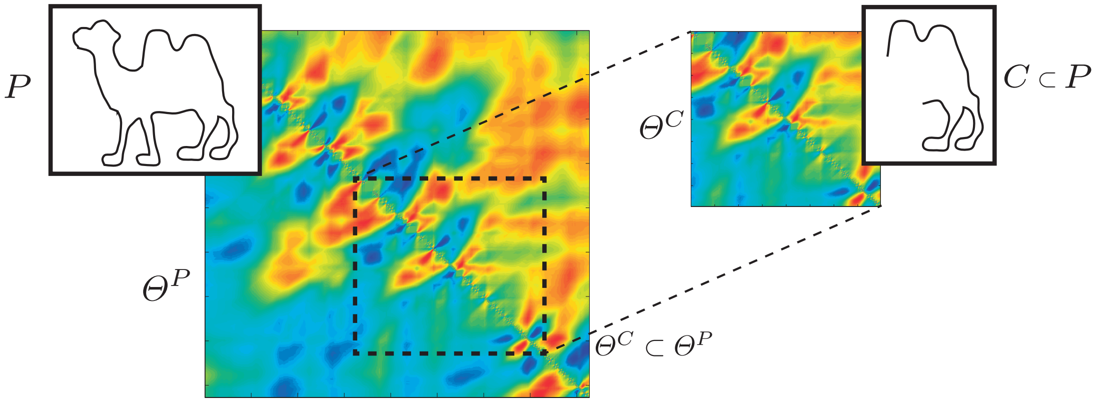

Figure 4.3: *(best seen in color.)* The OCTAR descriptor matrices, Θ^P and Θ^C, of two shapes, P and C, are shown. The self-containing property of the proposed descriptor can also be appreciated.

4.2 Proposed Partial Shape Matching Method

Given the set of contour fragments $\mathcal{F} = \{f_1, f_2, ..., f_K\}$ that represent the query shape image, where each fragment $f_k = \{p_1, p_2, ..., p_{N_k}\}, p_i \in \mathbb{R}^2$ is a sequence of N_k points, and the shape model $\mathcal{Q} = \{q_1, q_2, ..., q_M\}, q_i \in \mathbb{R}^2$, a sequence of M points; we want to find the best correspondence between a part $f_k(a, l) = \{p_a, ..., p_{a+l-1}\}, f_k(a, l) \subseteq f_k$ of a contour fragment and a part $\mathcal{Q}(b, l) = \{q_b, ..., q_{b+l-1}\}, \mathcal{Q}(b, l) \subseteq \mathcal{Q}$ of the model, where a and b are the initial points in f_k and $\mathcal{Q}$, respectively, and l is the part length.

Based on the proposed OCTAR descriptor, we introduce a method for finding partial matches between contour fragments and a model. In order to find partial matches of arbitrary sizes we have to compare all possible sub-blocks of the descriptor matrices to find the corresponding sub-blocks with the maximum similarity. With this aim, we build a 4D tensor $\mathbf{T}(k, a, b, l) = \Phi(f_k(a, l), \mathcal{Q}(b, l))$, where Φ is the similarity measure between descriptor matrices defined in Formula 4.3. To efficiently build $\mathbf{T}$, we use the integral image optimization to access the partial descriptor differences in constant time, as suggested in (Riemenschneider *et al.*, 2010). This optimization is possible thanks to the self-containing property of the OCTAR descriptor.

In order to select the best match between part $f_k(a,l) \subseteq f_k$ and $\mathcal{Q}(b,l) \subseteq \mathcal{Q}$, the simplest criterion could be to select those fragments with high similarity values in $\mathbf{T}$. However, given the observation that when very short fragments are involved in a matching, it is neither discriminative nor reliable, even when having the highest similarity values. To overcome this limitation, we propose a more robust alternative.

As we want to find which parts of a contour fragment match one or several parts of the model, we first find which parts of the model are more likely to appear in the contour fragments. With that aim we suppress the tensor $T(k,a,b,l)$, as indicated in Formula 4.4:

$$\mathcal{L}(k,l,b) = \sum_{h=1}^{l} \sum_{a=1}^{N_k} T(k,a,b,h). \tag{4.4}$$

Given the exhaustive character of $\mathbf{T}$, in a neighborhood of the best matching part there will be a large amount of strong matches in $\mathcal{L}$. Therefore, we identify the parts of the model more likely to be involved in a true partial match with one or several parts of the contour fragment from the shape image as the peaks on $\mathcal{L}$ for each length value l, denoted as $\mathcal{U}_l = \{u_1, u_2, ..., u_M\}, u_j \subseteq \mathcal{Q}$. Figure 4.4 a) represents a contour fragment of length l from the query image. Its correspondent parts in the swan model are shown in Figure 4.4 b). The detected peaks in $\mathcal{L}$ and their corresponding parts in the model are shown in Figure 4.4 c).

Once identified the parts of the model that will be involved in a match of length l, *i.e.*, $\mathcal{U}_l$, we perform the inverse procedure to find which parts of the contour fragment will match with each identified part in the model. For each part of the model $u_j \in \mathcal{U}_l$ we suppress the tensor $T(k,a,b,l)$, as indicated in Formula 4.5,

$$\mathcal{L}'(k,l,a) = \sum_{h=1}^{l} \sum_{b \in u_j} T(k,a,b,h), \tag{4.5}$$

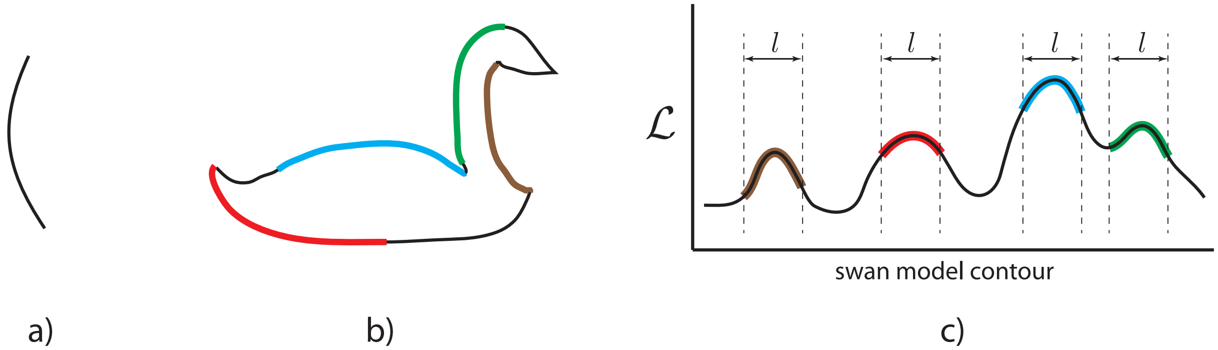

Figure 4.4: (*best seen in color*). Detection of the parts of the model more likely to be involved in a true partial match. In a) a contour fragment of length l from the query image, in b) its correspondent parts in the swan model, and in c) the detected peaks in $\mathcal{L}$.

and the peaks in $\mathcal{L}'$ will constitute the matching part of u_j in the contour fragment. Finally, we discard smaller matches contained in another match of larger length value l.

4.3 Object Hypotheses Formation and Evaluation

In presence of partial occlusion and noise, not every contour fragment $f_k \in \mathcal{F}$ has to be part of the object. Therefore, we have to select among the set of candidate matches those that really belong to the object. The number of possible combinations of contour fragments that can be joined to form the object is exponential with respect to the number of contour fragments. In order to reduce the number of possible combinations, spatial information is used. Each matched contour fragment is mapped to its corresponding part in the model and the object centroid estimated. Only matches with neighboring object centroid estimations can be later joined as an object hypothesis, an example on the *ceazanne* image of the EHTZ Shape Classes Dataset in shown in Figure 4.5. Beside reducing computational time, this step avoids false positives from an early stage.

In order to exploit further the spatial information in an object hypothesis, we extended the OCTAR shape descriptor, defined in Formula 4.2, such that it could express the spatial configuration between two contour fragments $\mathcal{P} = \{p_1, p_2, ..., p_N\}$ and $R = \{r_1, r_2, ..., r_M\}$, where each point $p_i \in \mathcal{P}$ is related with each point $r_j \in R$ through the area of the triangle

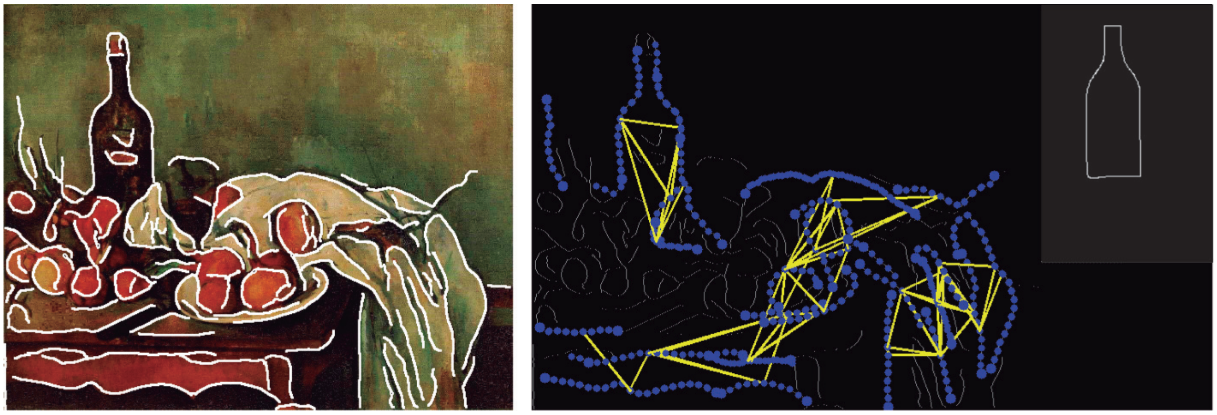

Figure 4.5: (*best seen in color*). Partial matches that according to their spatial relations can be later joined as an object hypothesis (connected by a yellow edge).

formed by p_i, r_j, and the first point in R (see Figure 4.6). The spatial configuration descriptor of two contour fragments $\mathcal{P}$ and R is defined as

$$\Theta^{\mathcal{P},R}(p_i, r_j) = \log\left(1 + \frac{TAR(p_i, r_j, r_1)}{\mathcal{A}(\{p_i, r_j, r_1\})}\right), \tag{4.6}$$

where $TAR(p_i, r_j, r_1)$ is the signed area (see Formula 4.1) of the triangle formed by the first point of the contour fragment R and the i^{th} and j^{th} points of the contour fragments $\mathcal{P}$ and R, respectively. $\mathcal{A}(\{p_i, r_j, r_1\})$ is the area of the equilateral triangle inscribed in the minimum enclosing circle of the point set $\{p_i, r_j, r_1\}$.

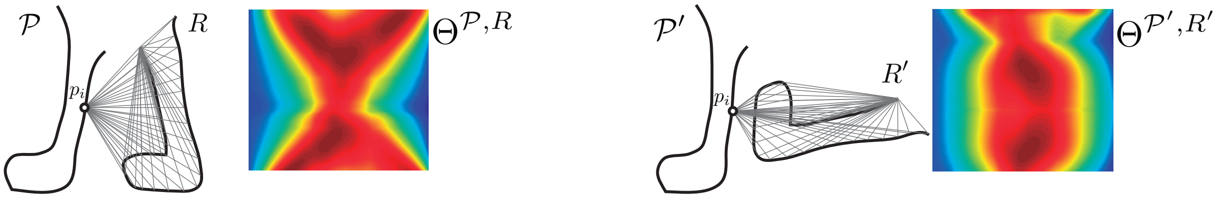

Figure 4.6: (*best seen in color*). Extended OCTAR descriptor for contours spatial configuration. The same two contours under different spatial configurations have different descriptor matrices.

In order to form object hypotheses, we use an agglomerative hierarchical approach in the spatial configuration space. Initially, each match is a hypothesis; later, in each iteration, the two hypotheses whose contour fragments configuration is more similar to its corresponding configuration of model parts are joined, restricted to those fragments with neighboring object centroid estimations.

Once the hypotheses hierarchy is obtained, each object hypothesis is evaluated according to four criteria. These criteria evaluate in what extent the object model is covered, the hypothesis global shape similarity with respect to the model, and its appearance. These hypothesis evaluation criteria are detailed in the following sections.

4.3.1 Covering Criterion

The first criterion is based on the coverage of the model contour by the hypothesis, and is defined as indicated in Expression 4.7.

$$\mathcal{E}_{COV} = \frac{1}{M} \sum_{i}^{M} w_i, \tag{4.7}$$

where w_i takes value of one or zero to indicate whether the i^{th} point of the model contour has been matched or not, and M is the number of points in the model contour.

4.3.2 Object Hypothesis Contour Estimation Criterion

The second hypothesis evaluation measure assesses the shape similarity in a global manner. An object hypothesis is a set of partial matches, therefore it is expressed as the correspondence between a subset of contour fragment points in the image and a subset of points in the model. The idea is to estimate the whole contour of the object hypothesis in the image based on the existing correspondences.

There is a mapping $T : \hat{\mathcal{Q}} \rightarrow \hat{\mathcal{F}}$, such that if $p \in \hat{\mathcal{Q}}, T(p) \in \hat{\mathcal{F}}$. The subset of points in the object hypothesis in the image is denoted as $\hat{\mathcal{F}} \in \mathcal{F}$ and the corresponding subset of points in the model is denoted as $\hat{\mathcal{Q}} \in \mathcal{Q}$. Usually, in an object hypothesis, there are some points in the model that have no correspondence in the image, *i.e.*, $\bar{\mathcal{Q}} = \{p \in \mathcal{Q} | p \notin \hat{\mathcal{Q}}\}$. For each point $p \in \bar{\mathcal{Q}}$, we estimate its correspondent point in the image based on a transformation Z, consisting on rotation and translation, which is estimated locally based on the correspondences between $\hat{\mathcal{F}}$ and $\hat{\mathcal{Q}}$. Therefore, the whole object hypothesis contour in the image is expressed as indicated in Formula 4.8.

$$\mathcal{H}(p) = \begin{cases} T(p), & \text{if } p \in \hat{\mathcal{Q}} \\ pZ_p, & \text{if } p \in \bar{\mathcal{Q}} \end{cases} \tag{4.8}$$

We estimate the transformation Z_p for each point $p \in \bar{\mathcal{Q}}$, as the rotation and translation transformation between a neighborhood $V_p \in \hat{\mathcal{Q}}$ of point p and their correspondent points $T(V_p)$ in the image. The neighborhood V_p of point p in $\hat{\mathcal{Q}}$ is defined as the closest points of p in the contour sequence, *i.e.*, the distance is stablished over the model contour indexes.

The transformation Z_p is computed using the Iterative Closest Point (ICP) algorithm (Besl and McKay, 1992; Chen and Medioni, 1992). The ICP algorithm aims to find the transformation between a point cloud and some another reference point cloud, by minimizing the squared errors between the corresponding points.

Finally, we evaluate each object hypothesis based on the OCTAR similarity score (Formula 4.3) between the whole object hypothesis contour in the image $\mathcal{H}$ and the model $\mathcal{Q}$:

$$\mathcal{E}_Z = \Phi(\mathcal{H}, \mathcal{Q}). \tag{4.9}$$

4.3.3 Fitted Object Hypothesis Criterion

Evaluating if the estimated object hypothesis contour $\mathcal{H}$ is consistent with the edge fragments in the image is also needed. With this purpose, we fit every point $p \in \mathcal{H}$ to its nearest point in the edge image $\mathcal{F}$, as expressed in Formula 4.10,

$$\mathcal{H}^*(p) = \begin{cases} p, & \text{if } p \in \hat{\mathcal{F}} \\ NN(p) \in \mathcal{F}, & \text{if } p \notin \hat{\mathcal{F}} \end{cases} \tag{4.10}$$

To find the nearest point of p in $\mathcal{F}$ we use the kd-tree algorithm. Later, each hypothesis evaluation is given by the OCTAR similarity between the estimated object contour and this same contour fitted to the image edges, as indicated in Formula 4.11.

$$\mathcal{E}_{Z^*} = \Phi(\mathcal{H}, \mathcal{H}^*). \tag{4.11}$$

4.3.4 Appearance-based Evaluation Criterion

As mentioned in Sections 1.1 and 2.3, appearance features may provide distinctive cues for the object recognition process. In our work, we use appearance information in the same way as (Biederman and Ju, 1988) suggested. In this work authors argue that appearance information is used by humans to recognize objects as a second-level feature. For appearance representation we use a BoW-based representation.

In order to build the visual vocabulary, positive samples for each class are taken from the ground-truth bounding boxes on the training set. The bounding boxes are resized to a reference size while keeping its aspect ratio. SIFT descriptors (Lowe, 2004) are computed over circular patches of radius M, at points on a regular grid with spacing also M pixels. From the dense features a visual vocabulary is obtained. For more details about the BoW representation used see Chapter 5, which presents our proposal on how to obtain a more discriminative, representative and compact BoW representation. Later, from the training set, we use Support Vector Machine (SVM) to learn a classifier.

For evaluating each object hypothesis, its bounding box is resized to the reference size, and the SIFT descriptors extracted over circular patches on a grid in the same way as it was explained above for the case of the training images. The object hypothesis is represented using the previously obtained vocabulary and then we measure its relevance to a class, using the confidence of the learned SVM model, denoted as $\mathcal{E}_{App}$.

Finally, we select as final match the hypothesis with the largest linear combination of $\mathcal{E}_{COV}$, $\mathcal{E}_{Z}$, $\mathcal{E}_{Z^*}$ and $\mathcal{E}_{App}$, defined as expressed in Formula 4.12,

$$\mathcal{M}^* = \arg\max\left[\alpha\mathcal{E}_{COV} + \beta\mathcal{E}_{Z} + \gamma\mathcal{E}_{Z^*} + \delta\mathcal{E}_{App}\right], \tag{4.12}$$

where α, β, γ and δ are the weights associated to $\mathcal{E}_{COV}$, $\mathcal{E}_{Z}$, $\mathcal{E}_{Z^*}$ and $\mathcal{E}_{App}$, respectively. In all our experiments we used $\alpha = \beta = \gamma = \delta = 1$ to equally favor the four criteria.

4.4 Experimental Results

4.4.1 Performance Evaluation on Real Scenes

We present results on the ETHZ Shape Classes Dataset (Ferrari *et al.*, 2006). This dataset contains images of five diverse shape-based classes: Apple logos, bottles, giraffes, mugs and swans, and contains a total of 255 images. Example images for each category could be seen in Figure 4.7. The ETHZ Shape Classes Dataset is highly challenging as there is considerable intra-class shape variation, the objects appear in a wide range of scales and many images are severely cluttered, with objects comprising only a fraction of the total image area. Most images contain a single instance of an object class, while some contain multiple instances. No image contains instances of different classes. Object ground-truth bounding boxes and object outlines are included. Also, edgemaps produced by the Pb edge detector (Martin *et al.*, 2004) are provided. Figure 4.8 shows the edgemaps of the ETHZ dataset examples images presented in Figure 4.7.

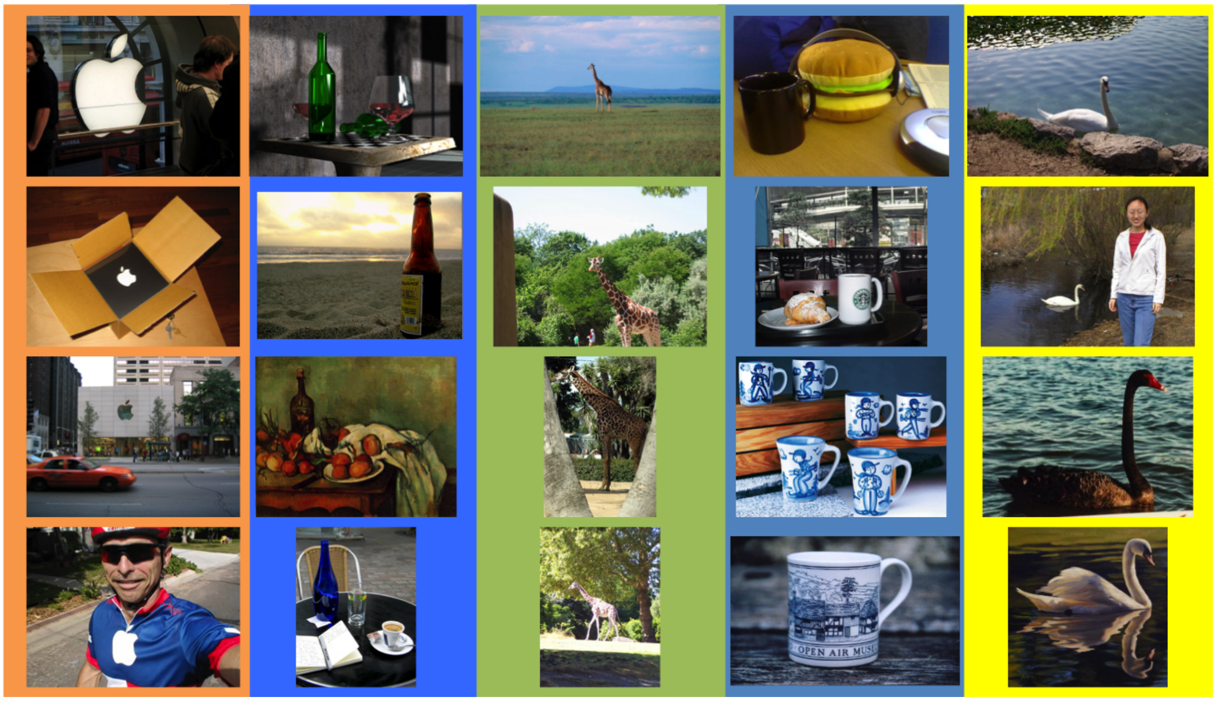

Figure 4.7: *(best seen in color.)* Example images from the ETHZ Shape Classes dataset. From left to right the Apple logo, bottle, giraffe, mug and swan class.

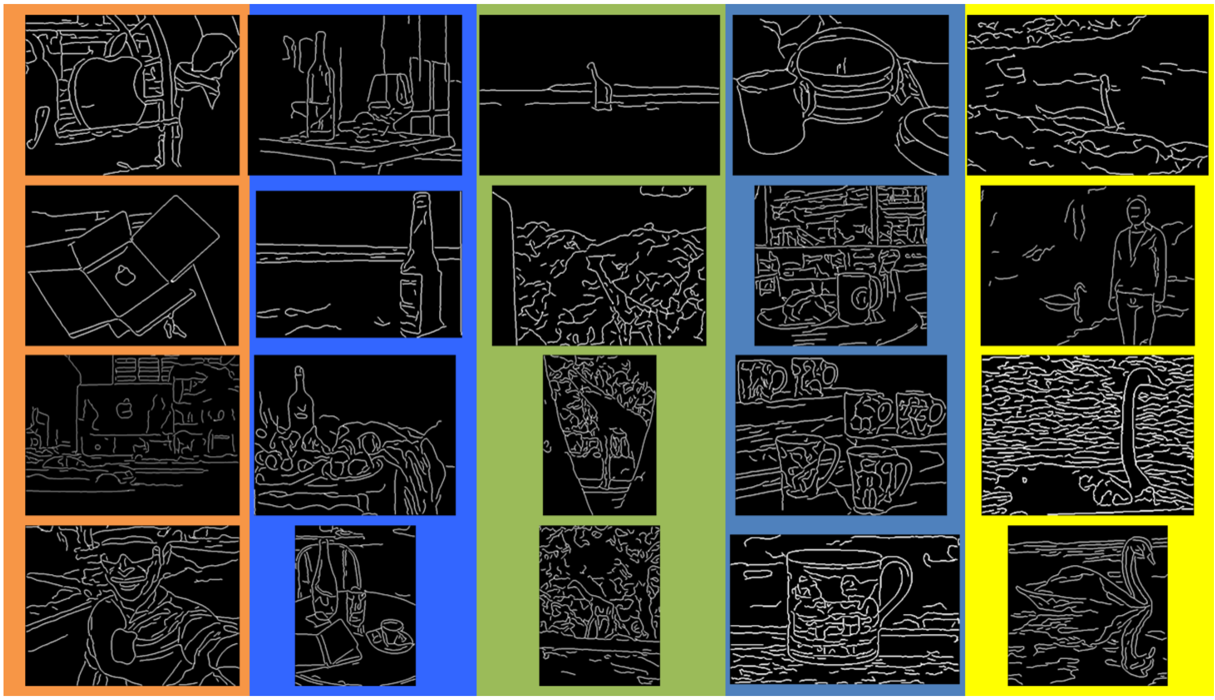

Figure 4.8: *(best seen in color.)* Example edgemap images from the ETHZ Shape Classes dataset. From left to right the Apple logo, bottle, giraffe, mug and swan class.

For the purpose of object detection evaluation we follow the protocol in (Ferrari *et al.*, 2010). We use the provided single hand-drawing shape models as the reference shape model $\mathcal{Q}$ for its corresponding class. We use the first half of images in each class for training the object appearance and the second half for testing. For evaluation, we use the PASCAL Challenge criterion, *i.e.*, a detection is counted as correct only if the intersection-over-union ratio with the ground-truth bounding box is greater than 50%, otherwise detections are counted as false-positives.

Table 4.1 shows the interpolated average precision (AP) in the ETHZ dataset and a comparison with several state-of-the-art shape-based methods. Our method obtained the best AP for the Giraffes class, given that Giraffes are highly textured objects we suspect that the use of appearance cues played an important role. Our AP is comparable with the other methods in the rest of the classes. Our mean average precision over the five classes is comparable with the best results. We also present results of our method without the appearance evaluation criterion (OCTAR - $\mathcal{E}_{App}$), in order to show the improvement

Table 4.1: Comparison of interpolated average precision (AP) on the ETHZ Shape Classes dataset.

	Applelogos	Bottles	Giraffes	Mugs	Swans	Mean
OCTAR	0.814	0.908	**0.799**	0.871	0.901	0.859
OCTAR - $\mathcal{E}_{App}$	0.807	0.916	0.713	0.860	0.854	0.830
Li *et al.* (2014)	0.823	0.900	0.692	**0.980**	0.810	0.841
Ma and Latecki (2011)	0.881	0.920	0.756	0.868	**0.959**	0.877
Srinivasan *et al.* (2010)	0.845	0.916	0.787	0.888	0.922	0.872
Maji and Malik (2009)	0.869	0.724	0.742	0.806	0.716	0.771
Felzenszwalb *et al.* (2008)	**0.891**	**0.950**	0.608	0.721	0.391	0.712

Table 4.2: Comparison of classification accuracy on the ETHZ Shape Classes dataset.

	Classification Accuracy (%)
OCTAR	**88.00**
OCTAR - $\mathcal{E}_{App}$	85.33
VLFeat (Vedaldi and Fulkerson, 2008)	77.33

introduced by using the appearance information.

In order to compare the performance of our proposed shape-based method against an appearance-based method we conducted experiments in a classification task. We randomly selected 15 images from each of the five categories of ETHZ Shape Classes dataset for training. For each category, 15 images were randomly selected as test images. To use our proposed OCTAR method in a classification task, we assigned to each test image the class of the highly ranked object hypothesis according to Equation 4.12. As a reference appearance-based classification method we used the VLFeat (Vedaldi and Fulkerson, 2008) categorization demo, which is a BoW based system. This method uses dense multi-scale SIFT descriptors (Bosch *et al.*, 2007) and spatial histograms, visual vocabularies built using Elkan's KMeans and a homogeneous kernel map to transform a χ^2 Support Vector Machine (SVM) into a linear one (Vedaldi and Zisserman, 2011). The classification accuracy for the appearance-based method and our proposed OCTAR method with and without using appearance information are reported in Table 4.2. As it can be seen, our proposed OCTAR method, using only shape information, and combining shape and appearance, outperformed the appearance-based method in this experiment.

4.4.2 Performance Evaluation on Occluded Shapes

In order to obtain a more clear evaluation of the robustness of the proposed OCTAR method to partial occlusion and missing edges, we performed a second set of experiments over artificially occluded shapes. The experiments were conducted on two different well-known datasets. The first dataset is the Kimia Shapes99 dataset (Sebastian *et al.*, 2004), which includes 9 categories and 11 shapes in each category with variations in form, occlusion, articulation and missing parts. The second dataset is the Kimia Shapes216 dataset (Sebastian *et al.*, 2004). The Shapes216 database consists of 18 categories with 12 shapes in each category. In the two datasets, in each image there is only one object, defined by its silhouette, and at different scales, rotations and positions.

In order to show the robustness of the proposed method to partial occlusion, we generated another 14 datasets by artificially introducing occlusion of different magnitudes (10%, 20%,...,70%) to the Shapes99 and Shapes216 datasets. Occlusion was added by randomly removing 2 to 5 fragments of the entire contour, whose total length represents the desired partial occlusion. A sample image from the Shapes216 dataset at different occlusion levels is shown in Figure 4.9.

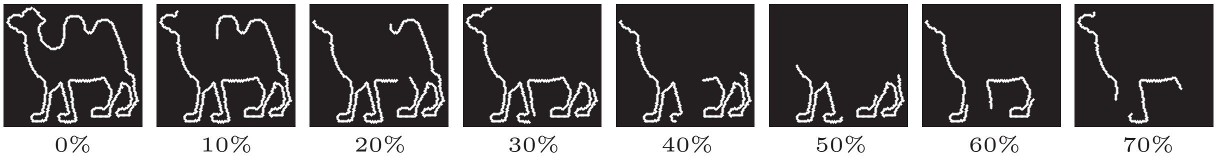

Figure 4.9: Example image from the Shapes216 dataset with different levels of occlusion (0%, 10%, 20%, 30%, 45% and 60%) used in the experiments.

As a measure to evaluate and compare the performance of the proposed shape matching schema in a shape retrieval scenario we use the so-called bull's eye score. Each shape in the database is compared with every other shape model, and the number of shapes of the same class that are among the $2N_c$ most similar is reported, where N_c is the number of instances per class. The bull's eye score is the ratio between the total number of shapes of the same class and the largest possible value. The results obtained by our proposed method were compared with those of the popular shape context (Belongie *et al.*, 2002) and IDSC (Ling and Jacobs, 2007) descriptors. Figure 4.10 shows the behavior of the bull's eye score of each method.

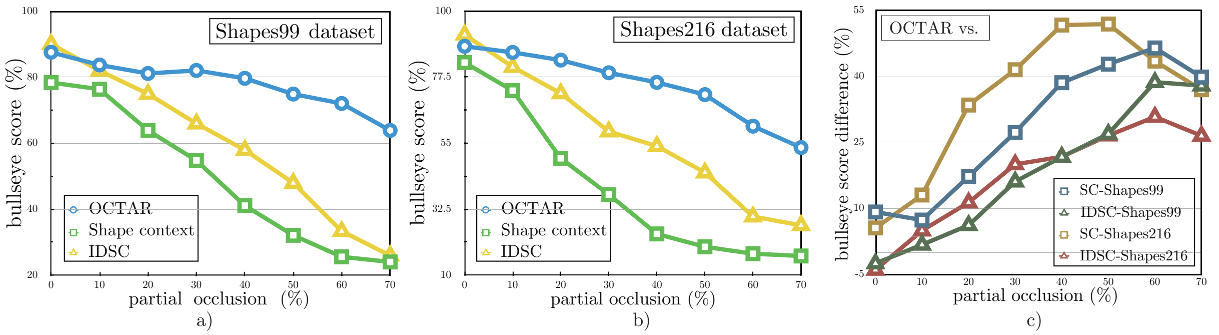

Figure 4.10: (*best seen in color*). Bull's eye score comparison between OCTAR, shape context and IDSC in the a) Shapes99 and b) Shapes216 datasets with different partial occlusions. In c) the OCTAR improvement compared to shape context and IDSC.

As expected, our proposed method outperformed the shape context and IDSC methods. Moreover, while increasing the occlusion level, the difference in terms of bull's eye score gets bigger, with about 30 - 50% higher bull's eye score across highly occluded images (see Figure 4.10(c)); which shows the advantages of OCTAR over the other two, in particular for highly occluded contours. The computation time of our proposed method has been also evaluated and compared against other methods. Table 4.3 shows the average time taken by OCTAR, shape context and IDSC for extracting and matching features of two shapes. These results were obtained on a single thread of a 2.2 GHz CPU and 8GB RAM PC. As it can be seen, OCTAR is faster than shape context and comparable to IDSC.

4.5 Summary

As a result of this work, a shape descriptor for open and closed contours, and a partial shape matching method have been proposed. The proposed descriptor and matching method allow us to find the best matching parts of a query object with a model in presence

Table 4.3: OCTAR average feature extraction and matching time for two images of the MPEG7 database, in milliseconds.

Method	Avg. computation time (ms)	Std dev
Shape context	1710	40.9
IDSC	6	0.1
OCTAR (our method)	45	3.2

of partial occlusion and noise. Also, the proposed method is invariant to rotation and translation. Unlike the LISF method, presented in Chapter 3, the OCTAR method is able to detect and recognize objects in complex real world images, as it is capable to deal with the intrinsic problems derived from using edgemaps obtained from real images. The OCTAR method allowed to evaluate object detection hypotheses according to several criteria, including the evaluation of the hypothesis appearance. In the next Chapter we present our proposed appearance-based representation method, which selects the most discriminative and representative visual words on a BoW-based representation.

Chapter 5

Improving Visual Vocabularies

Appearance-based features have proved to play an important role in object recognition. In our proposed method, OCTAR, presented in Chapter 4, we combined shape and appearance features for category-level object recognition, specifically by using appearance as a second level feature. In this Chapter we introduce our BoW-based appearance representation, which selects the most representative and discriminative visual words from a given visual vocabulary.

One of the most widely used approaches for representing images for object categorization is the Bag of Visual Words (BoW) approach (Csurka *et al.*, 2004). BoW-based methods have obtained remarkable results in recent years and they even obtained the best results for several classes in the recent PASCAL Visual Object Classes Challenge on object classification (Everingham *et al.*, 2011). The key idea of BoW approaches is to discretize the entire space of local features (*e.g.*, SIFT (Lowe, 2004)) extracted from a training set at interest points or densely sampled in the image. With this aim, clustering is performed over the set of features extracted from the training set in order to identify features that are visually equivalent. Each cluster is interpreted as a visual word, and all clusters form a so-called visual vocabulary. Later, in order to represent an unseen image, each feature extracted from the image is assigned to a visual word of the visual vocabulary; from which a histogram of occurrences of each visual word in the image is obtained, as illustrated in Figure 5.1.

One of the main limitations of the BoW approach is that the visual vocabulary is built

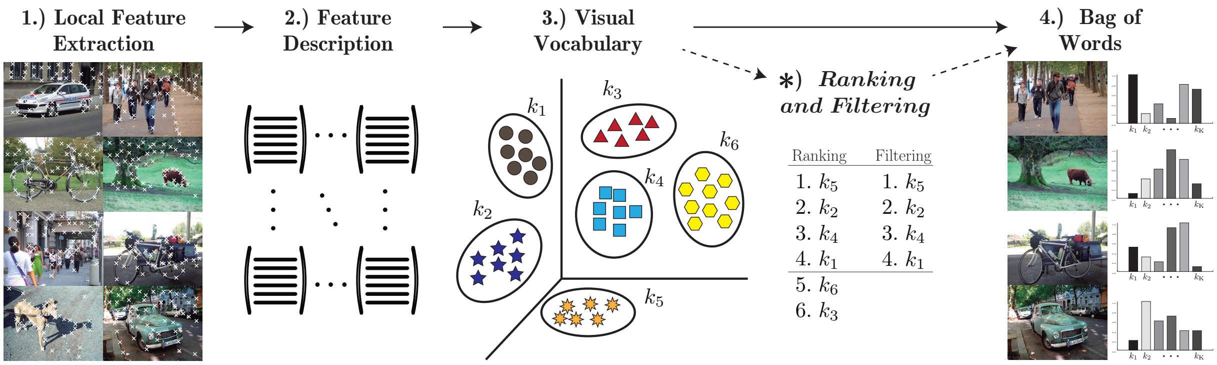

Figure 5.1: Classical BoW approach overview (steps 1 to 4). First, regions/points of interest are automatically detected and local descriptors over those regions/points are computed (step 1 and 2). Later in step 3, the descriptors are quantized into visual words to form the visual vocabulary. Finally, in step 4, the occurrences in the image of each specific word in the vocabulary for constructing the BoW feature are found. In this chapter, we propose to introduce step ($*$) in order to use only the most discriminative and representative visual words from the visual vocabulary in the BoW representation.

using features that belong to both the object and the background. This implies that the noise extracted from the image background is also considered as part of the object class description. Also, in the BoW representation, every visual word is used, regardless of its low representativeness or discriminative power. These elements may limit the quality of further classification processes. In addition, there is no consensus about which is the optimal way for building the visual vocabulary, *i.e.*, the clustering algorithm used, the number of clusters (visual words) that best describe the object classes, etc. When dealing with relatively small vocabularies, clustering can be executed several times and the best performing vocabulary can be selected through a validation phase. However, this becomes intractable for large image collections.

In this chapter, we propose three properties to assess the ability of a visual word to represent and discriminate an object class in the context of the BoW approach. We define three measures in order to quantitatively evaluate each of these properties. The visual words that best represent a class, best generalize over intra-class variability and best differentiate between object classes will obtain the highest scores for these measures. A methodology for reducing the size of the visual vocabulary based on these properties is also proposed. Our proposal does not depend on the clustering method used to create the visual vocabulary, the descriptor used (*e.g.*, SIFT, SURF, etc.) or the weighting scheme used (*e.g.*, *tf*, *tf-idf*, etc.). Therefore, it can be applied to a previously built vocabulary to improve its representativeness, since it does not build a new visual vocabulary, it rather finds the best visual words of a given visual vocabulary.

Experiments conducted on the Caltech-101 (Fei-Fei *et al.*, 2007) and Pascal VOC 2006 (Everingham *et al.*, 2006) datasets, in a classification task, demonstrate the improvement introduced by the proposed method. Tested with different vocabulary sizes, different interest points extraction and description methods, and different weighting schemas, the classification accuracies achieved using the entire vocabulary were always statistically inferior to those achieved by several of the vocabularies obtained by filtering the baseline vocabulary, using our proposed vocabulary size reducing methodology. Moreover, the best results were obtained with as few as the 13.4% and 34.5%, in average, of the baseline visual words for the Caltech-101 and Pascal VOC 2006 datasets, respectively. Compared with a state-of-the-art mutual information based method for feature selection our proposal obtains superior classification accuracy results for the highest compression rates and comparable results for the other filtering sizes.

5.1 Proposed Method

Visual vocabularies are commonly comprised by a lot of noisy visual words due to intra-class variability and the inclusion of features from the background during the vocabulary building process, among others. Later, for image representation every visual word is used, which may lead to an error-prone image representation.

In order to improve image representations, we introduce three properties and their corresponding quantitative evaluations to assess the ability of a visual word to represent and discriminate an object class in the context of the BoW approach. We also propose a methodology, based on these properties, for reducing the size of the visual vocabulary, discarding those visual words that worst describe an object class (*i.e.*, noisy visual words).

Reducing the vocabulary in such a manner will allow to have a more reliable and compact image representation.

We would like to emphasize that all the measures proposed in this section are used during the training phase; therefore, we can use all the knowledge about the data that is available during this phase.

5.1.1 Inter-class Representativeness Measure

A visual word could be comprised of features from different object classes, representing visual concepts or parts of objects common to those different classes. These common parts or concepts do not have necessarily to be equally represented inside the visual word because, even when similar, object classes should also have attributes that differentiate them. Therefore, we can say that, in order to best represent an object class, a property that a visual word must satisfy is to have a high representativeness of this class. In order to measure the representativeness of a class c_j in visual word k, the $\mathcal{M}_1$ measure is proposed as expressed in Formula 5.1.

$$\mathcal{M}_1(k, c_j) = \frac{f_{k,c_j}}{n_k}, \tag{5.1}$$

where n_k is the total number of features in visual word k and f_{k,c_j} represents the number of features of class c_j in visual word k, *i.e.*, the number of visual descriptors of class c_j that belong to the cluster corresponded to visual word k.

Figure 5.2 shows $\mathcal{M}_1$ values for two example visual words. In Figure 5.2 a) the circle class has a very high value of $\mathcal{M}_1$ because most of the features in the visual word belong to the circle class, being the opposite for the classes square and triangle that are poorly represented in the visual word. Figure 5.2 b) shows an example visual word where every class is nearly equally represented, therefore every class has similar $\mathcal{M}_1$ values.

5.1.2 Intra-class Representativeness Measure

A visual word could be comprised of features from different objects, many of them probably belonging to the same object class. Even when different, object instances from the

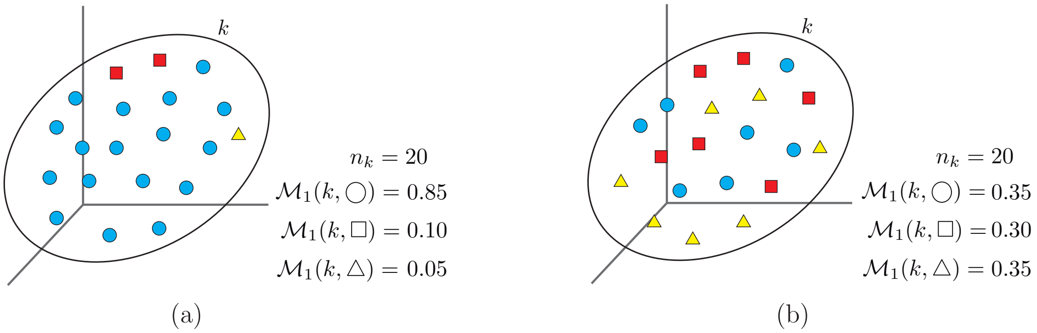
k
$n_k = 20$
$\mathcal{M}_1(k,\bigcirc) = 0.85$
$\mathcal{M}_1(k,\square) = 0.10$
$\mathcal{M}_1(k,\triangle) = 0.05$
(a)
k
$n_k = 20$
$\mathcal{M}_1(k,\bigcirc) = 0.35$
$\mathcal{M}_1(k,\square) = 0.30$
$\mathcal{M}_1(k,\triangle) = 0.35$
(b)

Figure 5.2: *(best seen in color.)* Examples of $\mathcal{M}_1$ measure values for a) a visual word with a well-defined representative class (circle class with high $\mathcal{M}_1$ value, square and triangle classes with low $\mathcal{M}_1$ values) and b) a visual word without any highly representative class (circle, square and triangle classes have low and very similar $\mathcal{M}_1$ values).

same class should share several visual concepts. Taking this into account, we can state that a visual word best describes a specific object class while more balanced are the features from that object class comprising the visual word, with respect to the number of different training objects belonging to that class. Therefore, we could say that, in order to represent an object class the best, a property that a visual word must satisfy is to have a high generalization or intra-class representativeness over this class.

To measure the intra-class representativeness of a visual word k for a given object category c_j, the μ measure is proposed, as expressed in Formula 5.2.

$$\mu(k, c_j) = \frac{1}{O_{c_j}} \sum_{m=1}^{O_{c_j}} \left| \frac{o_{m,k,c_j}}{f_{k,c_j}} - \frac{1}{O_{c_j}} \right|, \tag{5.2}$$

where O_{c_j} is the number of objects (images) of class c_j in the training set. o_{m,k,c_j} is the number of features extracted from object m of class c_j that belong to visual word k, and f_{k,c_j} is the number of features of class c_j that belong to visual word k. The term $1/O_{c_j}$ represents the ideal ratio of features of class c_j that guarantees the best balance, *i.e.*, the case where each object of class c_j is equally represented in visual word k.

The measure μ evaluates how much a given class deviates from its ideal value of intra-class variability balance. In order to make this value comparable with other classes and visual words, μ could be normalized using its maximum possible value, which is $\frac{2 \cdot O_{c_j} - 2}{O_{c_j}^2}$.

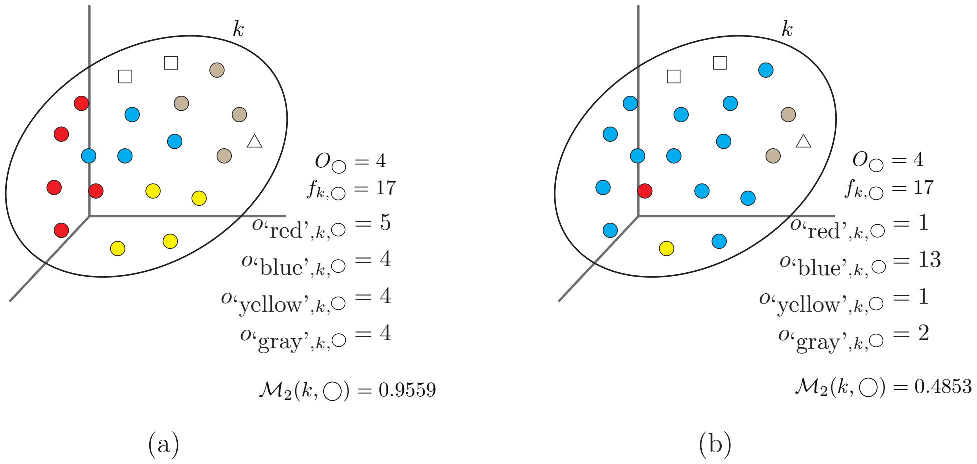
k
$O_{\bigcirc} = 4$
$f_{k,\bigcirc} = 17$
$o_{\text{'red'},k,\bigcirc} = 5$
$o_{\text{'blue'},k,\bigcirc} = 4$
$o_{\text{'yellow'},k,\bigcirc} = 4$
$o_{\text{'gray'},k,\bigcirc} = 4$
$\mathcal{M}_2(k, \bigcirc) = 0.9559$
(a)
k
$O_{\bigcirc} = 4$
$f_{k,\bigcirc} = 17$
$o_{\text{'red'},k,\bigcirc} = 1$
$o_{\text{'blue'},k,\bigcirc} = 13$
$o_{\text{'yellow'},k,\bigcirc} = 1$
$o_{\text{'gray'},k,\bigcirc} = 2$
$\mathcal{M}_2(k, \bigcirc) = 0.4853$
(b)

Figure 5.3: *(best seen in color.)* Examples of $\mathcal{M}_2$ measure values for the circle class in a) a visual word where there is a good balance between the number of features of different images of the circle class (high $\mathcal{M}_2$ value), and in b) the opposite case where only one image for the circle class is predominantly represented in the visual word (low $\mathcal{M}_2$ value). In the figure, different fill colors of each feature in the visual word represent features extracted from different object images of the same class.

Taking into account that μ takes its maximum value in the worst case of intra-class representativeness, the measure $\mathcal{M}_2$ is defined to take its maximum value in the case of ideal intra-class variability balance and to be normalized by $\max(\mu(k, c_j))$:

$$\mathcal{M}_2(k, c_j) = 1 - \frac{O_{c_j}}{2 \cdot (O_{c_j} - 1)} \sum_{m=1}^{O_{c_j}} \left| \frac{o_{m,k,c_j}}{s_{k,c_j}} - \frac{1}{O_{c_j}} \right|. \tag{5.3}$$

Figure 5.3 shows the values of $\mathcal{M}_2$ on two example visual words. In Figure 5.3 a), the number of features from the different images of the circle class in the visual word is well balanced, *i.e.*, the visual word generalizes well over intra-class variability for the circle class, hence this class presents a high $\mathcal{M}_2$ value. In contrast, in Figure 5.3 b) only one image from the circle class is well represented by the visual word. As the visual word represents a visual characteristic only present in one image, it is not able to well represent intra-class variability, therefore, the circle class will have a low value of $\mathcal{M}_2$ in this visual word.

5.1.3 Inter-class Distinctiveness Measure

$\mathcal{M}_1$ and $\mathcal{M}_2$ provide, under different perspectives, a quantitative evaluation of the ability of a visual word to describe a given class. However, we should not build a vocabulary just by selecting those visual words that best represent each object class, because this fact does not directly imply that the more representative words will be able to differentiate well one class from another, as a visual vocabulary is expected to do. Therefore, we can state that, in order to be used as part of a visual vocabulary, a desired property of a visual word is that it should have high values of $\mathcal{M}_1(k, c_j)$ and $\mathcal{M}_2(k, c_j)$ (represents well the object class), while having low values of $\mathcal{M}_1(k, \{c_j\}^C)$ and $\mathcal{M}_2(k, \{c_j\}^C)$ (misrepresents the rest of the classes), *i.e.*, it must have high discriminative power.

In order to quantify the distinctiveness of a visual word for a given class, the measure $\mathcal{M}_3$ is proposed. $\mathcal{M}_3$ expresses how much the object class that is best represented by visual word k is separated from the other classes in the $\mathcal{M}_1$ and $\mathcal{M}_2$ rankings.

Let $\Theta_{\mathcal{M}}(K, c_j)$ be the set of values of a given measure $\mathcal{M}$ for the set of visual words $K = \{k_1, k_2, ..., k_N\}$ and the object class c_j, sorted in descending order of the value of $\mathcal{M}$. Let $\Phi(k, c_j)$ be the position of visual word $k \in K$ in $\Theta_{\mathcal{M}}(K, c_j)$. Let $P_k = \min_{c_j \in C}(\Phi(k, c_j))$ be the best position of visual word k in the set of all object classes $C = \{c_1, c_2, ..., c_Q\}$. Let $c_k = \arg\min_{c_j \in C}(\Phi(k, c_j))$ be the object class where k has position P_k. Then, the inter-class distinctiveness (measure $\mathcal{M}_3$), of a given visual word k for a given measure $\mathcal{M}$, is defined as expressed in Formula 5.4.

$$\mathcal{M}_3(k, \mathcal{M}) = \frac{1}{(|C|-1)(|K|-1)} \sum_{c_j \neq c_k}^{C} (\Phi(k, c_j) - P_k). \tag{5.4}$$

In Figure 5.4, the $\mathcal{M}_3$ measure is calculated for two visual words (*i.e.*, k_2 and k_5) of a six visual words and three classes example. Visual word k_2 is among the top items of the representativeness ranking for every class in the example. Despite this, k_2 has low discriminative power because describing well several classes makes harder the process of differentiate one class from another. In contrast, visual word k_5 is highly discriminative because it describes well only one class.

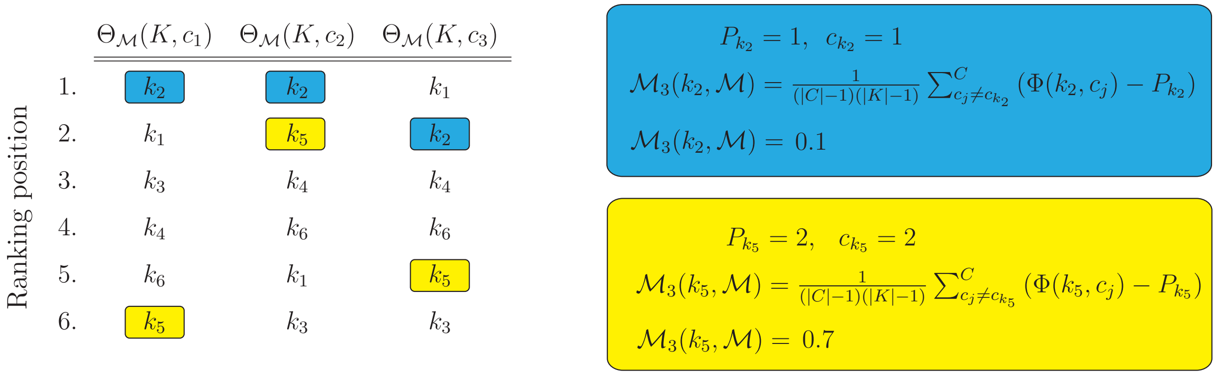

Ranking position	$\Theta_{\mathcal{M}}(K,c_1)$	$\Theta_{\mathcal{M}}(K,c_2)$	$\Theta_{\mathcal{M}}(K,c_3)$
1.	k_2	k_2	k_1
2.	k_1	k_5	k_2
3.	k_3	k_4	k_4
4.	k_4	k_6	k_6
5.	k_6	k_1	k_5
6.	k_5	k_3	k_3

$$P_{k_2} = 1, \quad c_{k_2} = 1$$
$$\mathcal{M}_3(k_2, \mathcal{M}) = \tfrac{1}{(|C|-1)(|K|-1)} \textstyle\sum_{c_j \neq c_{k_2}}^{C} \left(\Phi(k_2, c_j) - P_{k_2}\right)$$
$$\mathcal{M}_3(k_2, \mathcal{M}) = 0.1$$

$$P_{k_5} = 2, \quad c_{k_5} = 2$$
$$\mathcal{M}_3(k_5, \mathcal{M}) = \tfrac{1}{(|C|-1)(|K|-1)} \textstyle\sum_{c_j \neq c_{k_5}}^{C} \left(\Phi(k_5, c_j) - P_{k_5}\right)$$
$$\mathcal{M}_3(k_5, \mathcal{M}) = 0.7$$

Figure 5.4: *(best seen in color.)* Example of $\mathcal{M}_3$ measure for two visual words. k_2 has low discriminative power because it represents well several classes, while k_5 has high discriminative power because it describes well only one class.

5.1.4 On Ranking and Reducing the Size of Visual Vocabularies

The proposed measures provide a quantitative evaluation of the representativeness and distinctiveness of the visual words in a vocabulary for each class. The visual words that best represent a class, best generalize over intra-class variability and best differentiate between object classes, will obtain the highest scores for these measures. In this section, we present a methodology for ranking and reducing the size of the visual vocabularies, towards more reliable and compact image representations.

Let $\Theta^{\mathcal{M}_1}(K)$ and $\Theta^{\mathcal{M}_2}(K)$ be the rankings of vocabulary K, using measures $\mathcal{M}_3(K, \mathcal{M}_1)$ and $\mathcal{M}_3(K, \mathcal{M}_2)$, respectively. $\Theta^{\mathcal{M}_1}(K)$ and $\Theta^{\mathcal{M}_2}(K)$ provide a ranking of the vocabulary based on the distinctiveness of visual words according to inter-class and intra-class variability, respectively.

In order to find a consensus, $\Theta(K)$, between both rankings $\Theta^{\mathcal{M}_1}(K)$ and $\Theta^{\mathcal{M}_2}(K)$ a consensus-based voting method can be used; in our case, we decided to use the Borda Count algorithm (Emerson, 2013) although any other can be used as well. The Borda Count algorithm obtains a final ranking from multiple rankings over the same set. Given $|K|$ visual words, a visual word receives $|K|$ points for a first preference, $|K| - 1$ points for a second preference, $|K| - 2$ for a third, and so on for each ranking independently. Later, individual values for each visual word are added and a final ranking obtained.

From this final ranking a reduced vocabulary can be obtained by selecting the first N visual words. As pointed in (Liu and Shah, 2008), the size of the vocabulary affects the performance and there is a vocabulary size which can achieve maximal accuracy, which depends on the dataset, the number of classes and the data nature, among others. In our experiments, we explore different vocabulary sizes, over different datasets, different interest points extraction and description methods, different weighting schemas, and different classifiers.

5.2 Experimental Evaluation

In this chapter we have presented a methodology for improving BoW-based image representation by using only the most representative and discriminative visual words in the vocabulary. As it was stated in previous sections, our proposal does not depend on the algorithm used for building the set of visual words, the descriptor used nor the weighting scheme used. Therefore, the proposed methodology could be applied for improving the accuracy of any of the methods reported in the literature, which are based on a BoW approach.

The main goal of the experiments we present in this section is to quantitatively evaluate the improvement introduced by our proposal to the BoW-based image representation, over two standard datasets commonly used in object categorization. The experiments were focused on: a) to assess the validity of our proposal in a classic BoW-based classification task, b) to evaluate the methodology directly with respect to other kinds of feature selection algorithms in the state of the art, and c) to measure the time our methodology spent in order to filter the visual vocabulary built for each dataset. All the experiments were done on a single thread of a 3.6 GHz Intel i7 processor and 64GB RAM PC.

The experiments conducted in order to evaluate our proposal were done in two well-known datasets: Caltech-101 (Fei-Fei *et al.*, 2007) and Pascal VOC 2006 (Everingham *et al.*, 2006).

The Caltech-101 dataset (Fei-Fei *et al.*, 2007) consists of 102 object categories. There are about 40 to 800 images per category and most categories have about 50 images. The Pascal VOC 2006 dataset (Everingham *et al.*, 2006) consists of 10 object categories. In total, there are 5304 images, split into 50% for training/validation and 50% for testing. The distributions of images and objects by class are approximately equal across the training/validation and test sets.

5.2.1 Assessing the Validity in a Classic BoW-based Classification Task

As it was mentioned before, the goal of the first experiment is to assess the validity of our proposal. With this aim, we evaluate the accuracy in a classic BoW-based classification task, with and without applying our vocabulary filtering methodology.

In the experiments presented here, we use for image representation the BoW schema presented in Figure 5.1 with the following specifications:

- Interest points are detected and described using two methods: SIFT (Lowe, 2004) and SURF (Bay *et al.*, 2008).

- K-means, with four different K values, is used to build the visual vocabularies; these vocabularies constitute the baseline. For Caltech-101 dataset we used K=10000, 15000, 20000 and 25000, while for Pascal VOC 2006 dataset we used K=200, 1000, 5000 and 10000.

- Each of the baseline vocabularies is ranked using our proposed visual words ranking methodology.

- Later, nine new vocabularies are obtained by filtering each baseline vocabulary, leaving the 10%, 20%, ..., 90%, respectively, of the most representative and discriminative visual words based on the obtained ranking.

- Two weighting schemas are used for image representation: *tf* and *tf-idf*.

- For both datasets we randomly selected 10 images from all the categories for building the visual vocabularies. The rest of the images were used as test images; but, as in

(Lazebnik *et al.*, 2006), we limited to 50 the number of test images per category.

After that, we tested the obtained visual vocabularies in a classification task, using SVM (with a linear kernel) and KNN (where K is optimized with respect to the leave-one-out error) as classifiers. For each visual vocabulary, test images are represented using this vocabulary and, a 10-fold 10-times cross-validation process is conducted, where nine of the ten partitions are used for training and the other one for testing the trained classifier. The mean classification accuracy along the ten iterations is reported.

Figures 5.5 and 5.6 show the mean classification accuracy results over the cross-validation process using SVM and KNN, respectively, on the Caltech-101 dataset. Figures 5.7 and 5.8 show the same for the Pascal VOC 2006 dataset. In Figures 5.5 to 5.8, subfigures (a) and (b) show the results using SIFT descriptor; results for SURF are shown in subfigures (c) and (d). Results for the two different weighting schemas, *i.e.*, *tf* and *tf-idf*, are shown in subfigures (a) (c), and (b) (d), respectively.

It can be seen that in both datasets, for every configuration, our proposed methodology allows to obtain reduced vocabularies that outperformed the classical BoW approach (baseline).

Table 5.1 summarizes the results presented in Figures 5.5 and 5.6 for the Caltech-101 dataset. The results in Figures 5.7 and 5.8 are summarized in Table 5.2. For every experiment configuration, Tables 5.1 and 5.2 show the baseline classification accuracy against the best result obtained by the proposed method with both SVM and KNN classifiers. The size of the filtered vocabulary in which the best result was obtained is also showed.

Discussion

The experimental results presented in this section validate the claimed contributions of our proposed method. As it can be seen in Tables 5.1 and 5.2, the best results obtained with our proposed method outperform those obtained with the whole vocabularies. For the experiments conducted in the Caltech-101 dataset, our average best results outperformed the baseline by a 4.6% and 4.8% in mean classification accuracy using SVM and KNN, respectively. In the Pascal VOC 2006 dataset there was a 3.2% and 7% improvement for SVM and KNN, respectively. As noticed on Figures 5.5 to 5.8, the trend of the performance with respect to the filter size is not the same in the two considered datasets. In the Caltech-101 dataset, for smaller filter sizes higher accuracies, while in the Pascal VOC 2006 dataset a so well defined trend was not noticed. We suspect that the Pascal VOC 2006 dataset does not present a definite trend due to its specific characteristics, *i.e.*, a fewer number of classes, fewer number of training images and smaller sizes initial vocabularies. Nonetheless, despite not having a definite trend, and as mentioned before, the reduced vocabularies mostly obtained better classification accuracy than the entire vocabulary in the Pascal VOC 2006 dataset.

In order to validate the improvement obtained by the proposed method, the statistical significance of the obtained results was verified. For testing the statistical significance we used the Mann-Whitney test (Mann and Whitney, 1947), with a 95% of confidence. Appendix A presents the detailed explanation of this test. An implementation of the test can be found in (vas, 2013). As a result of the Mann-Whitney test, it has been verified that the results obtained in both datasets, by the proposed method, are statistically superior to those obtained by the baseline.

In addition, the best results using the filtered vocabularies were obtained with vocabularies several times smaller than the baseline vocabularies, *i.e.*, 6 and 10 times smaller in average using SVM and KNN, respectively, for the Caltech-101 datasets, and 2 and 5 times smaller in average for the Pascal VOC 2006 dataset with SVM and KNN, respectively. Furthermore, vocabularies 10 times smaller always obtained better accuracy results than the baseline vocabularies in the Caltech-101 dataset, and in the 78.1% of the experiments on the Pascal VOC 2006 dataset. Obtaining smaller vocabularies implies more compact image representations, that will have a direct impact on the efficiency of further processing based on these image representations, and less memory usage.

Also, the conducted experiments provide evidence that a large number of visual words in a vocabulary are noisy or little discriminative. Discarding these visual words allows for a better and more compact image representation.

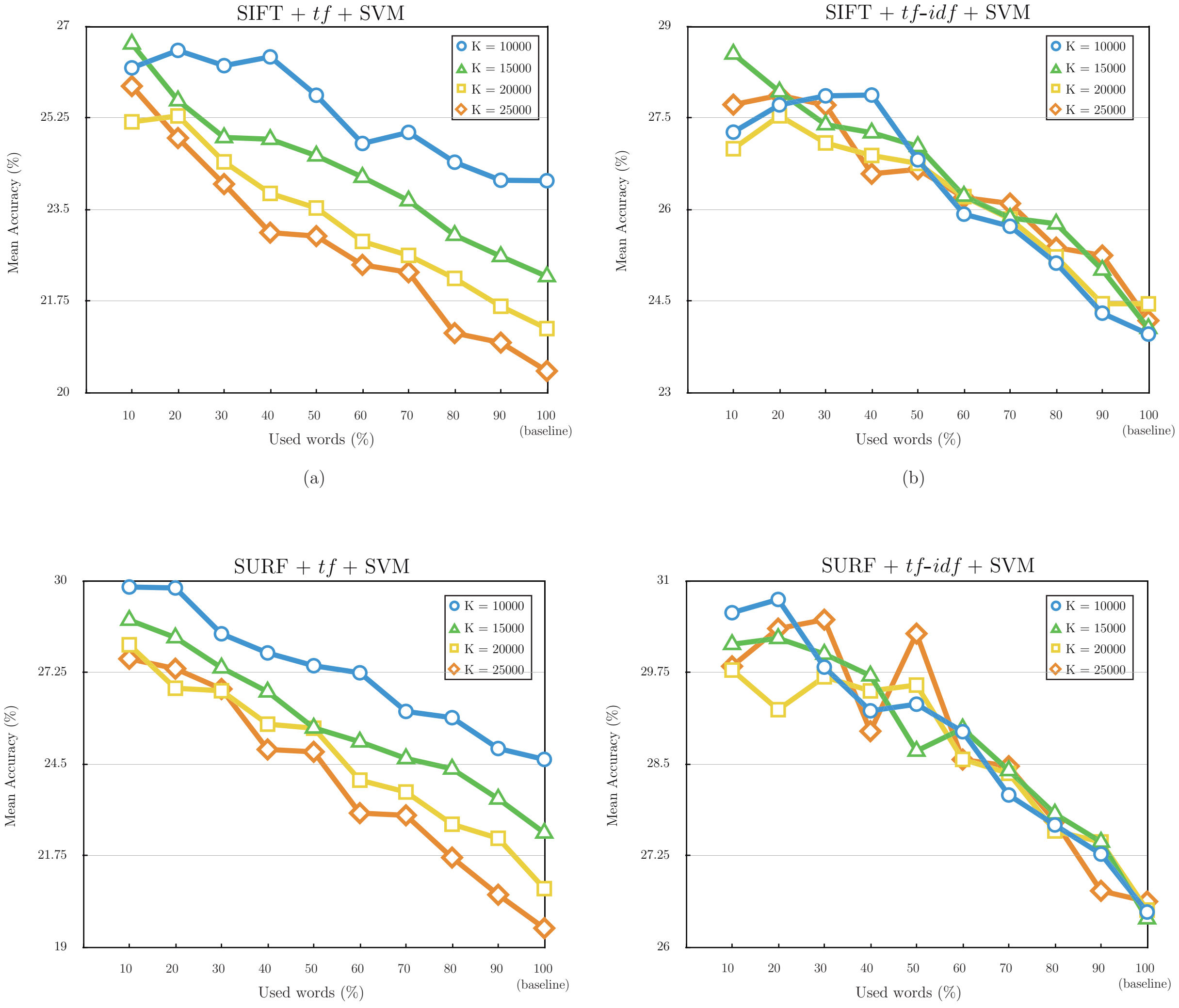

(a)

(b)

(c)

(d)

Figure 5.5: Mean classification accuracy results for SVM cross-validation on the Caltech-101 dataset. As can be seen, using the reduced vocabularies always resulted in better classification accuracies.

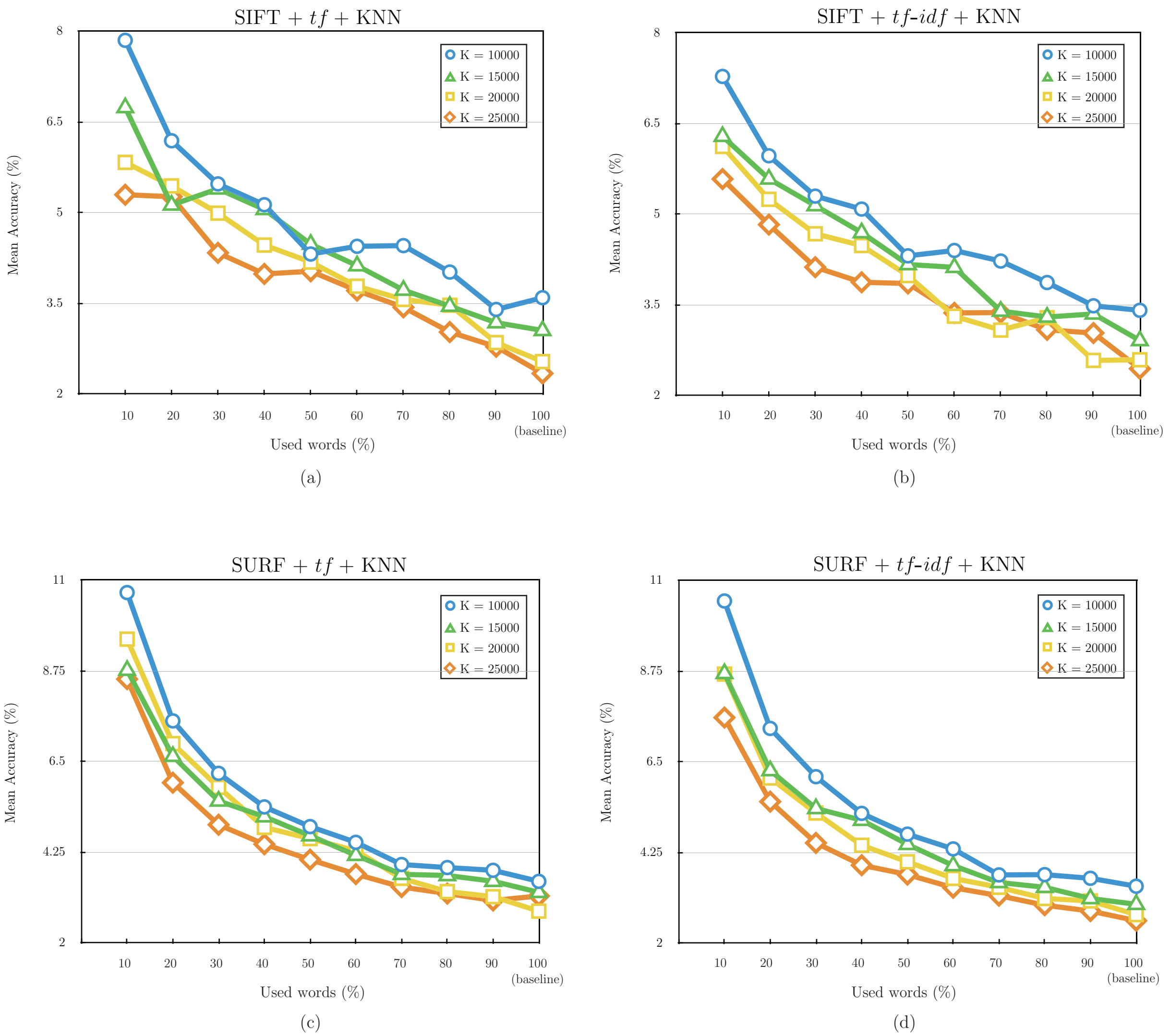

(a)

(b)

(c)

(d)

Figure 5.6: Mean classification accuracy results for KNN cross-validation on the Caltech-101 dataset. As can be seen, using the reduced vocabularies always resulted in better classification accuracies.

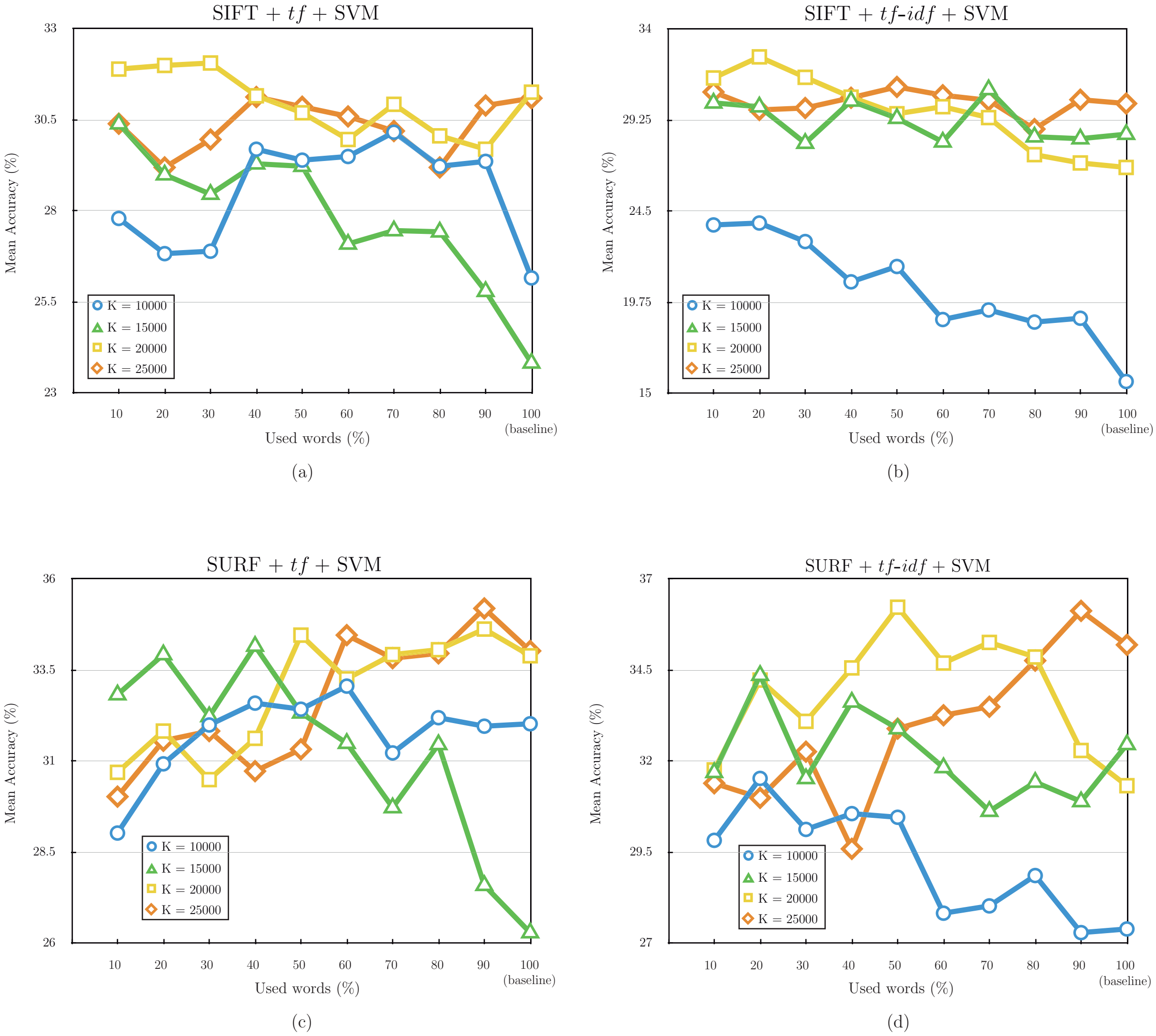

(a)

(b)

(c)

(d)

Figure 5.7: Mean classification accuracy results for SVM cross-validation on the Pascal VOC 2006 dataset. As can be seen, using the reduced vocabularies in most of the cases resulted in better classification accuracies.

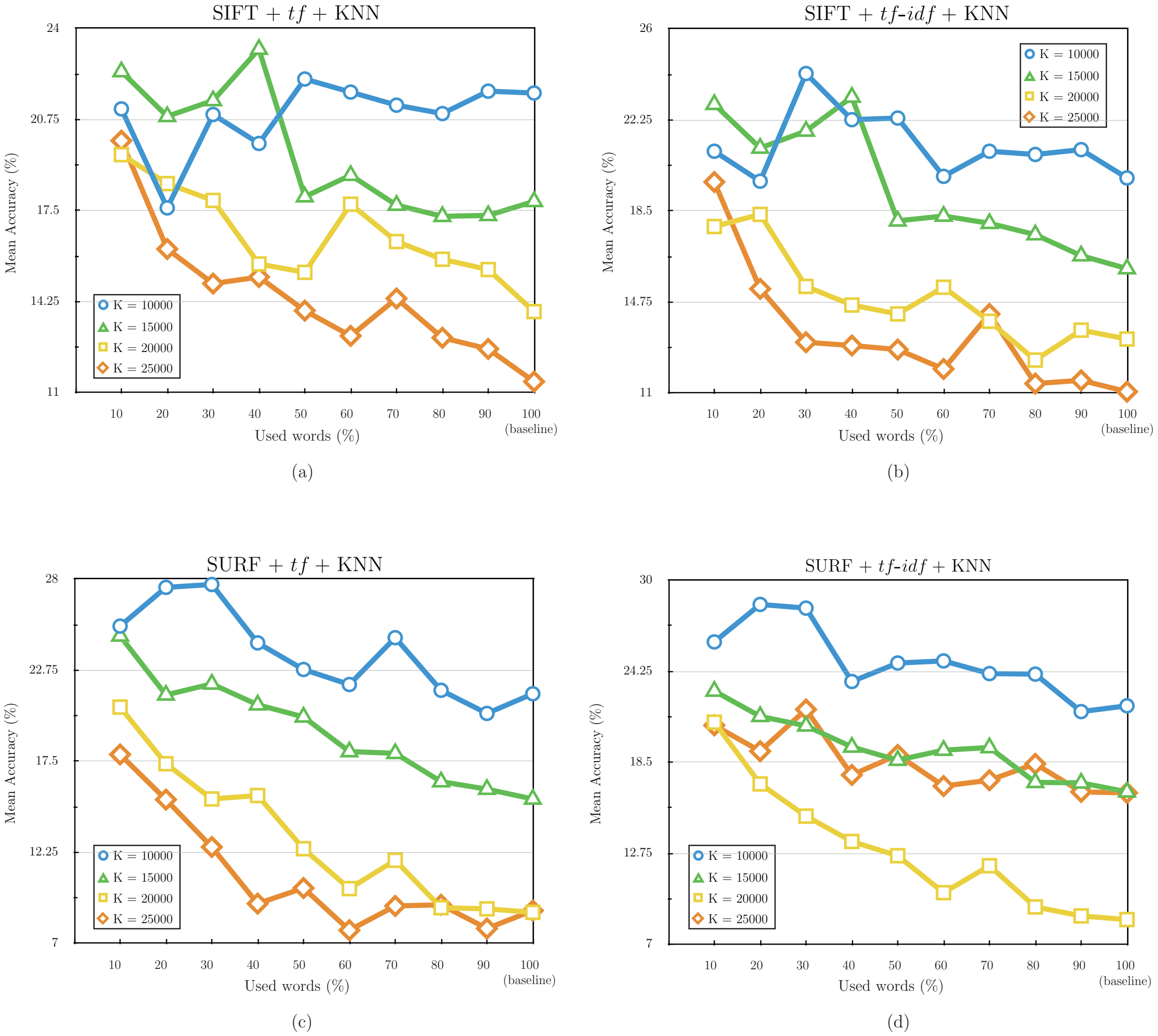

(a)

(b)

(c)

(d)

Figure 5.8: Mean classification accuracy results for KNN cross-validation on the Pascal VOC 2006 dataset. As can be seen, using the reduced vocabularies in most of the cases resulted in better classification accuracies.

Table 5.1: Summarized classification accuracy results for the Caltech-101 dataset.

Descriptor	**Weighting schema**	**K**	**SVM**			**KNN**		
			Base-line	**Best result**	**Best filter size (%)**	**Base-line**	**Best result**	**Best filter size (%)**
SIFT	*tf*	10000	24.05	**26.54**	20	3.60	**7.86**	10
		15000	22.22	**26.66**	10	3.06	**6.74**	10
		20000	21.22	**25.28**	20	2.54	**5.84**	10
		25000	20.41	**25.85**	10	2.34	**5.30**	10
	tf-idf	10000	23.96	**27.87**	40	3.41	**7.28**	10
		15000	24.05	**28.55**	10	2.91	**6.29**	10
		20000	24.45	**27.53**	20	2.60	**6.13**	10
		25000	24.18	**27.87**	20	2.45	**5.59**	10
SURF	*tf*	10000	24.63	**29.81**	10	3.53	**10.70**	10
		15000	22.43	**28.82**	10	3.26	**8.77**	10
		20000	20.75	**28.08**	10	2.80	**9.54**	10
		25000	19.56	**27.66**	10	3.17	**8.55**	10
	tf-idf	10000	26.48	**30.74**	20	3.42	**10.50**	10
		15000	26.39	**30.21**	20	2.97	**8.70**	10
		20000	26.50	**29.78**	10	2.72	**8.69**	10
		25000	26.62	**30.47**	30	2.57	**7.61**	10
Average			23.62	**28.23**	16.8	2.96	**7.76**	10

Table 5.2: Summarized classification accuracy results for the Pascal VOC 2006 dataset.

Descriptor	**Weighting schema**	**K**	**SVM**			**KNN**		
			Base-line	**Best result**	**Best filter size (%)**	**Base-line**	**Best result**	**Best filter size (%)**
SIFT	*tf*	200	26.17	**30.17**	70	21.70	**22.20**	50
		1000	23.83	**30.40**	10	17.83	**23.27**	40
		5000	31.27	**32.07**	30	13.90	**19.50**	10
		10000	31.10	**31.13**	40	11.40	**20.00**	10
	tf-idf	200	15.63	**23.90**	20	19.87	**24.17**	30
		1000	28.53	**30.87**	70	16.13	**23.20**	40
		5000	26.80	**32.57**	20	13.23	**18.37**	20
		10000	30.13	**31.00**	50	11.07	**19.70**	10
SURF	*tf*	200	32.03	**33.07**	60	21.40	**27.70**	30
		1000	26.30	**34.17**	40	15.33	**24.73**	10
		5000	33.90	**34.63**	90	8.80	**20.63**	10
		10000	34.03	**35.20**	90	8.90	**17.90**	10
	tf-idf	200	27.40	**31.53**	20	22.07	**28.47**	20
		1000	32.47	**34.37**	20	16.63	**23.00**	10
		5000	31.33	**36.23**	50	8.57	**21.03**	10
		10000	35.20	**36.13**	90	16.57	**21.83**	30
Average			29.13	**32.34**	48	15.21	**22.23**	21.25

Table 5.3: Computation time of visual vocabulary ranking compared to vocabulary building.

Dataset	K	Vocabulary building (K-means) computation time (s)	Vocabulary ranking (proposed method) computation time (s)
Caltech-101 (188 248 training features)	10000	4723.452	**8.111**
	15000	6711.089	**18.622**
	20000	7237.885	**33.890**
	25000	9024.024	**54.338**
Pascal VOC 2006 (114 697 training features)	200	119.274	**0.004**
	1000	490.028	**0.019**
	5000	1580.407	**0.228**
	10000	3803.964	**0.986**

5.2.2 Comparison with Other Kinds of Feature Selection Algorithms

The aim of the second experiment is to compare our proposal with respect to other kind of feature selection algorithm. With this purpose, we compare the accuracy of our vocabulary filtering methodology with respect to the accuracy of the MI-based method proposed in (Zhang *et al.*, 2014), in a classification task; the experiment was done over the Caltech-101 dataset. As it was mentioned in Chapter 2, the MI-based method proposed in (Zhang *et al.*, 2014) obtains the best results among the feature selection and compression methods of image representation for object categorization.

In the experiments presented here, we use for image representation a BoW-based schema with the following specifications:

- PHOW features (dense multi-scale SIFT descriptors) (Bosch *et al.*, 2007).
- Spatial histograms as image descriptors.
- Elkan's K-means (Elkan, 2003), with five different K values (K= 256, 512, 1024, 2048 and 4096), is used to build the visual vocabularies; these vocabularies constitute the baseline.
- Each of the baseline vocabularies is ranked using the MI-based method proposed in (Zhang *et al.*, 2014) and our proposed visual vocabulary ranking methodology.
- Later, nine new vocabularies are obtained by filtering each baseline vocabulary, leaving the 10%, 20%, ..., 90%, respectively.
- We randomly selected 15 images from each of the 102 categories of Caltech-101 dataset, in order to build the visual vocabularies. For each category, 15 images were randomly selected as test images.

We tested the obtained visual vocabularies in a classification task, using a homogeneous kernel map to transform a χ^2 Support Vector Machine (SVM) into a linear one (Vedaldi and Zisserman, 2011). The classification accuracy is reported in Figure 5.9.

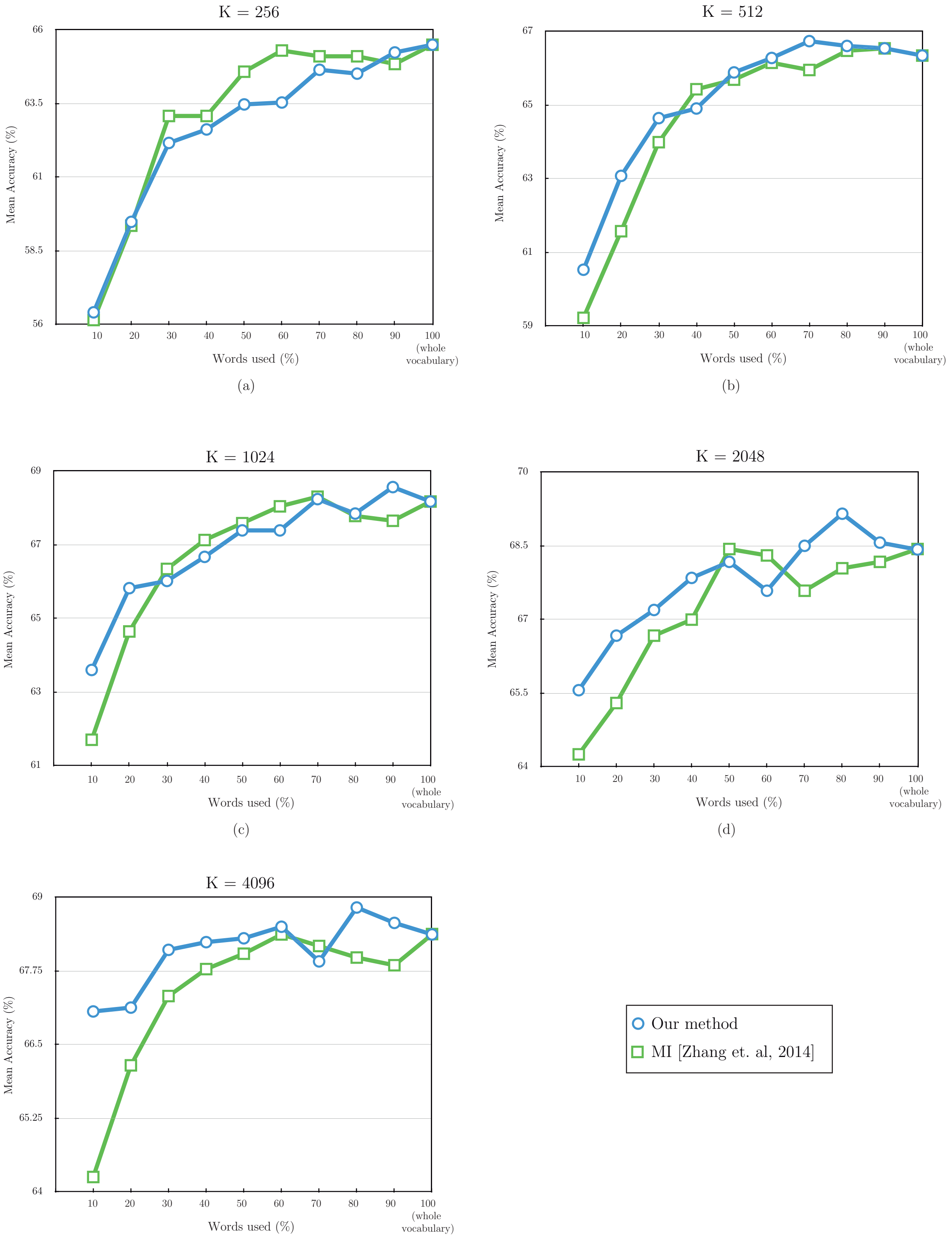

(a)

(b)

(c)

(d)

(e)

Figure 5.9: Comparison of classification accuracy results, on the Caltech-101 dataset, between the proposed methodology and the MI-based method proposed in (Zhang *et al.*, 2014).

As it can be seen in Figure 5.9, for each value of K used in the experiment, our proposal obtains the best classification accuracy results for the highest compression rates. Besides, for the other filtering sizes our proposal and the MI-based method attains comparable results.

5.2.3 Computation Time of the Visual Vocabulary Ranking

The computation time of the visual vocabulary ranking methodology has also been evaluated. Table 5.3 shows the time in seconds taken for the ranking method in different size vocabularies, for the Caltech-101 and the Pascal VOC 2006 dataset. In Table 5.3, the ranking time is compared with the time needed to build the visual vocabulary.

As can be seen in Table 5.3, the proposed methodology can be used to improve visual vocabularies without requiring much extra computation time.

5.3 Summary

In this chapter we devised a methodology for reducing the size of visual vocabularies that allows to obtain more discriminative and representative visual vocabularies for BoW image representation. The vocabulary reduction is based on three properties and their corresponding quantitative measures that express the inter-class representativeness, the intra-class representativeness and inter-class distinctiveness of visual words. The experimental results presented in this chapter showed that, in average, with only 25% of the ranked vocabulary, statistically superior classification results can be obtained, compared to the classical BoW representation using the entire vocabularies. Therefore, the proposed method, in addition to providing accuracy improvements, provides a substantial efficiency improvement. Also, compared with a mutual information based method our proposal obtained superior results for the highest compression rates and comparable results for the other filtering sizes. The method proposed in this Chapter provides a discriminative, representative and compact appearance representation of the object hypotheses formed by the OCTAR method, presented in Chapter 4.

Chapter 6

Conclusions

6.1 Summary and Conclusions

Shape information has shown to be useful in the representation of category-level objects, even in the presence of partial occlusion, changes in rotation, translation and scale, and noise in the contour.

As a result of this work, a method for shape feature extraction, description and matching of binary images, invariant to rotation, translation and scale, has been developed. The proposed method allowed to overcome the intrinsic disadvantages of only using local or global features by capturing the local structure of shape and later using it holistically for matching. In the conducted experiments, our method showed larger robustness to partial occlusion than other methods in the state of the art. Also, the proposal of a massively parallel implementation in CUDA of the two most time-consuming stages of LISF showed that significant speed-ups could be achieved, improving the efficiency of the systems.

In order to deal with the intrinsic problems derived from using edges extracted from real images, it was necessary to propose a shape descriptor that was particularly suitable for partial shape matching of both open and closed contours extracted from edgemap images. Furthermore, to propose a partial shape matching method robust to partial occlusion, noise, rotation and translation in the contour was needed. The use of a self-containing shape descriptor has shown to be essential for obtaining partial matches efficiently. The contour fragments configuration descriptor had a key role in forming object hypotheses coherently with the model, allowing to analyze the spatial relations and structure between edge fragments that could be joined to form an object hypothesis.

Appearance information has shown to provide important cues for object recognition. By combining shape and appearance through the evaluation of the appearance of the shape-based object detection hypotheses, allowed us to better discriminate object hypotheses, particularly in those classes with distinctive texture. Under the BoW approach, the results presented in this thesis, showed that not every visual word has the same relevance for the object representation. Using information about the class and object labels of the features in the visual vocabulary allowed us to obtain a more compact, discriminative and representative visual vocabulary, with considerable improvements in accuracy and efficiency.

6.2 Main Contributions

The main contributions of this thesis are:

a) A shape-based object recognition method, named LISF, that is invariant to rotation, translation and scale, and present certain robustness to partial occlusion. LISF, for highly occluded images largely outperformed other popular shape description methods and retain comparable results for not occluded images.

b) A massively parallel implementation in CUDA of the two most time-consuming stages of LISF, *i.e.*, the feature extraction and feature matching steps, which achieves speed-ups of up to 32x and 34x, respectively.

c) A shape-based object recognition method, named OCTAR, able to deal with the intrinsic problems derived from using edges extracted from real images, *i.e.*, broken and missing edge fragments that represent the target object, edge fragment wrongly connected to another object or background edges, and background cluttering. OCTAR, for highly occluded images largely outperformed other popular shape description methods and retained comparable results for not occluded images. Also, outperformed other methods in the state of the art in object detection in real images.

d) Three properties and their corresponding quantitative evaluation measures to assess the ability of a visual word to represent and discriminate an object class, in the context of the BoW approach. Also, based on these properties, we proposed a methodology for reducing the size of the visual vocabulary, retaining those visual words that best describe an object class. Using our reduced vocabularies the classification performance is improved with a significant reduction of the image representation size.

The combination of these contributions is a step forward on the development of the field of object recognition, an important and still open problem in Computer Vision.

6.3 Future Work

The results obtained in this thesis did not conclude the studies on shape and appearance-based category-level object recognition. Based on the obtained results, we propose as future work:

a) The OCTAR descriptor also provides information of the concavity/convexity of the contour. This information could be used to generate a binary OCTAR descriptor, based on its sign (concavity/convexity). The binary OCTAR descriptor could be used for shape indexing or for discarding not relevant object hypotheses with a smaller computational cost.

b) To propose a massively parallel implementation in GPU of the OCTAR method, specifically for the matching and hypotheses building stages.

c) The properties of visual words and their corresponding quantitative measures proposed in Chapter 5 could be further explored in order to propose a weighting schema to improve image representation, to propose a classifier that makes use of such information about the attributes and to define a measure that help us to automatically choose the more adequate filter size.

6.4 Publications

The following publications were generated as result of this doctoral research:

1. Leonardo Chang, Airel Pérez-Suarez, Miguel Arias-Estrada, José Hernández-Palancar, and L. Enrique Sucar. Improving visual vocabularies: a more discriminative, representative and compact bag of visual words. Submitted to Machine Vision and Applications journal. May 2014.

2. Leonardo Chang, Miriam M. Duarte, L. Enrique Sucar, and Eduardo F. Morales. A Bayesian approach for object classification based on clusters of SIFT local features. Expert Systems with Applications. 39, 2 (February 2012), 1679-1686, 2012.

3. Leonardo Chang, Miguel Arias-Estrada, L. Enrique Sucar, and José Hernández Palancar. LISF: An invariant local shape features descriptor robust to occlusion. In ICPRAM 2014 - Proceedings of the 3rd International Conference on Pattern Recognition Applications and Methods, ESEO, Angers, Loire Valley, France, 6-8 March, 2014, pages 429437, 2014.

4. Leonardo Chang, Miguel Arias-Estrada, José Hernández-Palancar, and L. Enrique Sucar. Partial shape matching and retrieval under occlusion and noise. In Progress in Pattern Recognition, Image Analysis, Computer Vision, and Applications - 19th Iberoamerican Congress, CIARP 2014, Puerto Vallarta, Mexico, November 2-5, 2014. Proceedings, pages 151158, 2014.

5. Leonardo Chang, Miguel Arias-Estrada, José Hernández-Palancar, and L. Enrique Sucar. An Efficient Shape Feature Extraction, Description and Matching Method using GPU. In Maria De Marsico, Antoine Tabbone and Ana Fred editors, ICPRAM 2014 - Best Papers, Lecture Notes in Computer Science. Springer. 2014.

6. Leonardo Chang, Miguel Arias-Estrada, L. Enrique Sucar, and José Hernández Palancar. Efficient Extraction and Matching of LISF Features in GPU. Poster Session of GTC 2014: GPU Technology Conference 2014, San José California, USA, 2014.

7. Leonardo Chang, Miguel Arias-Estrada, L. Enrique Sucar, and José Hernández Palancar. Efficient Local Shape Features Matching using CUDA. Poster Session of GTC 2013: GPU Technology Conference 2013, San José California, USA, 2013.

8. Leonardo Chang, Airel Pérez-Suárez, Máximo Rodríguez-Collada, José Hernández-Palancar, Miguel Arias-Estrada and L. Enrique Sucar. Assessing the Distinctiveness and Representativeness of Visual Vocabularies. Submitted to CIARP 2015.

9. Leonardo Chang, Miguel Arias-Estrada, José Hernández-Palancar, and L. Enrique Sucar. Object Detection through Partial Contour Fragments Matching. Submitted to CIARP 2015.

Bibliography

(2013) Concepts and applications of inferential statistics. URL http://vassarstats.net/textbook/. URL http://vassarstats.net/textbook/

Adamek T, O'Connor NE (2004) A multiscale representation method for nonrigid shapes with a single closed contour. IEEE Trans Circuits Syst Video Techn 14(5):742–753, URL http://dblp.uni-trier.de/db/journals/tcsv/tcsv14.html#Adamek004

Agarwal S, Awan A, Roth D (2004) Learning to detect objects in images via a sparse, part-based representation. IEEE Transactions on Pattern Analysis and Machine Intelligence 26(11):1475–1490, URL http://www.ncbi.nlm.nih.gov/pubmed/15521495

Agin GJ, Binford TO (1976) Computer Description of Curved Objects. IEEE Transactions on Computers C-25(4):439–449, DOI 10.1109/TC.1976.1674626, URL http://ieeexplore.ieee.org/lpdocs/epic03/wrapper.htm?arnumber=1674626

Alajlan N, Rube IE, Kamel MS, Freeman G (2007) Shape retrieval using triangle-area representation and dynamic space warping. Pattern Recognition 40(7):1911 – 1920, DOI http://dx.doi.org/10.1016/j.patcog.2006.12.005, URL http://www.sciencedirect.com/science/article/pii/S0031320306005188

Asada H, Brady M (1986) The curvature primal sketch. IEEE Transactions on Pattern Analysis and Machine Intelligence 8(1):2–14, URL http://ieeexplore.ieee.org/lpdocs/epic03/wrapper.htm?arnumber=4767747

Bai X, Yang X, Latecki LJ, Liu W, Tu Z (2010) Learning context-sensitive shape similarity by graph transduction. IEEE Trans Pattern Anal Mach Intell 32(5):861–874

Bay H, Ess A, Tuytelaars T, Van Gool L (2008) Speeded-Up Robust Features (SURF). Comput Vis Image Underst 110(3):346–359, DOI http://dx.doi.org/10.1016/j.cviu.2007.09.014

Belongie S, Malik J, Puzicha J (2001) Matching shapes. In: Proceedings Eighth IEEE International Conference on Computer Vision ICCV 2001, IEEE, IEEE Comput. Soc, vol 1, pp 454–461, DOI 10.1109/ICCV.2001.937552, URL http://ieeexplore.ieee.org/lpdocs/epic03/wrapper.htm?arnumber=937552

Belongie S, Malik J, Puzicha J (2002) Shape matching and object recognition using shape contexts. IEEE Transactions on Pattern Analysis and Machine Intelligence 24(4):509–522, DOI 10.1109/34.993558, URL http://ieeexplore.ieee.org/lpdocs/epic03/wrapper.htm?arnumber=993558

Besl PJ, McKay ND (1992) A method for registration of 3-d shapes. IEEE Trans Pattern Anal Mach Intell 14(2):239–256, DOI 10.1109/34.121791, URL http://dx.doi.org/10.1109/34.121791

Biederman I (1985) Human image understanding: Recent research and a theory. Computer Vision Graphics and Image Processing 32(1):29–73, DOI 10.1016/0734-189x(85)90002-7, URL http://www.sciencedirect.com/science/article/pii/0734189X85900027

Biederman I, Ju G (1988) Surface versus edge-based determinants of visual recognition. Cognitive Psychology 20(1):38–64, URL http://www.ncbi.nlm.nih.gov/pubmed/3338267

Binford TO (1971) Visual Perception by Computer. In: Grasselli A (ed) IEEE Conference on Systems and Control, IEEE, pp 277–284

Blum H (1967) A transformation for extracting new descriptors of shape. Models for the perception of speech and visual form 19(5):362–380, URL http://pageperso.lif.univ-mrs.fr/~edouard.thiel/rech/1967-blum.pdf

Bosch A, Zisserman A, Munoz X (2007) Image classification using random forests and ferns. IEEE 11th International Conference on Computer Vision (2007) 23(1):1–8, URL http://eprints.pascal-network.org/archive/00003046/

Bouchard G, Triggs W (2005) Hierarchical part-based visual object categorization. 2005 IEEE Computer Society Conference on Computer Vision and Pattern Recognition CVPR05 1:710–715, URL http://eprints.pascal-network.org/archive/00000801/

Brooks RA (1983) Model-Based 3-D Interpretation of 2-D Images. IEEE Transactions on Pattern Recognition and Machine Intelligence PAMI-5(2):140–150

Carneiro G, Lowe D (2006) Sparse Flexible Models of Local Features. 9th European Conference on Computer Vision ECCV 2006 3953:29–43, DOI 10.1007/11744078, URL http://www.springerlink.com/content/u7l072qn26147501

Chandra S, Kumar S, Jawahar CV (2012) Learning hierarchical bag of words using naive bayes clustering. In: Asian Conference on Computer Vision, pp 382–395

Chang L, Duarte M, Sucar L, Morales E (2010) Object Class Recognition Using SIFT and Bayesian Networks. Advances In Soft Computing pp 56—-66, URL http://www.springerlink.com/index/454413323066V860.pdf

Chang L, Duarte MM, Sucar LE, Morales EF (2012) A bayesian approach for object classification based on clusters of sift local features. Expert Systems with Applications 39:1679–1686, DOI http://dx.doi.org/10.1016/j.eswa.2011.06.059, URL http://dx.doi.org/10.1016/j.eswa.2011.06.059

Chang L, Arias-Estrada M, Palancar JH, Sucar LE (2014a) Partial shape matching and retrieval under occlusion and noise. In: Progress in Pattern Recognition, Image Analysis, Computer Vision, and Applications - 19th Iberoamerican Congress, CIARP 2014, Puerto Vallarta, Mexico, November 2-5, 2014. Proceedings, pp 151–158, DOI 10.1007/978-3-319-12568-8_19, URL http://dx.doi.org/10.1007/978-3-319-12568-8_19

Chang L, Arias-Estrada MO, Sucar LE, Palancar JH (2014b) Lisf: An invariant local shape features descriptor robust to occlusion. In: Marsico MD, Tabbone A, Fred ALN (eds) ICPRAM 2014 - Proceedings of the 3rd International Conference on Pattern Recognition Applications and Methods, ESEO, Angers, Loire Valley, France, 6-8 March, 2014, SciTePress, pp 429–437, DOI http://dx.doi.org/10.5220/0004825504290437

Chen Y, Medioni G (1992) Object modelling by registration of multiple range images. Image Vision Comput 10(3):145–155, DOI 10.1016/0262-8856(92)90066-C, URL http://dx.doi.org/10.1016/0262-8856(92)90066-C

Chetverikov D (2003) A Simple and Efficient Algorithm for Detection of High Curvature Points in Planar Curves. Proceedings of the 23rd Workshop of the Austrian Pattern Recognition Group pp 746–753, DOI 10.1007/978-3-540-45179-2_91, URL http://www.springerlink.com/index/VN2RGLUK251H3XCC.pdf

Chong CW, Raveendran P, Mukundan R (2004) Translation and scale invariants of legendre moments. Pattern Recognition 37(1):119–129

Csurka G, Dance CR, Fan L, Willamowski J, Bray C (2004) Visual categorization with bags of keypoints. In: Workshop on Statistical Learning in Computer Vision, ECCV, pp 1–22

De Winter J, Wagemans J (2004) Contour-based object identification and segmentation: stimuli, norms and data, and software tools. Behavior research methods instruments computers A journal of the Psychonomic Society Inc 36(4):604–624, URL http://www.ncbi.nlm.nih.gov/pubmed/15641406

Dickinson SJ (2009) Object Categorization. Computer and Human Vision Perspectives, Cambridge Books, chap The Evolution of Object Categorization and the Challenge of Image Abstraction, pp 1–37

Direkoglu C, Nixon M (2011) Shape classification via image-based multiscale description. Pattern Recognition 44(9):2134–2146, URL http://eprints.soton.ac.uk/272192/

Dork G, Schmid C (2005) Object class recognition using discriminative local features. Tech. rep., IEEE Transactions on Pattern Analysis and Machine Intelligence

Elkan C (2003) Using the triangle inequality to accelerate k-means. In: Fawcett T, Mishra N (eds) ICML, AAAI Press, pp 147–153

Emerson P (2013) The original borda count and partial voting. Social Choice and Welfare 40(2):353–358

Everingham M, Zisserman A, Williams CKI, Van Gool L (2006) The PASCAL Visual Object Classes Challenge 2006 (VOC2006) Results. http://www.pascal-network.org/challenges/VOC/voc2006/results.pdf

Everingham M, Van Gool L, Williams CKI, Winn J, Zisserman A (2011) The PASCAL Visual Object Classes Challenge 2011 (VOC2011) Results. http://www.pascal-network.org/challenges/VOC/voc2011/workshop/index.html

Fei-fei L, Fergus R, Perona P (2003) A Bayesian approach to unsupervised one-shot learning of object categories. Proceedings Ninth IEEE International Conference on Computer Vision 2(Iccv):1134–1141 vol.2, DOI 10.1109/ICCV.2003.1238476, URL http://ieeexplore.ieee.org/lpdocs/epic03/wrapper.htm?arnumber=1238476

Fei-Fei L, Fergus R, Perona P (2007) Learning generative visual models from few training examples: An incremental bayesian approach tested on 101 object categories. Comput Vis Image Underst 106(1):59–70

Felzenszwalb PF, Huttenlocher DP (2005) Pictorial Structures for Object Recognition. International Journal of Computer Vision 61(1):55–79, DOI 10.1023/B:VISI.0000042934.15159.49, URL http://www.springerlink.com/openurl.asp?id=doi:10.1023/B:VISI.0000042934.15159.49

Felzenszwalb PF, McAllester DA, Ramanan D (2008) A discriminatively trained, multiscale, deformable part model. In: CVPR, IEEE Computer Society, URL http://dblp.uni-trier.de/db/conf/cvpr/cvpr2008.html#FelzenszwalbMR08

Fergus R, Perona P, Zisserman A (2003) Object class recognition by unsupervised scale-invariant learning. In: Proceedings of the IEEE Conference on Computer Vision and Pattern Recognition, Madison, Wisconsin, vol 2, pp 264–271

Fernando B, Fromont , Muselet D, Sebban M (2012) Supervised learning of gaussian mixture models for visual vocabulary generation. Pattern Recognition 45(2):897–907

Ferrari V, Tuytelaars T, Gool LJV (2006) Object detection by contour segment networks. In: Leonardis A, Bischof H, Pinz A (eds) ECCV (3), Springer, Lecture Notes in Computer Science, vol 3953, pp 14–28, URL http://dblp.uni-trier.de/db/conf/eccv/eccv2006-3.html#FerrariTG06

Ferrari V, Jurie F, Schmid C (2010) From images to shape models for object detection. International Journal of Computer Vision 87(3):284–303, URL http://dblp.uni-trier.de/db/journals/ijcv/ijcv87.html#FerrariJS10

Ferrie FP, Lagarde J, Whaite P (1993) Darboux Frames, Snakes, and Super-Quadrics: Geometry from the Bottom Up. IEEE Transactions on Pattern Analysis and Machine Intelligence 15(8):771–784, DOI 10.1109/34.236252

Gehler PV, Nowozin S (2009) On feature combination for multiclass object classification. In: ICCV, IEEE, pp 221–228

Gong Y, Kumar S, Rowley HA, Lazebnik S (2013) Learning binary codes for high-dimensional data using bilinear projections. In: CVPR 2013

Gonzalez-Aguirre DI, Hoch J, Rhl S, Asfour T, Bayro-Corrochano E, Dillmann R (2011) Towards shape-based visual object categorization for humanoid robots. In: ICRA, IEEE, pp 5226–5232, URL http://dblp.uni-trier.de/db/conf/icra/icra2011.html#Gonzalez-AguirreHRABD11

Grimson WEL, Lozano-Perez T (1984) Model-Based Recognition and Localization from Sparse Range or Tactile Data. The International Journal of Robotics Research 3(3):3–

35, DOI 10.1177/027836498400300301, URL http://ijr.sagepub.com/cgi/doi/10.1177/027836498400300301

Hartigan JA, Wong MA (1979) A k-means clustering algorithm. JSTOR: Applied Statistics 28(1):100–108

Hu MK (1962) Visual pattern recognition by moment invariants. IRE Transactions on Information Theory 8(2):179–187, DOI 10.1109/TIT.1962.1057692, URL http://ieeexplore.ieee.org/xpls/abs_all.jsp?arnumber=1057692

Huttenlocher DP, Ullman S (1990) Recognizing solid objects by alignment with an image. International Journal of Computer Vision 5(2):195–212, DOI 10.1007/BF00054921, URL http://www.springerlink.com/index/10.1007/BF00054921

Jégou H, Douze M, Schmid C (2011) Product quantization for nearest neighbor search. IEEE Pattern Analysis and Machine Intellingence 33(1):117–128

Jiu M, Wolf C, Garcia C, Baskurt A (2012) Supervised learning and codebook optimization for bag of words models. Cognitive Computation 4:409–419

Kesorn K, Poslad S (2012) An enhanced bag-of-visual word vector space model to represent visual content in athletics images. IEEE Transactions on Multimedia 14(1):211–222

Khotanzad A, Hong YH (1988) Rotation invariant pattern recognition using zernike moments. Pattern Recognition, 1988, 9th International Conference on pp 326–328 vol.1, DOI 10.1109/ICPR.1988.28233

Kim WY, Kim YS (2000) A region-based shape descriptor using Zernike moments. Signal Processing Image Communication 16(1-2):95–102, DOI 10.1016/S0923-5965(00)00019-9, URL http://linkinghub.elsevier.com/retrieve/pii/S0923596500000199

Kimia BB (2009) Shapes and Shock Graphs: From Segmented Shapes to Shapes Embedded in Images, Cambridge University Press, p 430–450

Kirby M, Sirovich L (1990) Application of the Karhunen-Loeve procedure for the characterization of human faces. IEEE Transactions on Pattern Analysis and Machine Intelligence 12(1):103–108, DOI 10.1109/34.41390, URL http://ieeexplore.ieee.org/lpdocs/epic03/wrapper.htm?arnumber=41390

Kliot M, Rivlin E (1998) Invariant-Based Shape Retrieval in Pictorial Databases. Computer Vision and Image Understanding 71(2):182–197, DOI 10.1006/cviu.1998.0709, URL http://linkinghub.elsevier.com/retrieve/pii/S1077314298907093

Latecki LJ, Lakmper R, Eckhardt U (2000) Shape descriptors for non-rigid shapes with a single closed contour. In: CVPR, IEEE Computer Society, pp 1424–1429, URL http://dblp.uni-trier.de/db/conf/cvpr/cvpr2000.html#LateckiLE00

Lazebnik S, Schmid C, Ponce J (2006) Beyond Bags of Features: Spatial Pyramid Matching for Recognizing Natural Scene Categories. 2006 IEEE Computer Society Conference on Computer Vision and Pattern Recognition Volume 2 CVPR06 2(2169-2178):2169–2178, URL http://eprints.pascal-network.org/archive/00002929/

Leibe B, Leonardis A, Schiele B (2004) Combined Object Categorization and Segmentation with an Implicit Shape Model. Work 1(May):1–16, DOI 10.1.1.5.6272, URL http://citeseerx.ist.psu.edu/viewdoc/download?doi=10.1.1.5.6272&amp;rep=rep1&amp;type=pdf

Leibe B, Leonardis A, Schiele B (2007) Robust Object Detection with Interleaved Categorization and Segmentation. International Journal of Computer Vision 77(1-3):259–289, DOI 10.1007/s11263-007-0095-3, URL http://www.springerlink.com/index/10.1007/s11263-007-0095-3

Li T, Ye M, Ding J (2014) Discriminative hough context model for object detection. The Visual Computer 30(1):59–69, URL http://dblp.uni-trier.de/db/journals/vc/vc30.html#LiYD14

Ling H, Jacobs DW (2007) Shape classification using the inner-distance. IEEE TPAMI 29(2):286–299, URL http://dblp.uni-trier.de/db/journals/pami/pami29.html#LingJ07

Liu G (2010) Improved bags-of-words algorithm for scene recognition. Journal of Computational Information Systems 6(14):4933 – 4940

Liu J, Shah M (2008) Learning human actions via information maximization. 2013 IEEE Conference on Computer Vision and Pattern Recognition 0:1–8

Lopez-Sastre R, Tuytelaars T, Acevedo-Rodriguez F, Maldonado-Bascon S (2011) Towards a more discriminative and semantic visual vocabulary. Computer Vision and Image Understanding 115(3):415 – 425, special issue on Feature-Oriented Image and Video Computing for Extracting Contexts and Semantics

Lowe DG (1999) Object recognition from local scale-invariant features. Proceedings of the Seventh IEEE International Conference on Computer Vision 2([8):1150–1157 vol.2, DOI 10.1109/ICCV.1999.790410, URL http://ieeexplore.ieee.org/lpdocs/epic03/wrapper.htm?arnumber=790410

Lowe DG (2004) Distinctive image features from scale-invariant keypoints. International Journal of Computer Vision 60(2):91–110, DOI http://dx.doi.org/10.1023/B:VISI.0000029664.99615.94

Lu Z, Ip HHS (2009) Image categorization with spatial mismatch kernels. In: CVPR, IEEE, pp 397–404

Ma T, Latecki LJ (2011) From partial shape matching through local deformation to robust global shape similarity for object detection. In: CVPR, IEEE, pp 1441–1448, URL http://dblp.uni-trier.de/db/conf/cvpr/cvpr2011.html#MaL11

Maji S, Malik J (2009) Object detection using a max-margin hough transform. In: CVPR, IEEE, pp 1038–1045, URL http://dblp.uni-trier.de/db/conf/cvpr/cvpr2009.html#MajiM09

Mann HB, Whitney DR (1947) On a test of whether one of two random variables is stochastically larger than the other. Annals of Mathematical Statistics 18(1):50–60

Martin DR, Fowlkes CC, Malik J (2004) Learning to detect natural image boundaries using local brightness, color, and texture cues. IEEE TPAMI 26(5):530–49, DOI 10.1109/TPAMI.2004.1273918, URL http://ieeexplore.ieee.org/xpl/articleDetails.jsp?arnumber=1273918

Martínez JM (2004) MPEG-7 Overview. URL http://www.chiariglione.org/mpeg/standards/mpeg-7/mpeg-7.htm. URL http://www.chiariglione.org/mpeg/standards/mpeg-7/mpeg-7.htm

Matas J (2004) Robust wide-baseline stereo from maximally stable extremal regions. Image and Vision Computing 22(10):761–767, DOI 10.1016/j.imavis.2004.02.006, URL http://linkinghub.elsevier.com/retrieve/pii/S0262885604000435

McNeill G, Vijayakumar S (2006) Hierarchical procrustes matching for shape retrieval. In: CVPR (1), IEEE Computer Society, pp 885–894, URL http://dblp.uni-trier.de/db/conf/cvpr/cvpr2006-1.html#McNeillV06

Mikolajczyk K (2004) Scale & Affine Invariant Interest Point Detectors. International Journal of Computer Vision 60(1):63–86, DOI 10.1023/B:VISI.0000027790.02288.f2, URL http://www.springerlink.com/openurl.asp?id=doi:10.1023/B:VISI.0000027790.02288.f2

Mikolajczyk K, Schmid C (2002) An affine invariant interest point detector. Image Rochester NY 1(1):128–142, DOI 10.1007/3-540-47969-4, URL http://www.springerlink.com/openurl.asp?id=doi:10.1023/B:VISI.0000027790.02288.f2

Mikolajczyk K, Leibe B, Schiele B (2005) Local features for object class recognition. In: ICCV '05: Proceedings of the Tenth IEEE International Conference on Computer Vision, IEEE Computer Society, Washington, DC, USA, pp 1792–1799, DOI http://dx.doi.org/10.1109/ICCV.2005.146

Mokhtarian F, Bober M (2003) Curvature Scale Space Representation: Theory, Applications, and MPEG-7 Standardization. Kluwer

Murase H, Nayar SK (1995) Visual learning and recognition of 3-d objects from appearance. International Journal of Computer Vision 14(1):5–24, DOI 10.1007/BF01421486, URL http://www.springerlink.com/index/10.1007/BF01421486

Pentland AP (1986) Perceptual organization and the representation of natural form. Artificial Intelligence 28(3):293–331, DOI 10.1016/0004-3702(86)90052-4, URL http://linkinghub.elsevier.com/retrieve/pii/0004370286900524

Qin J, Yung NHC (2012) Feature fusion within local region using localized maximum-margin learning for scene categorization. Pattern Recognition 45(4):1671–1683

Riemenschneider H, Donoser M, Bischof H (2010) Using partial edge contour matches for efficient object category localization. In: ECCV'10, Springer-Verlag, Berlin, Heidelberg, pp 29–42, URL http://dl.acm.org/citation.cfm?id=1888150.1888154

Roh KS, Kweon IS (1998) 2-d object recognition using invariant contour descriptor and projective refinement. Pattern Recognition 31(4):441–455, URL http://dblp.uni-trier.de/db/journals/pr/pr31.html#RohK98

Rube IE, Alajlan N, Kamel M, Ahmed M, Freeman GH (2005) Robust multiscale triangle-area representation for 2d shapes. In: ICIP (1), IEEE, pp 545–548, URL http://dblp.uni-trier.de/db/conf/icip/icip2005-1.html#RubeAKAF05

Rublee E, Rabaud V, Konolige K, Bradski G (2011) ORB: An efficient alternative to SIFT or SURF. In: International Conference on Computer Vision, Barcelona

Sebastian TB, Klein PN, Kimia BB (2004) Recognition of shapes by editing their shock graphs. IEEE Transactions on Pattern Analysis and Machine Intelligence 26(5):550–571, DOI 10.1109/TPAMI.2004.1273924, URL http://dx.doi.org/10.1109/TPAMI.2004.1273924

Shu X, Wu XJ (2011) A novel contour descriptor for 2D shape matching and its application to image retrieval. Image and Vision Computing 29(4):286–294, DOI 10.1016/j.imavis.2010.11.001, URL http://linkinghub.elsevier.com/retrieve/pii/S0262885610001526

Silberberg TM, Harwood DA, Davis LS (1986) Object recognition using oriented model points. Comput Vision Graph Image Process 35:47–71, DOI 10.1016/0734-189X(86)90125-8, URL http://dl.acm.org/citation.cfm?id=16504.16507

Solina F, Bajcsy R (1990) Recovery of Parametric Models from Range Images: The Case for Superquadrics with Global Deformations. IEEE Transactions on Pattern Analysis and Machine Intelligence 12(2):131–147, DOI 10.1109/34.44401, URL http://ieeexplore.ieee.org/lpdocs/epic03/wrapper.htm?arnumber=44401

Srinivasan P, Zhu Q, Shi J (2010) Many-to-one contour matching for describing and discriminating object shape. In: The Twenty-Third IEEE Conference on Computer Vision and Pattern Recognition, CVPR 2010, San Francisco, CA, USA, 13-18 June 2010, pp 1673–1680, DOI 10.1109/CVPR.2010.5539834, URL http://dx.doi.org/10.1109/CVPR.2010.5539834

Stark M, Schiele B (2007) How Good are Local Features for Classes of Geometric Objects. IEEE 11th International Conference on Computer Vision (2007) pp 1–8, DOI 10.1109/ICCV.2007.4408878, URL http://ieeexplore.ieee.org/lpdocs/epic03/wrapper.htm?arnumber=4408878

Terzopoulos D, Metaxas D (1991) Dynamic 3D Models with Local and Global Deformations. IEEE Trans Pattern Anal Machine Intell 13(7):703–714

Toshev A, Taskar B, Daniilidis K (2011) Shape-based Object Detection via Boundary Structure Segmentation. International Journal of Computer Vision 99(2):123–146, DOI 10.1007/s11263-012-0521-z, URL http://www.springerlink.com/content/u71701604401086x/

Trinh NH, Kimia BB (2011) Skeleton Search: Category-Specific Object Recognition and Segmentation Using a Skeletal Shape Model. International Journal of Computer Vision 94(2):215–240, DOI 10.1007/s11263-010-0412-0, URL http://www.springerlink.com/index/10.1007/s11263-010-0412-0

Tsai CF (2012) Bag-of-words representation in image annotation: A review. ISRN Artificial Intelligence 2012

Turk M, Pentland A (1991) Eigenfaces for recognition. DOI 10.1162/jocn.1991.3.1.71, URL http://www.mitpressjournals.org/doi/abs/10.1162/jocn.1991.3.1.71

Tuytelaars T, Mikolajczyk K (2007) Local invariant feature detectors: A survey. Foundations and Trends in Computer Graphics and Vision 3(3):177–280, URL http://dblp.uni-trier.de/db/journals/ftcgv/ftcgv3.html

Van Otterloo PJ (1991) A contour-oriented approach to shape analysis. Prentice Hall International (UK) Ltd., Hertfordshire, UK, UK

Vedaldi A, Fulkerson B (2008) VLFeat: An open and portable library of computer vision algorithms

Vedaldi A, Zisserman A (2011) Efficient additive kernels via explicit feature maps. Pattern Analysis and Machine Intellingence 34(3)

Wang X, Bai X, Ma T, Liu W, Latecki LJ (2012) Fan shape model for object detection. In: CVPR, IEEE, pp 151–158, URL http://dblp.uni-trier.de/db/conf/cvpr/cvpr2012.html#WangBMLL12

Weber M, Welling M, Perona P (2000) Towards Automatic Discovery of Object Categories. Electrical Engineering 2(1063):101–108, DOI 10.1109/CVPR.2000.854754, URL http://ieeexplore.ieee.org/xpls/abs_all.jsp?arnumber=854754

Wu J, Tan WC, Rehg JM (2011) Efficient and effective visual codebook generation using additive kernels. Journal of Machine Learning Research 12:3097–3118

Yang X, Kknar-tezel S, Latecki LJ (2009) Locally constrained diffusion process on locally densified distance spaces with applications to shape retrieval. In: In: Proc. IEEE Conf. on Computer Vision and Pattern Recognition (CVPR

Yang X, Bai X, Kknar-Tezel S, Latecki L (2013) Densifying distance spaces for shape and image retrieval. Journal of Mathematical Imaging and Vision 46(1):12–28, DOI 10.1007/s10851-012-0363-x, URL http://dx.doi.org/10.1007/s10851-012-0363-x

Zhang D (2004) Review of shape representation and description techniques. Pattern Recognition 37(1):1–19, DOI 10.1016/j.patcog.2003.07.008, URL http://linkinghub.elsevier.com/retrieve/pii/S0031320303002759

Zhang D, Lu G (2002a) Generic Fourier descriptor for shape-based image retrieval. Proceedings IEEE International Conference on Multimedia and Expo 1(1):425–428, DOI 10.1109/ICME.2002.1035809, URL http://ieeexplore.ieee.org/lpdocs/epic03/wrapper.htm?arnumber=1035809

Zhang D, Lu G (2002b) Shape based image retrieval using generic fourier descriptors. In: Signal Processing: Image Communication 17, pp 825–848

Zhang J, Marszaek M, Lazebnik S, Schmid C (2007) Local Features and Kernels for Classification of Texture and Object Categories: A Comprehensive Study. International Journal of Computer Vision 73(2):213–238, DOI 10.1007/s11263-006-9794-4, URL http://www.springerlink.com/index/10.1007/s11263-006-9794-4

Zhang S, Tian Q, Hua G, Huang Q, Gao W (2011a) Generating descriptive visual words and visual phrases for large-scale image applications. IEEE Transactions on Image Processing 20(9):2664–2677

Zhang S, Tian Q, Hua G, Zhou W, Huang Q, Li H, Gao W (2011b) Modeling spatial and semantic cues for large-scale near-duplicated image retrieval. Computer Vision and Image Understanding 115(3):403–414

Zhang Y, Wu J, Cai J (2014) Compact representation for image classification: To choose or to compress? In: CVPR 2014

Appendix A

The Mann-Whitney Test

The Mann-Whitney U-test (Mann and Whitney, 1947) is used to test whether two independent samples of observations are drawn from the same or identical distributions. Specifically, in Section 5.2.1, the Mann-Whitney test is used to verify that the results obtained by the proposed method, are statistically superior to those obtained by the baseline.

This test is based on the idea that the particular pattern exhibited when m number of X random variables and n number of Y random variables are arranged together in increasing order of magnitude provides information about the relationship between their parent populations.

The Mann-Whitney test criterion is based on the magnitude of the Y's in relation to the X's, *i.e.*, the position of Y's in the combined ordered sequence. A sample pattern of arrangement where most of the Y's are greater than most of the X's or vice versa would be evidence against random mixing. This would tend to discredit the null hypothesis of identical distribution.

The test has two important assumptions. First the two samples under consideration are random, and are independent of each other, as are the observations within each sample. Second the observations are numeric or ordinal (arranged in ranks). In our application of the test, the two considered samples were the results of the baseline method, against the best result obtained by our proposed method. A test for each dataset and each used classifier was performed (see Tables 5.1 and 5.2).

In order to calculate the U statistics, the combined set of data is first arranged in ascending order with tied scores receiving a rank equal to the average position of those scores in the ordered sequence.

Let T denote the sum of ranks for the first sample. The Mann-Whitney test statistic is then calculated using $U = n_1n_2 + \{n_1(n_1+1)/2\} - T$, where n_1 and n_2 are the sizes of the first and second samples respectively.

We next compare the value of calculated U with the value given in the Tables of Critical Values for the Mann-Whitney U-test, where the critical values are provided for given n_1 and n_2 , and accordingly accept or reject the null hypothesis. Even though the distribution of U is known, the normal distribution provides a good approximation in case of large samples.

In order to perform our tests, we used the Mann-Whitney Test implementation provided in the VassarStats website (vas, 2013).

Appendix B

Acronyms

SIFT	Scale-Invariant Feature Transform
SURF	Speeded Up Robust Features
ORB	Oriented FAST and Rotated BRIEF
MSER	Maximally Stable Extremal Regions
GPU	Graphics Processing Unit
3D	Three-dimensional
GPGPU	General-Purpose Computing on Graphics Processing Units
CAD	Computer Aided Design
BoW	Bag of Words
CSS	Curvature Scale Space
MCC	Multi-scale Convexity Concavity
SC	Shape Context
TAR	Triangle-Area Representation
MTAR	Multi-scale Triangle-Area Representation
GMM	Gaussian Mixed Model
HIK	Histogram Intersection Kernel
LISF	Invariant Local Shape Features
CUDA	Compute Unified Device Architecture
RGB	Red, Green and Blue
OCTAR	Open/Closed contours Triangle Area Representation
ICP	Iterative Closest Point
IDSC	Inner Distance Shape Context
CPU	Central Processing Unit
GHz	GigaHertz
RAM	Random-Access Memory
GB	GigaByte
PC	Personal Computer
SVM	Support Vector Machine
KNN	K-Nearest Neighbor
tf	Term frecuency
$tf - idf$	Term frequency - inverse document frequency
fps	Frames per second

Appendix C

Notations

d_{min}	Lower scale limit for the LISF feature extraction method
d_{max}	Upper scale limit for the LISF feature extraction method
α_{min}	Lower sharpness limit for the LISF feature extraction method
α_{max}	Upper sharpness limit for the LISF feature extraction method
H_i	LISF feature descriptor
Ω	Matching measure of LISF method
$TAR(i,j,k)$	Signed area of the triangle formed by points $\{i,j,k\}$
$\Theta^{\mathcal{P}}(i,j)$	OCTAR descriptor value for points pair (i,j)
$\Phi(P,Q)$	Similarity measure between two OCTAR descriptors Θ^{P} and Θ^{Q}
$\Theta^{\mathcal{P},R}$	OCTAR spatial configuration descriptor of two contour fragments $\mathcal{P}$ and R
$\mathcal{E}_{COV}$	OCTAR covering criterion
$\mathcal{E}_{Z}$	OCTAR object hypothesis contour estimation criterion
$\mathcal{E}_{Z^*}$	OCTAR fitted object hypothesis criterion
$\mathcal{E}_{App}$	OCTAR appearance-based evaluation criterion
$\mathcal{M}_1(k,c_j)$	Inter-class representativeness measure of class c_j in visual word k
$\mathcal{M}_2(k,c_j)$	Intra-class Representativeness Measure of class c_j in visual word k
$\mathcal{M}_3(k,\mathcal{M})$	Distinctiveness measure of a given visual word k for a given measure $\mathcal{M}$